APPLIED PHYSICS REVIEWS

Electron emission from ferroelectrics

G. Rosenman[a] and D. Shur
Department of Electrical Engineering–Physical Electronics, Faculty of Engineering, Tel Aviv University, Ramat Aviv 69978, Israel

Ya. E. Krasik and A. Dunaevsky
Department of Physics, Technion-Israel Institute of Technology, Haifa 32000, Israel

(Received 13 September 1999; accepted for publication 16 August 2000)

Electron emission from ferroelectrics (FEE) is an unconventional electron emission effect. Methods of FEE excitation are quite different compared to classic electron emission from solids. Two kinds of FEE have been observed, ''weak'' and ''strong.'' ''Weak'' electron emission (current density 10^{-12}–10^{-7} A/cm^2) occurs from polar surfaces of ferroelectric materials in the ferroelectric phase only. A source of the electric field for ''weak'' FEE excitation is an uncompensated charge, generated by a deviation of macroscopic spontaneous polarization from its equilibrium state under a pyroelectric effect, piezoelectric effect, or polarization switching. The FEE is a tunneling emission current which screens uncompensated polarization charges. It is shown that the FEE is an effective tool for direct domain imaging and studies of electronic properties of ferroelectrics. ''Strong'' FEE, which is 10–12 orders of magnitude higher than ''weak'' FEE, achieves 100 A/cm^2 and is plasma-assisted electron emission. Two modes of the surface flashover plasma formation followed by strong electron emission have been studied. The plasma of ferroelectric origin has been observed only in the ferroelectric phase and it is induced by polarization switching or a field-enforced phase transition, such as antiferroelectric–ferroelectric or relaxor–ferroelectric. The second mode of plasma is conventional surface flashover which may be initiated by a high voltage application in any phase from any dielectric, including ferroelectrics. In this review paper we consider numerous experimental results, as well as mechanisms of both types of electron emission from ferroelectrics. The main stress is placed on the material aspect in order to clarify the influence of ferroelectricity (ferroelectric phase transitions, polarization switching, etc.) on electron emission. Another aspect which is broadly discussed is the potential applications of these unconventional FEE emitters in various devices for development of high density FEE cathodes for microwave devices, as well as FEE converters of IR irradiation into visible light, x-ray imaging, FEE flat panel displays, etc.
 [S0021-8979(00)02323-9]

TABLE OF CONTENTS

I. INTRODUCTION

Two sorts of electron emission overbarrier and tunneling are observed from solids. Overbarrier electron emission (photoelectron or thermionic) occurs when a source of an external energy (light source or thermal heater) excites electrons to an energy exceeding the work function. For thermionic emission, for instance, the cathode temperature T should be around $T=2500-3000$ K. In the case of tunneling emission the external electric field gives rise to narrowing the potential barrier resulting in tunneling of electrons to the vacuum. Despite the absolute different mechanisms of the overbarrier and tunneling effects, the only common feature should be noted for all classic types of electron emission. Electron emission from conventional cathodes occurs due to changes in the electron subsystem of solids (changes of a spectrum of electronic states, work function, or penetrability of the potential barrier). No alterations arise in a crystal lattice itself, which serves as a reservoir for electrons.

The first observations of electron emission from ferroelectrics (FEE) during the pyroelectric effect by Rosenblum *et al.*[1] and the piezoelectric effect by Rosenman and Pechorskii[2] in $LiNbO_3$ crystals showed that FEE differs strongly from classic types of electron emission from solids. The temperature variation needed for pyroelectrically induced FEE was only a few degrees.[1] FEE in a $LiNbO_3$ crystal was observed from polar surfaces only: on heating, from the Z^+ polar face; and, surprisingly, on cooling from the opposite Z^- face. The measured electron energy was as high as several keV without an external accelerating field.[1] In the case of the piezoelectric effect, the FEE was studied from $LiNbO_3$ under mechanical pressing. It was found that the Y^+ face of the crystal emits electrons on pressing, whilst the opposite Y^- face emits on unloading along the X direction.[2] The measured FEE current did not exceed $10^{-9}-10^{-14}$ A/cm^2. Studies of FEE during spontaneous polarization reversal by Rosenman *et al.*[3] in ferroelectric $Pb_5Ge_3O_{11}$ allowed the observation of FEE current several orders of magnitude higher, reaching 10^{-7} A/cm^2. The results (Rosenblum *et al.*,[1] Rosenman *et al.*[2,3]) showed an important distinguishing feature of FEE compared to the classic types of electron emission from solids. It was shown that the only reason for FEE is an electrostatic field, generated due to a deviation of spontaneous polarization from the equilibrium state under pyroelectric, piezoelectric effects, or polarization reversal. FEE occurs from the negatively charged faces of ferroelectrics. The FEE current cannot be observed as a steady state current. This current is a transient emission current which screens spontaneous polarization. Investigations of numerous ferroelectrics showed that the FEE effect is a useful tool for studies of electronic properties of ferroelectrics. Developing the FEE imaging technique[3,4] allowed an attractive method for ferroelectric domains observation to be proposed[1,3] as well as the development of some FEE devices, such as a FEE flat panel display based on local polarization switching.[5] These FEE studies are related to the first period of studies of the ''weak'' FEE.

An explosive interest in FEE arose at the second stage of studies of this phenomenon, after publications by Gundel *et al.*[6,7] and other consequent publications by Riege, Gundel, and their co-authors at CERN, reported huge FEE currents reaching 10^2 A/cm^2. The FEE effect was observed by use of PLZT (lead lanthanum zirconate titanate) ferroelectric ceramics subjected to a high pulsed voltage stress. The re-

a)Electronic mail: gilr@eng.tau.ac.il

corded FEE current[6,7] exceeded 12 orders of magnitude the ''weak'' FEE current observed by Rosenman *et al.*[3] It became clear that a new generation of electron cathodes could be developed. Dozens of laboratories all over the world joined this activity (Gundel, Riege *et al.*,[6,8] Ivers *et al.*,[9] Schachter,[153] Jiang *et al.*,[10] Sampayan *et al.*,[11] Cavazos *et al.*,[12] Averty *et al.*,[13] Biedrzycki,[91] Okuyama *et al.*,[14] Airapetov *et al.*,[15] Shur *et al.*,[16] Miyake *et al.*,[17] Riege *et al.*,[18] Shannon *et al.*,[84] Krasik *et al.*,[87] Boscolo *et al.*,[89] Advani *et al.*,[131] Zhang *et al.*,[83]).

In the present review we also discuss a third stage of FEE studies. We firmly believe that this third stage is the starting point of applying FEE in different technological areas and for diverse devices. Promising examples are the first applications of high density FEE cathodes for microwave generation in a slow-wave tube,[19] traveling wave tube,[20] and observation of high frequency modulation.[21] It should be noted that despite the immense efforts undertaken during the last 10 years there is no definite opinion about the physics of the phenomenon, especially about the strong FEE reaching hundreds of amperes per square centimeter. Experimentally FEE is observed in diverse effects, such as spontaneous polarization reversal, dielectric polarization, or various field-enforced phase transitions (antiferroelectric–ferroelectric, relaxor–ferroelectric, paraelectric–ferroelectric). The electron emission was measured in different phase states (ferroelectric, antiferroelectric, relaxor, paraelectric) from electrically poled and unpoled ferroelectric crystals and ceramics.

We firmly believe that the ''mystery'' of the effect is hidden in the physics of ferroelectricity. This paper is a comprehensive review of numerous experimental data on FEE. Analysis of the presented results and models are presented based on ferroelectric materials science. The goal of the review is to show the current state of the understanding of the phenomenon and to estimate the areas of its possible application.

PART A: FERROELECTRIC ELECTRON EMISSION

1. Screening of the depolarization field and the work function of a ferroelectric crystal near polar surfaces

Ferroelectrics are spontaneously polarized crystals. The macroscopic dipole moment P_s (spontaneous polarization) of a ferroelectric is stable without the application of an electric field. For a ferroelectric crystal with finite dimensions, spontaneous polarization is homogeneous in the crystal bulk, but abrupt changes occur at the polar faces where $\mathbf{P}_s=0$. The nonhomogeneous distribution of $\mathbf{P}_s$ near the surface gives rise to a strong depolarization field because $\mathrm{div}\,\mathbf{P}_s\neq 0$. Two different ways for minimizing the depolarization field energy which allows a stable polarized state have been found.[22] The first way is a domain-divided ferroelectric crystal where screening the depolarization field occurs by electric charges of opposite signs of 180°-ferroelectric domains. The second way was proposed for monodomain ferroelectrics by Ivanchik[23] and Guro *et al.*[24,25] It was assumed that in the equilibrium state the bounded polarization charges are compensated by screening charges of a ferroelectric semiconductor [Fig. 1(a)]. The positive end of a spontaneous polarization vector is screened by electrons, while the negative end by holes. This model allowed the prediction of the existence of surface layers near opposite polar faces possessing *n*- and *p*-type conductivity.[22] The electron concentration n_s near the positive polar face can be determined by a simple equation[24]

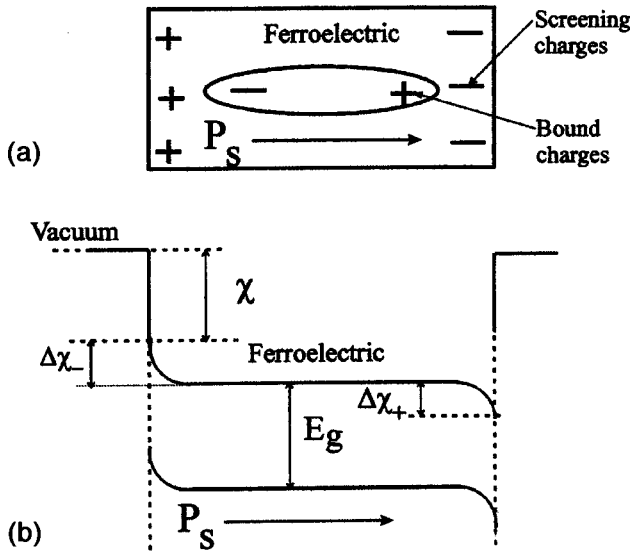

FIG. 1. (a) A ferroelectric crystal in an equilibrium state; (b) asymmetry of the electronic work function near the polar faces of a ferroelectric crystal.

$$4\pi q\,\delta n_s = D, \tag{1}$$

where δ is the thickness of the surface layer where the screening charge is localized, q is the electronic charge, and D is the electric field induction. For $BaTiO_3$ expression (1) gives $n_s=10^{19}\,\mathrm{cm}^{-3}$.[24] An equilibrium electron concentration in a neutral bulk region n_i for any semiconductor is given by

$$n_i = N_c \exp(-E_g/kT), \tag{2}$$

where N_c is the density of states, E_g is the energy gap. For the ferroelectric crystal $BaTiO_3$ possessing the energy gap of $E_g=3.2\,\mathrm{eV}$, the parameter $n_i=10^{-9}\,\mathrm{cm}^{-3}$. Hence $n_i \ll n_s$. This allowed Ivanchik[23] and Guro *et al.*[24,25] to assume that the compensation of the depolarization field in a monodomain ferroelectric crystal is provided by strong band bending $\Delta\chi_+$ and $\Delta\chi_-$ which are of the opposite sign. Figure 1(b) shows that a work function A for the opposite polar faces A_{Z^+} and A_{Z^-} may be written as follows:

$$A_{Z^+} = E_g + \chi - \Delta\chi_{Z^+}, \tag{3}$$

$$A_{Z^-} = E_g + \chi + \Delta\chi_{Z^-}, \tag{4}$$

where χ is the electron affinity and E_g is the band gap. These expressions lead to a strong asymmetry of the work functions ΔA for Z^+ and Z^- faces. Theoretical estimations[24,25] showed that for ideal pure single crystals:

$$\Delta A = A_{Z^-} - A_{Z^+} = E_g, \tag{5}$$

which is very large for $LiNbO_3$ ($\Delta A=3.9\,\mathrm{eV}$). However, experimental measurements demonstrated much lower values. LeBihan and Chartier[26] measured by the electron mirror

microscopy method the difference in the work function of 180° domains and observed $\Delta A = 0.975$ eV for TGS crystals. Another experimental result obtained by a Kelvin probe showed a much larger value of $\Delta A = 4.5$ eV for the TGS ferroelectric, and $\Delta A = 1$ eV for the GASH crystal.[27] The photoemission yield studied by Boikova and Rosenman[28] gave $\Delta A = 0.4$ eV for $LiNbO_3$ and $\Delta A = 0.6$ eV for $BaTiO_3$.[29] Low ΔA indicated that the screening charges are localized mainly on surface states with the concentration for $LiNbO_3$ $4\times10^{14}\,cm^{-2}$.[30] The estimated band bending was $\Delta\chi_+ = 0.15$ eV and $\Delta\chi_- = 0.25$ eV and electron affinity $\chi = 0.25$ eV. Akhaian *et al.*[31,32] studied the photoemission work function in $LiNbO_3$. The measurements showed $\Delta A = 0.7$ eV and allowed the observation of a zero electron affinity $\chi = 0$ at the Z^+ face. However, the measurements implemented by the Anderson method[32] did not reveal any difference in potential barriers for electrons from opposite polar faces. It was interpreted as direct evidence of complete screening of spontaneous polarization by charges localized on the surface states.

II. BASIC CONDITIONS FOR FEE GENERATION

The concept of minimization of the depolarization field (Ivanchik,[23] Guro *et al.*[24,25]) in a monodomain ferroelectric allows the consideration of two systems of charges [Fig. 1(a)]. The first system is a system of the bound charges responsible for spontaneous polarization. The second is a system of the screening charges compensating P_s near polar faces. The properties of these two systems are quite different. The system of the bound charges is determined by the properties of a ferroelectric crystal lattice. The screening charges are charges whose properties depend on electronic parameters of the ferroelectric semiconductor. Any deviation of spontaneous polarization P_s from its equilibrium value during, for example, polarization switching or the pyroelectric effect, gives rise to imbalance charges ΔP_s. The screening process of ΔP_s occurs by means of various compensation currents. The relative contribution of different screening processes to the total screening charge $Q_\Sigma = \Delta P_s$ depends on the experimental setup, the bulk conductivity of a ferroelectric crystal, interface conditions, etc. The general equation maybe written as follows:

$$Q_\Sigma = \int_0^t J_c\,dt + \int_0^t J_b\,dt + \int_0^t J_{\rm em}\,dt. \tag{6}$$

The first term is a conventional switching (pyroelectric, piezoelectric) charge $Q_{\rm ext}$ brought about by the transient switching (pyroelectric, piezoelectric) compensated current J_c to the electrodes that coat the polar faces via the external circuit during the time $t_{\rm sw}$ [Fig. 2(a)]. The second term is a screening charge Q_b which is provided by the bulk conductive current J_b. The charge Q_b is a space charge, which is redistributed near each polar surface inside a ferroelectric crystal bulk, in accordance with the following simple equation:

$$Q_b = Q_{b0}\exp(-t/\tau), \tag{7}$$

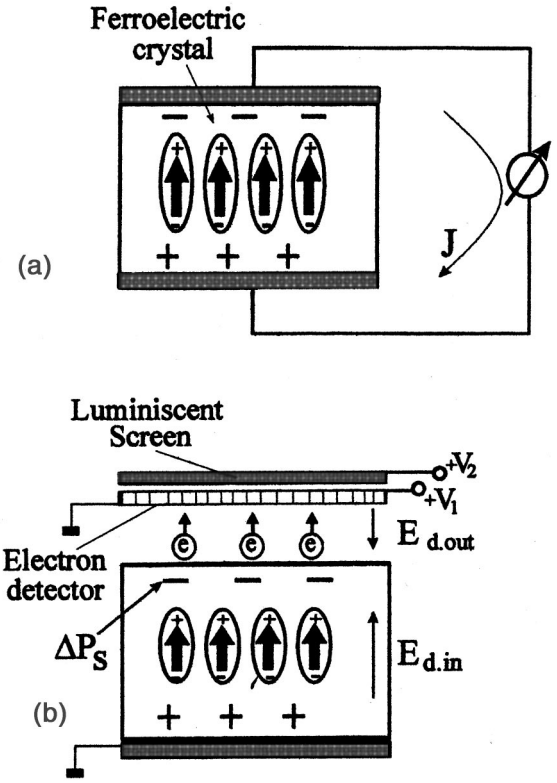

FIG. 2. Methods and conditions of generating ferroelectric electron emission. (a) A conventional experimental setup; (b) an experimental setup for FEE measurements. Uncompensated charges may be generated during pyroelectric, piezoelectric, and polarization switching effects.

where τ is the relaxation time. The relaxation time τ is defined as $\tau = \varepsilon\varepsilon_0/\sigma$ (ε is the dielectric permittivity, σ is the bulk conductivity). For the conventional setup [Fig. 2(a)] the current through the external short circuit is much higher than that in the crystal bulk $J_c \gg J_b$ because the conductivity σ of the ferroelectric crystal is very low. For the $LiNbO_3$ crystal where $\varepsilon = 50$ and $\sigma = 10^{-16}$–$10^{-18}\,\Omega^{-1}\,cm^{-1}$, the value of τ is as large as 10^5–10^7 s. Therefore, the contribution of the bulk current J_b to the screening process in this case is negligibly small.

The situation dramatically changes when ferroelectric polar faces are not coated by the electrodes [Fig. 2(b)]. A temperature variation (pyroelectric effect) or mechanical stress (piezoelectric effect) applied to a ferroelectric crystal gives rise to the generation of pyroelectric or piezoelectric charges ΔP_s. For a sample without electrodes, the first term in Eq. (6) describing the external current J_c is zero. The bulk screening process occurs very slowly with relaxation time $\tau = \varepsilon\varepsilon_0/\sigma$. So far the generated pyroelectric or piezoelectric charges will be the source of electrostatic fields in a gap ferroelectric sample-input plate of an electron detector $E_{d\,\rm out}$ and in the crystal bulk of the ferroelectric crystal $E_{d_{\rm in}}$ [Fig. 2(b)]. Figure 2b shows that the field $E_{d\,\rm out}$ is responsible for the FEE current. A simple estimation may be implemented for $LiNbO_3$ in the case of the pyroelectric effect ($\Delta T = 10$ K, pyroelectric coefficient $\gamma = 10^{-8}\,C\,cm^{-2}\,K^{-1}$). Taking a ferroelectric sample of $d = 1$ mm thick along the polar direction Z, and a gap of 10 μm results in the field $E_{d\,\rm out}$

$=\Delta P_s/\varepsilon_0=10^6$ V/cm ($\Delta P_s=\gamma\Delta T=10^{-7}$ C/cm^2). According to the estimations in the case of polarization switching, the field $E_{d\,\mathrm{out}}$ should be much stronger-up to 10^7-10^8 V/cm. A field 10^6-10^8 V/cm is enough for the field electron emission effect. Figure 2 demonstrates that FEE from a ferroelectric crystal may occur from a negatively charged polar surface only. In the case of positive charges, the field will cause field emission from a metal input plate of the electron detector toward the ferroelectric crystal [Fig. 2(b)]. The generated electron emission current will be a transient current, screening (neutralizing) uncompensated charges on the ferroelectric surface [see, the third term in Eq. (6)]. The FEE current flows in the short circuit containing the upper ferroelectric crystal surface, the vacuum gap, the electron detector, the luminescent screen, the voltage source (V_1,V_2), and the bottom ferroelectric surface. It should be emphasized that the FEE current from the charged ferroelectric surface gives rise to a new neutral state of the crystal. An alternative possibility for the relaxation of this high electric field [Fig. 2(b)] is a surface discharge effect and subsequent screening process by electrons and ions from the surface flashover plasma. It should be noted that the considered model is based on the assumption of a stable unmodified ferroelectric domain configuration. The influence of this very important factor was demonstrated in studies of FEE from undoped TGS and isomorphic crystals implemented by Sidorkin, Kostsov, and Biedrzycki (see Sec. I D).

Thus, uncompensated electrostatic charges are generated on polar surfaces of ferroelectrics by the pyroelectric effect, piezoelectric effects, and spontaneous polarization switching. The strong electrostatic field causes an unavoidable screening process when a ferroelectric crystal uncoated by electrodes may relax to a new fully compensated state by emitting electrons (FEE) into the vacuum.

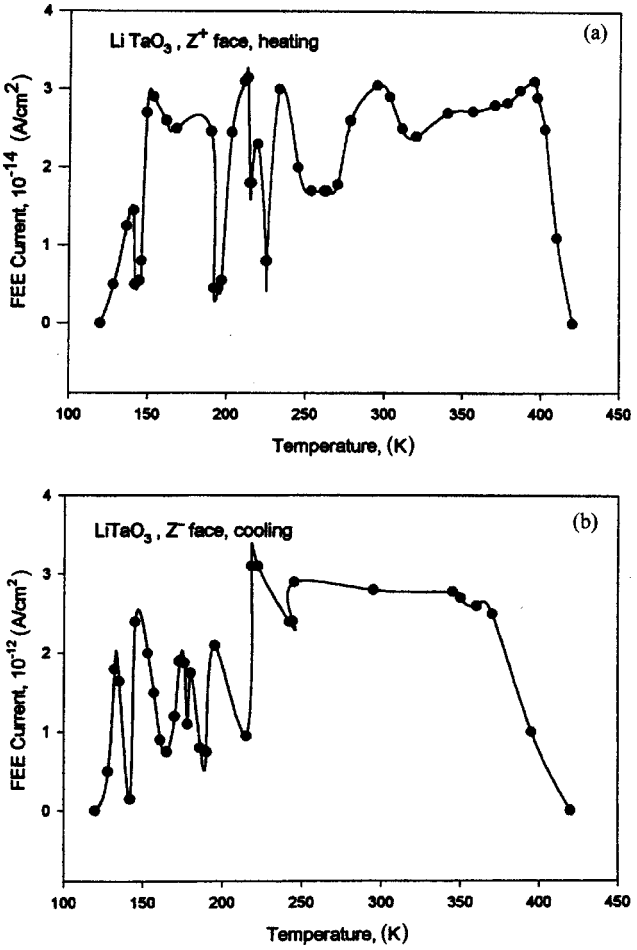

FIG. 3. FEE in a $LiTaO_3$ crystal during the pyroelectric effect: (a) upon heating; (b) upon cooling.

III. FEE INDUCED BY THE PYROELECTRIC EFFECT

To the best of our knowledge the first measurements of electron emission from ferroelectrics was undertaken by Beliaev and Bendrikova,[33] who studied the influence of spontaneous polarization on photostimulated electron emission yield versus time in TGS and Seignette salt crystals in air. The authors observed an increase of photoelectron emission current from the negatively charged surface and a decrease for the positively charged one. Another pioneer paper published by Kortov and Minz[34] reported the observation of photostimulated electron emission during ferroelectric–paraelectric phase transitions from the ceramics, $BaTiO_3$ and $(Pb,Ba)Nb_2O_6$. An anomalous increase of the electron emission current occurred in the vicinity of the Curie point.

The first detailed investigations of FEE during the pyroelectric effect was conducted by Rosenblum *et al.*,[1] who studied $LiNbO_3$ crystals. The experiments were conducted in a vacuum of 10^{-6} Torr, restricting to some extent surface discharges. A chevron electron multiplier consisting of two microchannel plates (MCP) served as a position-sensitive electron detector. The electron flux amplified by the detector was imaged by a phosphor screen [Fig. 2(b)]. This setup allowed the measurement and visualization of the electron flux with a resolution of 300 μm. The main result[1] was the observation of FEE without any photostimulation, which was used in the previously published works (Beliaev and Bendrikova,[33] Kortov and Minz,[34]). Heating the $LiNbO_3$ monodomain crystal from room temperature to $T=400$ K and its subsequent cooling induced persistent FEE from the Z^+ face during heating and sporadic bursts during cooling. The opposite Z^- face of the monodomain sample emitted FEE on cooling and electron bursts were observed from this face on heating. Multidomain samples emitted electrons during heating as well as cooling. The FEE images showed a pronounced picture of ring-shape ferroelectric domains, identical to the optical image of the domain structure in multidomain $LiNbO_3$. The emission current density was of the order of $10^{-9}-10^{-10}$ A/cm^2. Measurements of electron energy by a retarding potential gave a high value of $W_e=5$ keV. The results were interpreted in terms of thermally stimulated field emission where the thermal stimulation serves as a method of pyroelectric charges generation. These charges produce an electrostatic field E in the vacuum gap, which according to the presented estimations[1] was as high as $E=1.35\times10^7$ V/cm. The data by Rosenman and Boikova,[35] obtained by the use of $LiNbO_3$: Fe, demonstrated a long-time persistent emission current which was ascribed to the dynamic equilibrium state between two processes: pyroelectric

charge generation and bulk charge relaxation process. The upper temperature of FEE was $T=420\,\mathrm{K}$, and it was ascribed to the activation of Fe^{+2}-donor centers and correspondingly increasing the bulk conductivity.[35]

FEE was studied in detail by Rosenman, Rez, and co-workers[36,37] by the use of the isomorphic ferroelectric crystal $LiTaO_3$ [Fig. 3(a)]. The sample temperature was varied from 150 up to 773 K with different rates of α in the range of 1–12 K/min. Luminescent spark radiation was measured by a photomultiplier. A persistent electron emission current was unipolar and observed from the Z^+ face on heating and the Z^- face on cooling when negative pyroelectric charges are generated. Sharp drops of the persistent FEE current occurred for $\alpha>4$ K/min and disappeared for $\alpha=1$ K/min. These sharp electron emission drops were observed simultaneously with spark radiation pulses. The temperature of the FEE generation was limited for both low temperature $T_L=100\,\mathrm{K}$ and high temperature $T_H=400\,\mathrm{K}$ [Fig. 3(b)]. It is obvious that the observed FEE is of a pyroelectric origin. The pyroelectric field is screened in three ways. The first one is electron emission current FEE. The second mode of screening occurs via a ferroelectric crystal bulk. The third way is observed when the surface pyroelectric field exceeds the breakdown electric field. The surface flashover gives rise to screening of the pyroelectric field by positive ions from the surface plasma. It should be emphasized that all kinds of charge relaxation lead to the renovation of the neutral state. The grounded bottom face of the sample and input plate of the electron detector creates short circuit conditions providing the needed neutrality [Fig. 2(b)]. The measured FEE current density was $J_{\mathrm{em}}=10^{-12}\,\mathrm{A/cm^2}$ and the emitted electron charge per second was $Q_{\mathrm{em}}=10^{-12}\,\mathrm{C/cm^2}$. The persistent FEE arises upon heating beyond $\Delta T\approx 3-4$ K and for a $LiTaO_3$ deviation of the spontaneous polarization $\Delta P_s\approx 10^{-7}\,\mathrm{C/cm^2}$. So far the electron emission charge Q_{em} is much less than the generated pyroelectric charge ΔP_s and it may be neglected in the charge balance. The following equation for the uncompensated charge $\Delta\rho$ causing FEE, considering the processes of pyroelectric charge generation $d\rho_t=-\gamma dT$, (γ is the pyroelectric coefficient) and their screening by compensation via the ferroelectric crystal bulk, may be obtained.

$$\Delta\rho=\gamma\alpha\tau\left(1-\frac{\Delta T}{2\alpha\tau}\right). \tag{8}$$

Direct evidence of the influence of the bulk screening process was demonstrated in the $Ba_2NaNb_5O_{15}$(BNN) ferroelectric.[38] Its dark conductivity σ_d is close to that of $LiNbO_3$ and $LiTaO_3$ crystals. However, this ferroelectric crystal possesses a very high photoconductivity σ_{ph}. The temperature dependence of the FEE current measured in the dark was similar to that obtained for other low conductive ferroelectrics.[1,37] Illumination of the ferroelectric crystals by a He–Cd laser ($\lambda=0.44\,\mu$m) gave rise to a total extinction of FEE (Fig. 4). The process of the FEE relaxation was studied at different temperatures and under different laser beam intensities. It is obvious [see Eq. (8)] that the laser illumination of the photosensitive crystal BNN leads to a sharp decrease of the relaxation time τ due to a conductivity increase.

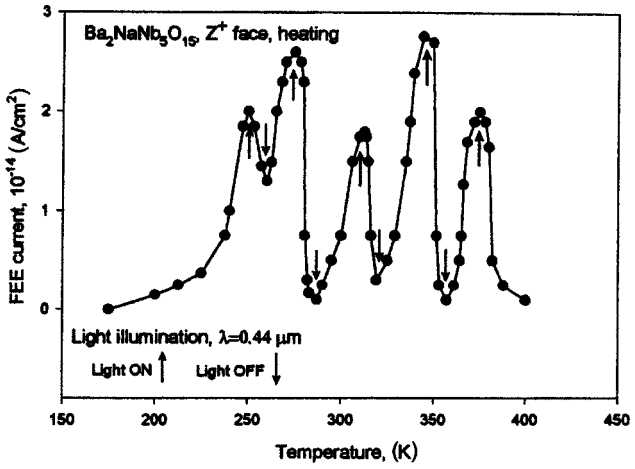

FIG. 4. The effect of light illumination on the extinction of FEE in $Ba_2NaNb_5O_{15}$ crystals. The arrows show the time of switching the illumination ''on'' and ''off.''

The experimental linear dependence of the photoconductivity of the BNN crystals allowed one to estimate several important electronic parameters: photosensitivity, the product $\mu\beta\tau$ (where μ is the electron mobility, β is the quantum yield, and τ is the lifetime), and electron mobility of the thermalized photoelectrons screening pyroelectric charge $\mu=1\,\mathrm{cm^2\,s^{-1}\,V^{-1}}$.[38]

The FEE effect was also studied from linear pyroelectrics. It was first observed in BeO ceramics[39] and monocrystals.[40] The electron emission peak was measured in the temperature range $T=150-350\,\mathrm{K}$ and the effect was ascribed to the pyroelectric properties of this composition. Measurements of FEE and pyroelectric properties[41] confirmed the proposed model and showed that the FEE current depends strongly on the poling field. The electron energy observed from polarized ceramics of BeO achieved 1 keV.

Detailed investigations of other linear pyroelectrics were implemented later by use of lithium sulphate monohydrate and Resorzin monocrystals.[42,43] Two kinds of FEE were found: pyroelectrically induced FEE and FEE of the electret origin. The FEE effect was highly irreproducible for these crystals. It was assumed that the unstable FEE may be related to modification of the spectrum of the surface states.

IV. FEE DURING PHASE TRANSITIONS

The ferroelectric phase transition is the region where all physical parameters such as structural symmetry, spontaneous polarization, pyroelectric coefficient, dielectric permittivity are changed critically. Anomalous photoemission was observed in monodomain ferroelectric monocrystals $BaTiO_3$ during all three well-known phase transitions, both in crystals[44–46] and thin films.[47] The photostimulated FEE current was asymmetric: The current from the Z^+ face was almost twice as much as the current from the opposite polar face. The effect was ascribed to two different causes: (a) band bending of the opposite sign near opposite polar faces and (b) an asymmetric potential barrier for electrons in ferroelectric crystals during their transport to the emitting surfaces.[48] It should be noted that $BaTiO_3$ is a high conduc-

tive ferroelectric crystal ($\sigma \approx 10^{-9}$ S/cm) and ''dark'' ferroelectric electron emission cannot be observed in these crystals.

The most attractive ferroelectric crystal for studies of FEE during ferroelectric phase transitions is a TGS crystal. The Curie temperature of this crystal is near room temperature, $T_C = 49\,^{\circ}\mathrm{C}$, and the conductivity is several orders of magnitude less than that in $BaTiO_3$, being close to the parameter in $LiNbO_3$ ($\sigma \approx 10^{-16}$–10^{-18} S/cm). Numerous papers have been published on FEE from TGS and isomorphic crystals. Sujak and Syslo performed the first observation of FEE in TGS, TGSe, and TGFB.[49] FEE was observed within the temperature range of the ferroelectric phase transition upon heating from the positive polar face. The peak of FEE occurred at the Curie temperature. The absorption method used in β spectrometry was applied to estimate the electron energy W_e. A value of W_e about 130 keV was obtained. The authors ascribed the effect to the pyroelectric properties of TGS crystals. Detailed studies of FEE from virgin TGS with different domain structures during ferroelectric phase transition were carried out by Kostsov *et al.*,[50] Sidorkin *et al.*,[51,52] and Biedrzycki *et al.*[53–55] Biedrzycki[53] studied 35 virgin undoped TGS crystals. It was demonstrated that FEE occurs mainly in two electron emission peaks. The first strong FEE current maximum was observed 6–13 K below the phase transition point $T_C = 322$ K, and the second smaller peak was recorded at 2–3 K above the Curie temperature. The proposed interpretation of the obtained data was based on direct observations of the domain structures in the studied TGS samples by nematic liquid crystals.[54] The virgin TGS possesses a highly mobile domain structure, which was especially unstable several degrees below the Curie point. Heating up the TGS samples causes a generation of the pyroelectric field. The field may be screened by the bulk conductive current and partly by FEE, as was observed for $LiTaO_3$ and $LiNbO_3$ crystals. Another way to minimize the depolarization field is a reconstruction of the domain configuration.[50,54] The process of domain structure modification is individual for different virgin TGS samples, and it is consistent with ''irreproducibility'' of the FEE spectra observed by Biedrzycki.[53]

A stable unipolar monodomain configuration in TGS crystals is observed when TGS is doped with L-α alanine. It occurs due to the internal electric field of built-in polar molecules of L-o alanine. The samples of doped TGS crystals demonstrated a reproducible unipolar FEE effect.[56] The structure of the FEE temperature spectrum (temperature was varied within the region of 300–390 K) consisted of two peaks from both polar surfaces [Figs. 5(a) and 5(b)]. The first one was observed in the ferroelectric phase, while the second peak in the paraelectric phase. It was ascribed to FEE caused by an electret field and it was highly reproducible for both faces upon heating. Studies of the FEE effect in doped TGS crystals at low temperature showed that persistent electron emission is observed in the ferroelectric phase.[57] Estimations, fulfilled in the work by Rosenman *et al.*,[57] showed that near the Curie temperature the relaxation time τ is very high because of a sharp growth of the dielectric permittivity ε. The results allowed one to simplify Eq. (8) and describe the

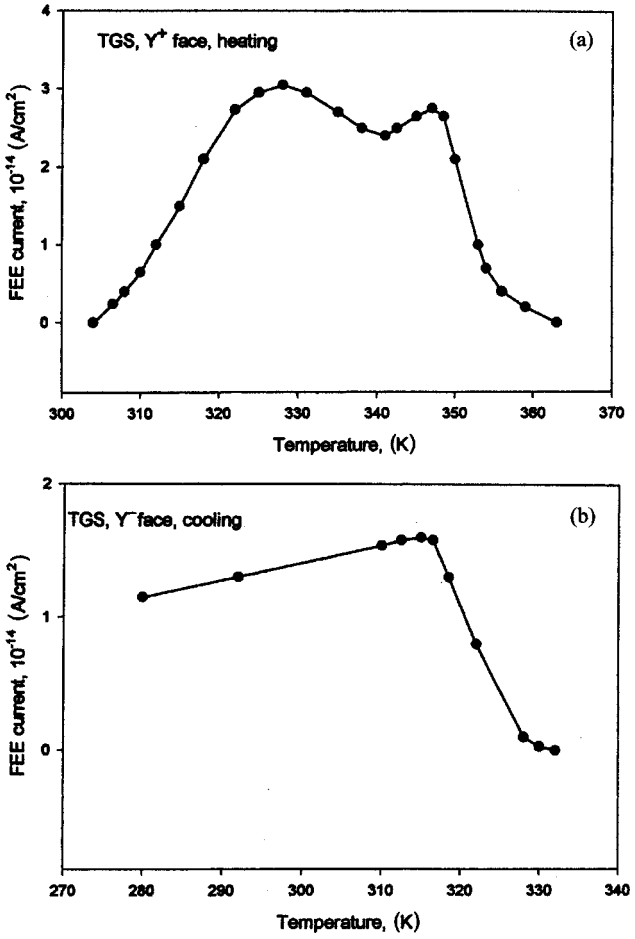

FIG. 5. FEE from TGS crystals doped with L-o alanine: (a) from the Y^+-polar face; (b) from the Y^--polar face.

field in the gap ferroelectric sample-electron detector E_{gap} which causes FEE, in the following form:

$$E_{\mathrm{gap}} = \frac{\gamma(T)\Delta T}{\varepsilon_0 \varepsilon(T)\dfrac{d_g}{d_{\mathrm{cr}}}}, \tag{9}$$

where d_{cr} is the thickness of the crystal along the polar axis and d_g is the distance between the upper polar surface of the ferroelectric sample and input plate of the electron detector. Equation (9) shows that the field E_{gap} is proportional to the ratio γ/ε. Both parameters change strongly in the region of the phase transition. Measurements of FEE and the dependence of γ/ε implemented for highly doped TGS with immobile domain structure, demonstrated that the FEE current behavior is similar to the temperature dependence of the parameter γ/ε.[57]

Recently, comparative studies of several ferroelectric crystals and ferroelectric PLZT ceramics were implemented by Shur and Rosenman.[58] PLZT ceramic samples and undoped monodomain $LiNbO_3$, TGS, $Gd_2(MoO_4)_3$, and $Pb_5Ge_3O_{11}$ crystals were studied in the experiments. Perovskite PLZT ceramic compositions 2/65/35 and 7/65/35 related to a rhombohedral ferroelectric phase were used. The ceramic samples were prepoled before measurements.

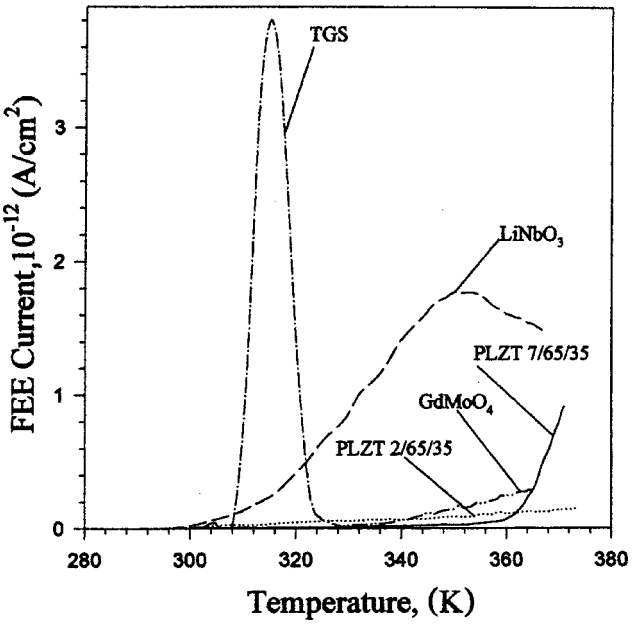

FIG. 6. A comparison between FEE properties of various ferroelectric crystals and PLZT ceramics.

Dielectric permittivity of the samples was measured at a frequency of 1 kHz by an LCR meter ELC-131D. Two kinds of FEE curves were observed (Fig. 6). The first one has a sharp maximum that was recorded for TGS crystals only in the vicinity of the Curie point and the data are consistent with the results.[49–57] The second one is a rather smooth graph of the FEE current density that increases with temperature. These curves were compared for $\Delta T \approx 40\,^{\circ}\mathrm{C}$ for all samples when the temperature change rate is approximately constant. For this ΔT the highest FEE current density $j_{\mathrm{em}}(T \approx 337\,^{\circ}\mathrm{K}) \approx 1.25\times 10^{-12}\,\mathrm{A/cm^2}$. The electron emission image showed that FEE was uniform from the entire surface of the sample. The electron current appeared just after the heating started when ΔT was just a few degrees. The FEE current density was much lower for the studied ferroelectric ceramics (Fig. 6). It was two orders of magnitude lower for PLZT composition 7/65/35, and 20 times for 2/65/35. Electron emission was observed from PLZT 2/65/35 compositions from the edges of the sample only because of fringing fields. The FEE current density was also very weak for $Gd_2(MoO_4)_3$ ($j_{\mathrm{em}} \approx 2\times 10^{-14}\,\mathrm{A/cm^2}$). It was not observed at all for lead germanate crystals because of their very high conductivity, which was $\sigma \approx 10^{-9}$ S/cm. It should be noted that abrupt growth of the FEE current for PLZT 7/65/35 started at the temperature $T \approx 363$ C and reached the value of $10^{-12}\,\mathrm{A/cm^2}$ within the several degrees of temperature change (Fig. 6).

Table I shows basic material values and FEE data for the studied ferroelectrics. It is obvious that for low conductive ferroelectrics and for a relatively short heating time, the process of bulk screening may be neglected.[58] The field in the gap in this case is described by Eq. (9) where E_{gap} is proportional to the relation γ/ε. The data in Table I demonstrate a very good correlation between the γ/ε relation and the FEE current. The smallest FEE current was observed for ferroelectric ceramics PLZT. In spite of the fact that they have the largest pyroelectric coefficient, they also possess a very high dielectric permittivity, which suppresses growth of the field E_g.

Two very important points should be emphasized. The first one is related to the sharp rise of emission current density occurring at a temperature of about 363 °C for the PLZT 7/65/35 sample (Fig. 6). We assume that this cannot be explained by the enhancement of the field in the gap due to rather strong changes of the temperature ΔT. No rise of emission current was observed for PLZT 2/65/35 in spite of the lower conductivity. We believe that this anomalous FEE current growth in 7/65/35 composition is due to the ferroelectric–relaxor phase transition that occurs well below the dielectric permittivity maximum, when the macroscopic spontaneously polarized state disappears.[59]

The studied PLZT compositions are very popular materials for strong ferroelectric cathodes. The presented studies showed the opposite result: PLZT ceramics demonstrate the worst FEE figures of merit. They generate the smallest, negligible FEE current. For ''weak'' FEE observed under pyroelectric, piezoelectric, and spontaneous polarization switching, the higher the dielectric permittivity the smaller the FEE current. As will be shown in Part B, which is devoted to strong ferroelectric cathodes, the critical parameter for them is also the dielectric permittivity. The larger the permittivity, the higher the ''strong'' FEE current. This discrepancy proves that the origin of these two effects is quite different. It will be shown in the following that ''weak'' FEE is a tunneling electron emission from a charged ferroelectric surface while ''strong'' FEE is a plasma-assisted effect.

V. FEE IMAGING OF STATIC DOMAIN STRUCTURES

The observed FEE effect allowed development of a new method of imaging of static ferroelectric domains in $LiNbO_3$.[1] The electron imaging method is shown in Fig.

TABLE I. FEE and basic physical parameters for studied ferroelectrics (Shur and Rosenman—Ref. 58).

Sample	Pyroelectric coefficient γ, $\mathrm{C/(cm^2\,K)}$	Relative dielectric permittivity ε	Relaxation time τ, s	Relation γ/ε	j_{em} $\mathrm{pA/cm^2}$
TGS	2.63×10^{-8}	49	876	5.36×10^{-10}	3.8
$LiNbO_3$	0.82×10^{-8}	31	7720	2.64×10^{-10}	1.27
PLZT 2/65/35	3.04×10^{-8}	581	836	5.23×10^{-11}	0.07
PLZT 7/65/35	6.9×10^{-8}	2184	876	3.16×10^{-11}	0.01
$Gd_2(MoO_4)_3$	4.4×10^{-10}	9	1717	4.8×10^{-11}	0.02

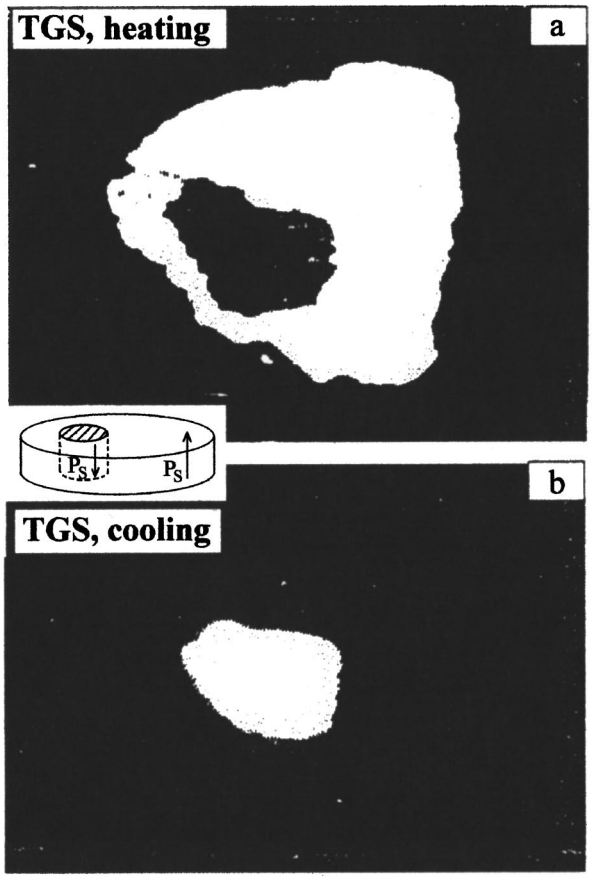

FIG. 7. FEE imaging of the ferroelectric bidomain configuration in a doped TGS crystal: (a) upon heating; (b) upon cooling.

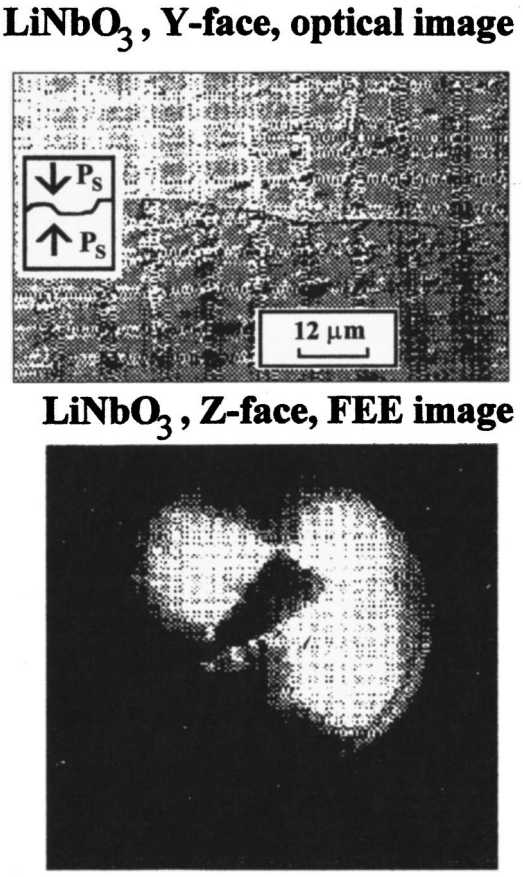

FIG. 8. The optical and FEE image of the ''head-to-head'' domain configuration induced by the pyroelectric effect.

2(b). TGS crystals doped by *L*-α alanine were studied by Rosenman *et al.*[60] for the visualization of artificially fabricated bidomain configurations (Fig. 7). Due to a high concentration of doping, the FEE domain images demonstrated a high stability. It was shown that any electron image may be obtained for a properly fabricated domain structure and it may also serve as a solid state electron imaging test.

Another type of a bidomain configuration was imaged by Kugel for $LiNbO_3$ where ''head-to-head'' domain structures with various thicknesses of the inverted layers and multilayer domain configurations were built-in by outdiffusion heat treatment at $T=1100\,^{\circ}\mathrm{C}$.[61] Figure 8 depicts a ''head-to-head'' bidomain configuration. The electric field E_{gap}, of pyroelectric origin, generated in the gap ferroelectric sample-electron detector for low conductive ferroelectrics like $LiNbO_3$ may be written as follows:[61]

$$E_{\mathrm{gap}}=\frac{1}{\varepsilon_0}\,\frac{-\gamma\delta T}{\varepsilon_0 d_{\mathrm{cr}}+\varepsilon_{\mathrm{cr}} d_g}\,(d_{\mathrm{cr}}-2\Delta), \tag{10}$$

where d_{cr} and $\varepsilon_{\mathrm{cr}}$ are the crystal thickness and dielectric permittivity along the polar axis of the ferroelectric, respectively, and d_g is the gap between the electron detector and ferroelectric sample, δT is the temperature change, and Δ is the thickness of the domain inverted layer. For a monodomain structure $\Delta=0$ and conventional unipolar FEE occurs from both polar faces.[1,37] For the ''head-to head'' symmetric bidomain structure $\Delta=0.5d_{\mathrm{cr}}$ the field E_{gap} is zero and no emission current was recorded from any *Z*-polar face. However, the FEE current was generated from the boundary between domains into the vacuum where the negative pyroelectric charges were accumulated during heating (Fig. 8).

VI. FEE DURING THE PIEZOELECTRIC EFFECT

Another method to generate FEE is the piezoelectric effect. FEE from $LiNbO_3$ crystals induced by the piezoelectric effect was initially observed by Rosenman and Pechorskii.[2,62] It was studied from monodomain samples which were subjected to uniaxial deformation. Electrons were emitted from the (010)-Y^+ face and the $(0\bar{1}0)$-Y^- face when the ferroelectric crystal was deformed along the $[100]$-*X* direction. Figure 9 shows the FEE current versus mechanical stress. The observed FEE effect was unipolar. Electron emission was observed from the (010)-Y^+ face when the sample was stressed and from the $(0\bar{1}0)$-Y^- face under unloading (Fig. 9). The FEE current was generated either from the Y^+ face above a definite threshold of the mechanical pressure (Fig. 9) or from the opposite face when the pressure on a tightly pressed sample decreased after a definite time of pressure application. The current magnitude depended on the loading rate. The observed electron current was $10^{-12}\,\mathrm{A/cm^2}$, which is comparable to the FEE current induced by the pyroelectric field. Obviously, FEE observed from piezoelectric $LiNbO_3$ crystals is a field electron emis-

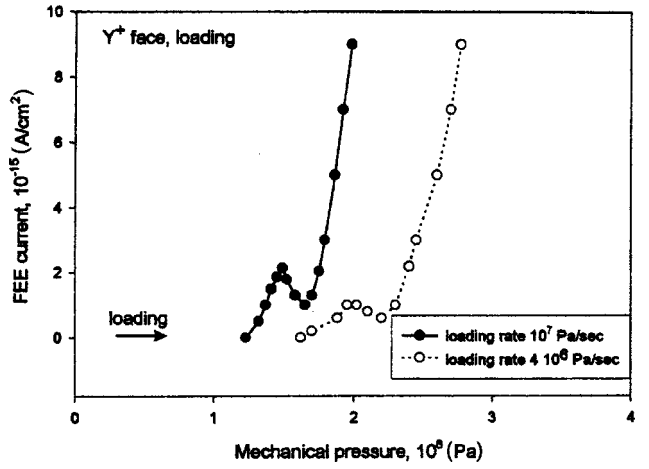

FIG. 9. FEE induced by the piezoelectric effect at different rates of mechanical loading.

sion where the field is generated by the piezoelectric effect. The field generated on the emitting surface is given by[62]

$$E_{\mathrm{gap}}=\frac{d_{21}\alpha\varepsilon}{2\sigma}\left[1-\exp\left(-\frac{\sigma}{\varepsilon\varepsilon_0}\tau\right)\right], \tag{11}$$

where d_{21} is the piezoelectric coefficient, α is the rate of deformation, and σ is the conductivity. Estimations based on real experimental parameters allowed the authors to obtain a value of the field of about 2.3×10^6 V/cm, which is sufficient for field electron emission.

VII. FEE INDUCED BY POLARIZATION SWITCHING

Previously reviewed results indicate that the FEE effect is generated by an uncompensated field of pyroelectric or piezoelectric origin. Different methods used for estimating the intensity of the generated field showed that it does not exceed $(2-3)\times10^6$ V/cm. The measured FEE current varied within the range $10^{-9}-10^{-14}$ A/cm^2. The FEE imaging method allowed the visualization of static domain configurations.

It was proposed that polarization switching should be the most effective method for FEE generation.[3] This field-induced reorientation of the ferroelectric polar axis may be performed in a short time, which is much less than that of the dielectric relaxation time. Fast changes of spontaneous polarization from $+P_s$ to $-P_s$ allows the neglection of bulk screening processes and a prediction of an appearance of much higher uncompensated fields which were generated upon the pyroelectric or piezoelectric effect.

The first observation of FEE during polarization reversal was performed by Rosenman *et al.*[3] FEE was studied in lead germanate $Pb_5Ge_3O_{11}$. A previously described electron detector[60] allowed the detection of the FEE current and a simultaneous observation of the FEE images, illustrating the switching process in real time. A detailed analysis of FEE was performed using a TV system for recording the FEE process during polarization reversal. The time resolution was limited by the TV method of recording, 40 ms. An external switching field was applied to two electrodes from a high voltage generator [Fig. 2(b)]. The first electrode was a rear

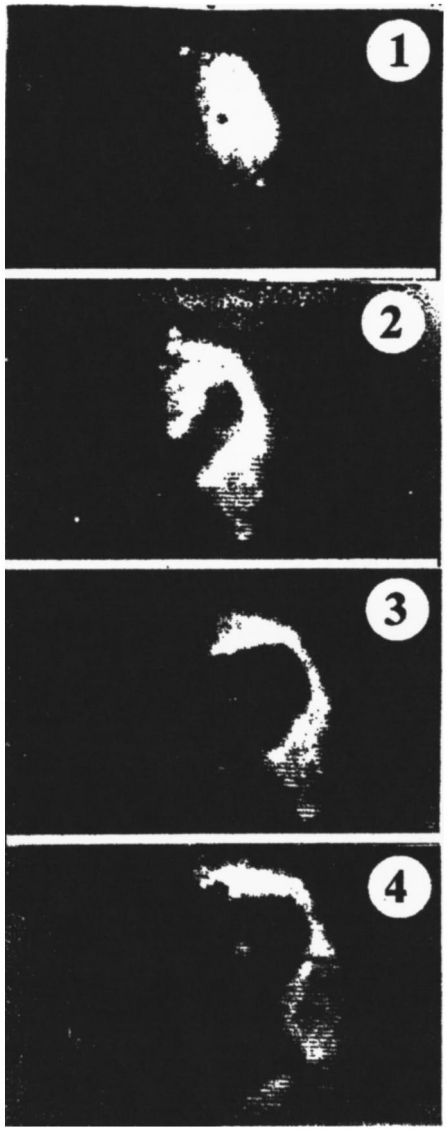

FIG. 10. FEE images (×10) illustrating the polarization switching process in $Pb_5Ge_3O_{11}$. The applied switching field is 3.4×10^3 V/cm. The FEE images were taken every 0.12 s.

electrode deposited on the ferroelectric sample. The second electrode was the input plate of the electron multiplier. Thus the sample was placed directly on the microchannel plate. A small gap remained between the polar ferroelectric surface and the electron detector, which also served as the switching electrode. Our subsequent measurements of capacities gave an estimation of this distance as 10–20 μm.

The studied lead germanate plates were $10\times10\times1$ ($X\times Y\times Z$) mm in size. The switching field was varied in the range of $E_{\mathrm{sw}}=(3-6)\times10^3$ V/cm. Figure 10 shows several fragments of the video movie. Application of the switching pulse ($E_{\mathrm{sw}}=3.4\times10^3$ V/cm) gives rise to a bright emission spot. The intensity decreased fast in the center and the emission ring of an irregular form moved to the crystal periphery. This FEE movie was recorded when the switching voltage pulse of a negative polarity was applied to the rear electrode. The switching voltage causes the appearance of the negative end of the domain at the crystal surface which was placed on

the input plate of the electron detector. Application of a pulse of an opposite polarity did not lead to any electron emission except for the appearance of sporadic flashes.

The FEE images[63] demonstrate the development of the switching process. It is known that polarization switching occurs in three separate stages: an increase of a nucleus with inverse polarization, its growth through ferroelectric crystal bulk toward opposite polar face, and a sideways motion of domain walls.[64] The illustrated FEE images demonstrate two stages. The bright emission spot (Fig. 10) generated upon applying the switching field is the starting point of the switching process and it corresponds to the nucleation stage. The macroscopic nucleus increases its size by means of broadening. This stage of domain wall movement is illustrated by other FEE images (Fig. 10). The moving domain boundary leaves behind the emission trace. It may be assumed that this trace is a region of uncompensated switching charge. This conclusion is consistent with the classic model developed by Miller and Savage,[65] who predicted an appearance of the uncompensated polarization charge $2P_s$ behind a moving 180° domain wall. They also proposed a mechanism of screening of this depolarization field. This may occur by means of field electron emission from the region of uncompensated charges into the surface dielectric (nonferroelectric) layer of a ferroelectric crystal. The observed FEE[3] is direct experimental evidence of the discussed theoretical model.[65] The domain wall velocity was estimated directly from the FEE data ($v = 3.6$ cm/s). This parameter is 10 times less than that for lead germanate crystals.[66]

The developed imaging method allowed the observation of the FEE current contribution to the screening depolarization field generated during polarization reversal. The experiments were performed by use of ferroelectric–ferroelastic gadolinium molibdate crystals $Gd_2(MoO_4)_3$.[67] The samples prepared were plane parallel wafers 1.5 mm thick. Polar surfaces were rectangular with sides parallel to the (110) and $(1\bar{1}0)$ directions and sized 2×8 mm^2. Figure 11 shows TV fragments of a video movie whose frames were taken every 40 ms. Application of a switching voltage of 500 V led to the appearance of an emission spot at the edge of the sample. It grew along the short crystal side in the form of a thin bright line. The line started to traverse the crystal along the other side and electron emission was observed from the whole polar face of the sample (Fig. 11). The FEE images illustrate all stages of polarization switching in the ferroelectric–ferroelastic crystal $Gd_2(MoO_4)_3$: nucleation of a tapered domain at the crystal edge, penetration of the tapered domain through the crystal and formation of a strip domain, and finally, the sideways motion of the 180° domain wall.

Ferroelectric–ferroelastic crystals $Gd_2(MoO_4)_3$ have a very low conductivity ($\sigma = 10^{-14}$ S/cm) and its dielectric relaxation time is $\tau = 88.5$ s.[67] Hence, in the case of an uncoated polar face bulk screening of the depolarization field is strongly limited. The last FEE image (Fig. 11) showed an intensive extinction of the FEE picture brightness in a short time, $\tau_{em} \approx 10^{-2}$ s. This time is four orders of magnitude less than the estimated dielectric relaxation time of this crystal. This is evidence that the FEE current contributes significantly to the screening process in low conductive ferroelectric crystals.

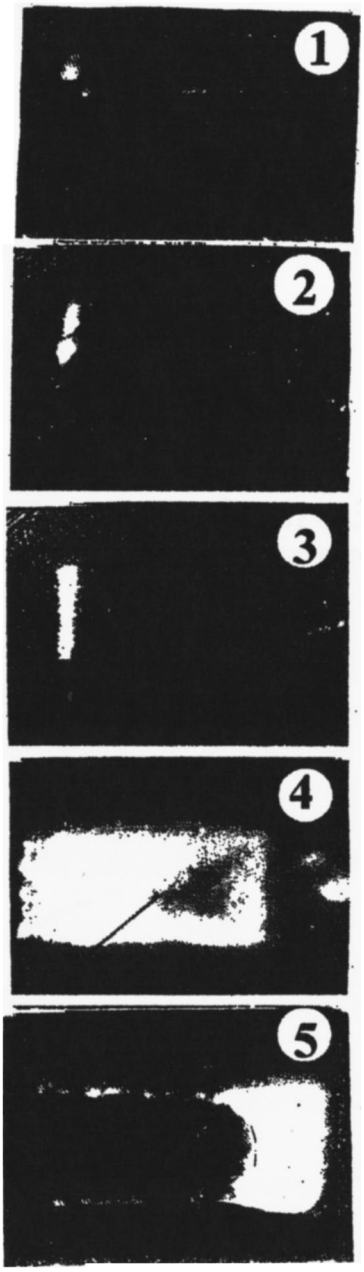

FIG. 11. FEE images (×10) illustrating the polarization switching process in $Gd_2(MoO_4)_3$. The switching field is 3.3×10^3 V/cm. The FEE images were taken every 0.04 s.

FEE during polarization switching was also thoroughly studied by Biedrzycki and LeBihan[68] and Rosenman *et al.*[63,69] in TGS crystals, by Biedrzycki and LeBihan[70] in $BaTiO_3$ and PLZT ceramics, and by Sujak and Biedrzycki[71] in KDP crystals. FEE was excited in TGS crystals by the application of a 50 Hz sinusoidal switching field. The observed results (see Refs. 63 and 70) showed that the FEE current is generated when the applied field reaches a value sufficient for polarization reversal, which was controlled by simultaneous measurements of hysteresis loops. FEE was observed only in a ferroelectric phase at $T \leqslant T_C$ and the effect appeared from a negatively charged ferroelectric polar

face when the negative end of the polar axis extended to the surface.

Direct measurements of FEE current density from a TGS crystal in a 50 Hz switching field[63] resulted in $j_{em} = 10^{-7}$ A/cm^2. Similar results were observed in a 50 Hz switching field for other ferroelectrics, including PLZT ceramics.[68,71]

It should be noted that in the reviewed papers the FEE parameters were measured in a ''plane'' geometry when the upper electrode (the input plate of the used electron detector) was mounted parallel to studied ferroelectric faces [Fig. 2(b)]. The resulting FEE current was weak and did not exceed 10^{-7} A/cm^2. This experimental setup differed from the setup developed by Gundel *et al.*[6,7] where a patterned (strip, grid) electrode was deposited directly on the studied polar face. As a result, the distribution of the applied electric field is drastically altered from a ''plane'' geometry. We firmly believe that the experimental setup with patterned electrode led to absolutely new results when an extremely strong FEE current reaching 100 A/cm^2 was obtained.[6,7]

VIII. NATURE OF ''WEAK'' FEE

A. Basic features of FEE

The presented review of the experimental results in the previous sections shows that the FEE effect is observed from different ferroelectric crystals and ceramics. A list of studied ferroelectrics includes almost all well-known ferroelectrics ($LiNbO_3$, $LiTaO_3$, TGS, $Ba_2NaNb_5O_{15}$, $Ba_xSr_{1-x}Nb_2O_6$, $Pb_5Ge_3O_{11}$, $Gd_2(MoO_4)_3$, $BaTiO_3$, and PLZT). They were studied under various conditions. FEE was observed for pyroelectric, piezoelectric effects, and during polarization switching. Despite different compositions of the investigated ferroelectrics and diverse methods of electron emission excitation, the common features of the FEE should be noted:

(a) FEE is observed in the ferroelectric phase only,
(b) FEE is generated due to a deviation of spontaneous polarization from its equilibrium state,
(c) FEE is an electron current into a vacuum screening depolarization field,
(d) FEE current density is 10^{-9}–10^{-12} A/cm^2 for pyroelectric, piezoelectric effects and it reaches 10^{-7} A/cm^2 if induced by polarization switching,
(e) FEE electron energy may reach the value 10^5 eV

B. Electric field distribution of a charged ferroelectric crystal

Analysis of the studied basic features of the FEE effect results in an important conclusion about the field origin of electron emission from ferroelectrics. The source of this electrostatic field is charges of spontaneous polarization ΔP_s generated on ferroelectric polar surfaces.

A conventional experimental setup, which was developed for all FEE measurements showing weak FEE currents, is considered in Fig. 12. A ''plane'' geometry was used when the plate of the electron detector is parallel to the flat ferroelectric surface. The studied front crystal surface is noncovered by an electrode. The ferroelectric sample of thickness d_{cr} is mounted on a sample holder. The rear face of the sample with an electrode attached and the input plate of the electron detector are grounded. The detector is mounted at a distance d_{gap} from the front polar ferroelectric face.

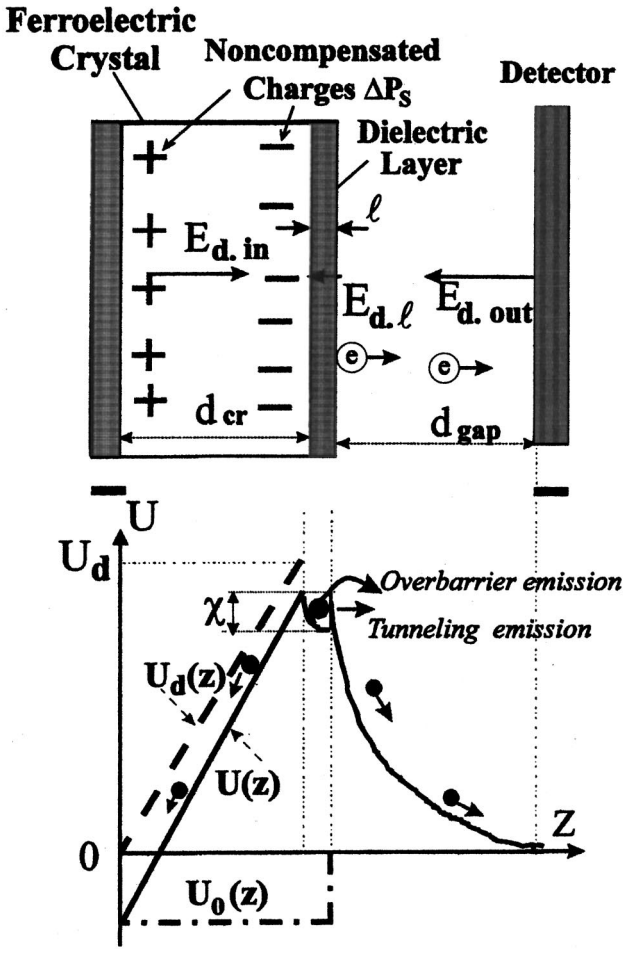

FIG. 12. Electron energy diagram in the depolarization field. The field may be generated during pyroelectric, piezoelectric, and upon polarization switching. $U_0(z)$ is the potential energy of an electron in the equilibrium state, χ is the electronic work function, $U_d(Z)$ is the distribution of the potential of the depolarization field created by uncompensated polarization charges, and $U(Z)$ is the potential energy of an electron in the depolarization field.

Any changes of the ferroelectric crystal temperature, mechanical pressure, or polarization reversal causes a deviation of the spontaneous polarization ΔP_s. Charges (positive and negative) are generated near the polar surfaces. They are localized at the boundary between the ferroelectric crystal and the dielectric layer (Fig. 12). The existence of the surface layer of nonferroelectric origin is a well-known experimental and theoretical fact. It may also be considered as a layer of localization of screening charges.[22] This charge is a source of three electrostatic fields (Fig. 12): the field inside the ferroelectric crystal bulk $E_{d\,\mathrm{in}}$, in the dielectric layer E_{dl}, and outside the ferroelectric crystal bulk $E_{d\,\mathrm{out}}$. Numerous experimental data and direct measurements have shown that FEE is observed from a negatively charged surface. To estimate the probability of electron emission from a ferroelectric crystal, the fields $E_{d\,\mathrm{in}}$, E_{dl}, and $E_{d\,\mathrm{out}}$ should be estimated. The calculations were done by assuming a uniform distribu-

TABLE II. Calculated electrostatic fields and measured FEE currents for ferroelectric crystals and thin films for pyroelectric and polarization switching effects. [The estimation of the fields are performed for ferroelectric TGS crystal and PLZT ceramics in accordance with the plane geometry of the experimental setup of Fig. 12 and Eqs. (12)–(14); $d_{gap}=10\ \mu$m.]

	Pyroelectric effect				Polarization switching			
	Crystal (ceramics), $d_{cr}=1$ mm		Thin film, $d_{cr}=1\ \mu$m		Crystal (ceramics), $d_{cr}=1$ mm		Thin film, $d_{cr}=1\ \mu$m	
	TGS	PLZT	TGS	PLZT	TGS	PLZT	TGS	PLZT
Electric field E_{din}, V/cm	0.9×10^4	4.7×10^2	3.7×10^4	4.9×10^2	5.2×10^5	3.2×10^6	2.2×10^6	3.3×10^5
Electric field E_{dl}, V/cm	1.8×10^5	9.4×10^3	7.5×10^2	50	1×10^7	6.4×10^6	4.5×10^4	6.7×10^3
Electric field E_{dout}, V/cm	0.9×10^6	4.7×10^4	3.7×10^3	250	5.2×10^7	3.2×10^7	2.2×10^5	3.3×10^4
Measured FEE current, A/cm^2	10^{-9}–10^{-12}	10^{-14}	⋯	⋯	10^{-7}–10^{-9}	⋯	⋯	⋯

tion of the fields for a flat surface. The expressions for the fields are given as follows:

$$E_{d\,\mathrm{in}}=\frac{\Delta P_s}{\varepsilon_0}\times\frac{1}{\varepsilon_{\mathrm{cr}}+\dfrac{d_{\mathrm{cr}}}{d_{\mathrm{gap}}}}, \tag{12}$$

$$E_{dl}=\frac{\Delta P_s}{\varepsilon_0}\times\frac{1}{\varepsilon_l\left(1+\dfrac{d_{\mathrm{gap}}}{d_{\mathrm{cr}}}\varepsilon_{\mathrm{cr}}\right)}, \tag{13}$$

$$E_{d\,\mathrm{out}}=\frac{\Delta P_s}{\varepsilon_0}\times\frac{1}{1+\dfrac{d_{\mathrm{gap}}}{d_{\mathrm{cr}}}\varepsilon_{\mathrm{cr}}}. \tag{14}$$

Figure 12 and Eqs. (12)–(14) allow one to explain and predict some important experimental results.

C. The problem of FEE from ferroelectric thin films: ''Size'' effect

Figure 12 and Eqs. (12)–(14) show that the field intensities strongly depend on the size relation d_{cr}/d_{gap}, the value of uncompensated charges ΔP_s, and the dielectric permittivity ε_{cr} of the ferroelectric sample. We will consider the ''size'' effect for the plane geometry where a ferroelectric sample (crystal or thin film) with a flat surface is mounted above the flat surface of the electron detector. It may be called a ''plane-to-plane'' setup. This experimental setup was used in all works on ''weak'' FEE.[1,35–37,42,49–58]

Two sorts of materials, ferroelectric crystals TGS and ferroelectric ceramics PLZT 7/65/35, will be considered. They differ strongly in the value of spontaneous polarization ($P_{s,\mathrm{PLZT}}/P_{s,\mathrm{TGS}}\approx10$) and in the dielectric permittivity ($\varepsilon_{\mathrm{cr,PLZT}}/\varepsilon_{\mathrm{cr,TGS}}\approx50$). In the case of the pyroelectrically induced FEE, measurements of ΔP_s showed $\Delta P_s\sim10^{-7}$ C/cm^2. This value will be taken for further estimates. For polarization switching ΔP_s may be as high as $\Delta P_s\sim2P_s$ [$\Delta P_s(\mathrm{TGS})=6\times10^{-6}\ \mu$C/cm^2 and $\Delta P_s(\mathrm{PLZT\ 7/65/35})=68\times10^{-6}\ \mu$C/cm^2]. It is of great interest to estimate and compare the induced fields for ferroelectric crystals and thin films for these two sorts of materials.

Conventionally used ferroelectric crystals for FEE studies have a thickness $d_{cr}=1$ mm and the measured minimum value of the gap is $d_{gap}=10\ \mu$m (Fig. 12). For estimation of the fields in ferroelectric thin films the thickness of the film is chosen to be 1 μm.

Table II shows the field intensity redistribution versus the sample thickness. The thinner the ferroelectric sample, the lower the field $E_{d\,\mathrm{out}}$ responsible for FEE, and the higher the field $E_{d\,\mathrm{in}}$ is in the bulk. The pyroelectrically induced field $E_{d\,\mathrm{out}}$ for a TGS crystal with a thickness $d_{cr}=1$ mm is about $E_{d\,\mathrm{out}}=10^6$ V/cm. Experimental studies demonstrated explicitly that the field is sufficient for a FEE current $j=10^{-9}$–10^{-12} A/cm^2.[1,35–37,42,49–58] For a thin ferroelectric TGS film $d_{cr}=1\ \mu$m, the same pyroelectric uncompensated charge ΔP_s gives a field $E_{d\,\mathrm{out}}$ three orders of magnitude less ($E_{d\,\mathrm{out}}=3.7\times10^3$ V/cm). It is obvious that such a low field cannot cause electron emission. We did not find any published experimental data for pyroelectrically induced FEE from TGS thin films. The ''size'' effect of pyroelectrically induced FEE was studied in ferroelectric crystals $LiNbO_3$, and $LiTaO_3$ crystals of different thickness varying from 1 cm to 100 μm. It was shown that the FEE current from $LiNbO_3$ decreased appreciably for samples 100 μm thick.[72] The estimation the minimal thickness along the polar axis d_{cr} ($\varepsilon\sim50$, $J\sim10^{-9}$ A/cm^2) of a ferroelectric crystal when FEE might be observed results in a value of $d_{cr,min}\sim50\ \mu$m. In the paper by Rosenman,[73] a 50-μm-thick ferroelectric disk of $LiTaO_3$ showed a very weak FEE current induced by CO_2-laser heating. In this experiment the imaging IR radiation with $\lambda=10.6\ \mu$m was enabled only when a bias dc electric field was applied to the sample.

Polarization switching of the TGS crystal permits the generation of uncompensated charges of more than 1.5 orders of magnitude. The field $E_{d\mathrm{out}}$ reaches 5.2×10^7 V/cm and a much higher FEE current of 10^{-7} A/cm^2 was measured.[63] The estimates (Table II) made for TGS thin films 1 μm thick show a low value of the field $E_{d\,\mathrm{out}}$ under

polarization switching ($E_{d\,\mathrm{out}}=2.2\times10^5$ V/cm). This field is not sufficient to produce field-induced FEE current.

Let us consider the fields and FEE currents for the PLZT 7/65/35 composition in the case of the pyroelectric effect and polarization switching. The field $E_{d\,\mathrm{out}}$ may be estimated for the same uncompensated pyroelectric charge $\Delta P_s=10^{-7}$ C/cm^2. The estimation gives the field $E_{d\,\mathrm{out}}$ for a PLZT ceramic sample 1 mm thick 10 times less than that for TGS because of the very high dielectric permittivity of the ceramic $\varepsilon=2.3\times10^3$. The estimated field $E_{d\,\mathrm{out}}=4.7\times10^4$ V/cm (Table II) is too small for field emission. It is consistent with FEE measurements[58] during the pyroelectric effect when no emission was observed from PLZT compositions except in the region of the phase transition (Fig. 6). During polarization switching, ΔP_s of PLZT is very large ($\Delta P_s=68\times10^{-6}$ μC/cm^2). According to the estimates the field $E_{d\,\mathrm{out}}$ for the 1-mm-thick sample may be as high as $E_{d\,\mathrm{out}}=3.2\times10^7$ V/cm. A comparison between a TGS crystal (Table II) and PLZT ceramics shows that there is no noticeable difference in the field $E_{d\,\mathrm{out}}$ induced by polarization switching of the PLZT and TGS samples with a thickness $d_{\mathrm{cr}}=1$ mm. Despite much higher spontaneous polarization of the PLZT ceramics, its extremely large dielectric permittivity suppresses the field $E_{d\,\mathrm{out}}$ [Eq. (14)] needed for FEE generation. FEE from PLZT was excited by polarization switching in a 50 Hz sinusoidal field.[68] The experimental setup used was a conventional plane geometry with an electron detector mounted in the vicinity of the uncoated ferroelectric surface. The observed electron emission current from PLZT ceramics was very weak.

In the case of ferroelectric PLZT thin films, reducing the ferroelectric sample thickness to 1 μm leads to a strong decrease of the field $E_{d\,\mathrm{out}}$ responsible for FEE. It is two to three orders of magnitudes less than that which may be achieved for crystals 1 mm thick under identical experimental conditions (Table II). Obviously, the estimated field values of 10^3-10^5 V/cm are not enough to generate field electron emission, especially of strong electron emission currents reaching 100 A/cm^2. It can be concluded that generation of the FEE current from ferroelectric thin films is highly problematic because of the pronounced ''size'' effect. The only explicit physical reason is as follows: The FEE effect is generated by the electrostatic field outside the charged ferroelectric capacitor. The thinner the ferroelectric sample along the polar axis, the smaller the field that ejects electrons into a vacuum from a negatively charged surface. The additional effect for PLZT ferroelectric thin films that leads to a decrease of the field $E_{d\,\mathrm{out}}$ is caused by its high dielectric permittivity.

To the best of our knowledge the experimental studies of FEE from ferroelectric thin films are very limited. We have found only four papers where the FEE effect was studied from ferroelectric thin films [Asano *et al.*,[74] Auciello *et al.*,[75] Averty *et al.*,[13] and Sviridov *et al.*[76]]. In the experimental setup used in the papers referred to previously, a patterned electrode was deposited on the ferroelectric polar surface for polarization switching, as was also done for strong ferroelectric cathodes.[6,7] It will be shown in the second part of the review devoted to ferroelectric cathodes that this setup drastically changes the distribution of the applied electric field, and leads, as a result, to other physical processes, such as surface flashover plasma generation.

D. Electron energy distribution

A high electron energy $W_e=5$ keV was observed by Rosenblum *et al.*[1] during FEE from $LiNbO_3$. These data were later confirmed for TGS by Sujak and Syslo,[49] who observed electron energies up to $W_e=130$ keV, and by Rosenman *et al.*[77] for $LiTaO_3$ (up to $W_e=100$ keV). Figure 12 shows that the electrons emitted from a ferroelectric crystal are accelerated by the field $E_{d\,\mathrm{out}}$ and the electron energy is determined by a ferroelectric surface potential φ_{cr}, Two charged capacitors, the ferroelectric crystal C_{cr}, and the capacitor C_{gap}, formed by two plates, the input plate of the electron detector and the upper surface of the sample, are connected in parallel (Fig. 12). The potential of the system φ_{cr} of the two capacitors may be written as

$$\varphi_{\mathrm{cr}}=\frac{\Delta P_s}{C_{\mathrm{cr}}+C_{\mathrm{gap}}}. \tag{15}$$

Obviously, the changes of the crystal thickness d_{cr} or the vacuum gap d_{gap} between the input plate of the electron detector and the upper surface of the ferroelectric sample cause variation of the C_{cr} and C_{gap}, Equation (15) shows that it should lead to potential variation φ_{cr} and, therefore, it should change the measured electron energy W_e.

Detail analysis and calculations of the surface potential φ_{cr} were implemented in the work by Rosenman[78] where the problem was solved using the principle of superposition of electrostatic fields. The calculated data were in a good agreement with the experimental results obtained for $LiTaO_3$, where FEE was excited by the pyroelectric effect. The electron energy was changed smoothly from $W_e=120$ keV down to 600 eV by varying the gap d_{gap} from 3 cm to 10 μm. The same effect of the electron energy alteration was observed when the ferroelectric sample thickness was varied, whilst the vacuum gap was kept constant.[78]

E. Transient character of FEE

The fields distribution (Fig. 12) shows that generation of the uncompensated charges ΔP_s and electrostatic fields $E_{d\,\mathrm{in}}$, E_{dl}, and $E_{d\,\mathrm{out}}$ leads to three induced by the field $E_{d\,\mathrm{in}}$, $J_b=\sigma_{\mathrm{cr}}E_{d\,\mathrm{in}}$. The second current J_l is a conductive current in the dielectric layer of the surface $J_l=\sigma_1 E_{dl}$. The third current is the FEE current J_{em}. Figure 12 distinctly shows that the field $E_{d\,\mathrm{in}}$, on the one hand, and fields E_{dl} and $E_{d\,\mathrm{out}}$, on the other hand, are of opposite directions. As a result the generated pyroelectric effect or polarization switching charge ΔP_s causes two screening currents: J_{in} in the crystal bulk and J_{em} into the vacuum. Both currents cause a decreasing generated uncompensated charge ΔP_s and lead to sample neutrality. Finally we may write that $\Delta P_s=Q_b+Q_{\mathrm{em}}$ or

$$\Delta P_S=\int_0^t J_{\mathrm{in}}\,dt+\int_0^t J_{\mathrm{em}}\,dt. \tag{16}$$

The most convenient way to observe a contribution of the FEE current in screening process and to prove its transient property is to use a low conductive ferroelectric and to generate high density ΔP_s for a short time to limit the screening process into the ferroelectric crystal bulk.[79] The FEE depletion effect was obtained during polarization switching of $Gd_2(MoO_4)_3$. Weakening the FEE image indicates that screening of ΔP_s occurred during 10^{-2} s, which is four orders of magnitude lower than the dielectric relaxation time in this crystal.[37] It proves that the FEE emitted charge contributes significantly to polarization screening.

F. Tunneling mechanism of FEE

Numerous studies of the ''weak'' FEE effect allowed a proposal for the only mechanism for this phenomenon. The effect was interpreted as field electron emission by all groups participating in the studies. Figure 12 shows an electron energy diagram. At the equilibrium state, when spontaneous polarization is compensated by the screening charges ($\Delta P_s = 0$), an electron is in a potential well $U_0(Z)$ (Fig. 12). The uncompensated charges ΔP_s, generated at the polar faces by the pyroelectric or piezoelectric effect, leads to strong changes of the potential energy of the electrons. A curve $U_d(Z)$ (Fig. 12) depicts a schematic distribution of the potential of the induced depolarization field. As a result, the electron energy $U(Z)$ may be written as follows:

$$U(Z) = U_0 + U_d(Z). \tag{17}$$

The schematic presentation of $U(Z)$ results in definite conclusions concerning the electron emission from ferroelectrics.[72]

Two optional mechanisms of FEE from a charged ferroelectric surface may be considered (marked by the arrows in Fig. 12). The first one is an overbarrier effect when the electron energy inside a crystal lattice exceeds the work function $W_{\text{el in}} > A$. The presented picture of the electrostatic fields distribution shows that the field E_{dl} moves the electrons to the boundary between the crystal and the vacuum. The initial energy of the electrons may be increased in this field because of the acceleration in the lattice. One should take into account the fact that acceleration of electrons may occur along the mean free path. Ferroelectric crystals possess very high electron–phonon coupling,[22] which was confirmed by estimating that the coefficient of the electron–phonon interaction in the ferroelectrics, $LiTaO_3$ and $LiNbO_3$,[77] is as high as $\alpha = 11$. It enables the choice of the value of the mean free path to be equal to the lattice constant $\approx 10^{-8}$ cm. The electron energy $W_{\text{el in}} = E_{dl} \times l$ (the magnitude of the field is given in Table II); for its maximum value (polarization switching) $E_{dl} = 6.7 \times 10^5$ V/cm. Therefore, one can get $W_{\text{el in}} = 6.7 \times 10^{-3}$ eV. The data from the measurements of the electronic work function for $LiNbO_3$ showed[30] that its electron affinity is $\chi = 0.25$ eV, which is three orders of magnitudes higher than $W_{\text{el in}}$. Therefore overbarrier electron emission is unlikely to occur.

The second option, which may be considered for FEE, is a tunneling effect. The model presented in the work included two steps for FEE. The first step is an electron current flowing in the dielectric layer toward the surface

$$J_{\text{FEE}\,l} = \sigma E_{dl}. \tag{18}$$

The second step is tunneling emission into the vacuum

$$J_{\text{FEE}} = J_{\text{FEE}\,l} D(E_{d\,\text{out}}), \tag{19}$$

where $D(E_{d\,\text{out}})$ is the penetrability of the electrons through the potential barrier. The estimations were performed[72] using the known expression:

$$D(E_{d\,\text{out}}) = \exp\left\{ -\frac{6.83 \times 10^7}{E_{d\,\text{out}}} (\psi - W_{x_0})^{1.5} \vartheta \times \left[\frac{3.79 \times 10^{-4} E_{d\,\text{out}}^{0.5}}{\psi - W_{x_0}} - \left(\frac{\varepsilon_l - 1}{\varepsilon_l + 1} \right)^{0.5} \right] \right\}. \tag{20}$$

The following groups of electrons were considered in verifying the model: free electrons which are in the region of surface band bending, electrons which are in a polaron band, and electrons which are localized on surface states. The concentration of free electrons is negligibly small for the considered ferroelectrics which possess a wide energy gap, which for $LiNbO_3$ is as large as $E_g = 3.9$ eV. The second group of electrons, which may contribute to FEE are electrons localized on surface states. Negatively charged acceptors (occupied by electrons) screen the positive end of the spontaneous polarization. The donors occupied by electrons are neutral. The negative end of P_s is screened by positive charges of ionized donors. Therefore, the concentration of electrons available for electron emission into vacuum is very different for the Z^+ and Z^- faces. However, experimental measurements of FEE from these faces demonstrated equal FEE currents. A good agreement with experimental results for pyroelectrically induced FEE current was achieved when the penetrability of the barrier was estimated for electrons occupying the polaron band.[72] It should be noted that the developed theoretical model of FEE from surface states[5] successfully described the experimental results observed from TGS crystals in the region of the phase transition.

All the above-mentioned models of weak FEE were based on a concept of the field emission induced by the pyroelectric effect or polarization switching. The field causing FEE was a macroscopic electrostatic field. A strong influence of local microscopic fields near polar faces was recently observed by Kugel and Rosenman.[80] Bidomain (head-to-head) configuration of Ti-induffused $LiNbO_3$ was studied. A thin crystal layer possessing inverted spontaneous polarization totally suppressed the FEE current induced by the pyroelectric field. A fabricated layer 13 μm thick could not affect the macroscopic pyroelectric field of the 1-mm-thick sample. A model of electrons localized in quantum wells at the surface[50] showed a definite discrepancy with the experimental results. A correction was made by assuming that electrons are localized in the exterior surface polaron states, where the additional barrier is influenced by a local positive pyroelectric potential created by inverted spontaneous polarization.[80]

IX. CLASSIC AND FERROELECTRIC ELECTRON EMISSION

The review of the published experimental results allows a comparison of classic types of electron emission from solids with FEE. All known electron emissions are based on either exciting electrons in solids by increasing their kinetic energy, or changing the penetrability of the potential barrier near the surface. Electron emission from ferroelectrics (FEE) is quite different as it does not need an external field or light irradiation. Electron emission occurs from ferroelectric crystal surfaces normal to the axis of spontaneous polarization by using ''plane-to-plane'' setup in contrast to classic field emitters utilizing ''point-to-plane'' geometry. FEE takes place in the ferroelectric phase only. It is excited by unconventional methods such as polarization inversion or mechanical stress (piezoelectric effect). The energy of emitted electrons may reach a huge value of 100 keV without any external accelerating voltage.

FEE arises due to the ability of ferroelectrics to generate electrostatic charges on their polar faces. The density of these charges is high enough to cause field emission from a ferroelectric by means of electron tunneling. FEE represents the electron current into vacuum screening uncompensated polarization charges. It should be emphasized that this type of emission occurs because of the deviation of spontaneous polarization from its equilibrium state. Thus, in comparison with well-known classic types of electron emission, FEE occurs due to changes in a crystal lattice of a ferroelectric. This fact, and unusual methods of electron emission generation, make FEE a new type of electron emission from solids.

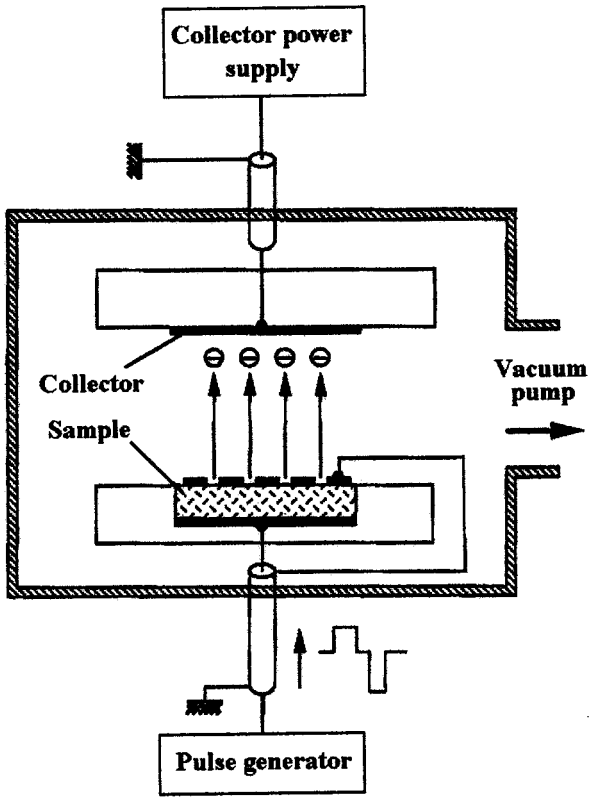

FIG. 13. A typical experimental setup for electron emission generation (see Refs. 8 and 74, and other papers).

PART B: STRONG ELECTRON EMISSION FROM FERROELECTRICS

I. ANALYSIS OF DATA ON STRONG ELECTRON EMISSION FROM FERROELECTRICS

The data reviewed in the previous part, devoted to the FEE effect, showed that electrons are emitted from a charged ferroelectric surface due to pyroelectric, piezoelectric, or polarization switching effects. The observed electron current is a field emission current screening generated charges of ferroelectric origin. The FEE current measured by using electron multipliers is really weak, and is as small as $10^{-7}-10^{-10}$ A/cm^2.

Numerous publications starting from 1989, reported electron emission from ferroelectric ceramics with a very high current density of 10^2-10^5 A/cm^2. A huge divergence in the electron currents from the same ferroelectric materials, reaching 9–12 orders of magnitude, is a good reason for assuming a basic difference between these two sorts of electron emission.

We would like to call the reader's attention to the fact that the experimental setup (electrode configuration) used in studies of strong FEE was quite different from that used for the weak emission. Weak FEE exploited plane-to-plane geometry (Part A). In experiments with polarization inversion, an electron detector serving as a switching electrode was mounted parallel to the polar surface of a ferroelectric crystal. This electrode induced only a normal component of the applied electric field needed for polarization reversal.

Strong emission was excited by all researchers using a patterned electrode (strip, grid, or ring) deposited on the polar ferroelectric surface. This type of electrode induces not only the normal component, but also a tangential component of the applied electric field, which may cause a dramatic effect of accelerating the emitting electrons along the ferroelectric surface, followed by surface flashover-plasma generation. A second important peculiarity of the patterned electrode is that the polarization switching effect occurs below the electrode, whilst the electron emission arises from an uncovered part of the surface where polarization inversion is problematic.

Strong FEE is generated in different phase states of ferroelectric ceramics (ferroelectric, antiferroelectric, relaxor, and paraelectric) subjected to an external electric field. As a result, diverse field-produced effects of different origin may induce the electron emission. One can assume that electron emission parameters (current density, delay time, pulse duration, etc.) should be different and this may be revealed by a thorough analysis of numerous experimental results.

In Part B, Sec. I detailed data on experimental technique, calculations of the electric field distribution in ferroelectrics with patterned electrode, results and models for strong FEE are presented. Specific stress is given to the material science aspect, the physics of polarization switching, and field-enforced phase transitions.

A. Experimental technique

1. Electrode configuration and electrode materials

For studying strong electron emission from ferroelectrics almost all researchers used an experimental setup similar to that shown schematically in Fig. 13 (the schematic drawing is based on Gundel *et al.*,[8] Asano *et al.*,[74] and other papers). The above-mentioned experiments were conducted under various vacuum conditions: from a vacuum of 10^{-7} Torr[11] to the pressure as high as 0.1 Torr.[74] Two quite different kinds of electrodes were applied to the ferroelectric samples. A solid electrode is deposited on the back of disk-shaped (typically about 1-mm-thick and 1-cm-diam) ceramic samples. A patterned electrode of different shapes (grid, strip, or ring) was used as a top electrode applied to the emitting surface. A patterned electrode consisting of interconnected metal strips 200 μm wide, that were separated by bare strips of equal width, was employed by Gundel *et al.*,[81] Ivers *et al.*,[9] and Asano *et al.*[74] This electrode configuration became a ''standard'' for further studies. Some authors used a metal grid mechanically pressed to the front (emitting) surface of the sample (see Cavazos *et al.*,[12] Sampayan *et al.*,[11] Airapetov *et al.*,[15] Shur *et al.*,[82,83] Rosenman *et al.*[84]). Sampayan *et al.*[11] studied ceramic samples with a grid electrode in the form of a square mesh composed of 0.025-mm-diam tungsten wires spaced 0.75 mm on the centers. The standard grid electrode configuration was also used by Airapetov *et al.*,[15] Zhang and Huebner,[85] and Shannon *et al.*[86] A copper fine grid (4 μm wire diameter, 16 μm period) was employed in studies by Shur *et al.*[82] and Rosenman *et al.*[84] Averty *et al.*[13] used a patterned electrode with typical dimensions of several hundreds of μm. In some experiments a set of interconnected strips or a ring electrode was glued to the sample surface by conductive silver paint.[16,87,88] In a study by Shur *et al.*,[16] a ring metal electrode (the external diameter, internal diameter, and thickness of the ring were 6, 3.4, and 0.2 mm, respectively) was mounted on the emitting (front) surface of PLZT 12/65/35 ceramic samples by silver paint. Boscolo *et al.*[89] proposed a front electrode consisting of a pattern of unconnected patches contained within a ring as one way of improving emission stability.

Different metals including Cu, W, Au, Ag, Pt, Al were deposited in order to form the above-mentioned patterned grid electrode. Various deposition techniques, such as evaporation (Gundel *et al.*,[81] Asano *et al.*,[74] Shannon *et al.*[86]), ion beam sputtering (Auciello *et al.*[75]), photochemical etching (Jiang *et al.*[10]), and screen printing (Zhang and Huebner[85]) were employed. The electrodes issue was considered in detail by Riege *et al.*,[18] who used 1- to 2-μm-thick Au electrodes evaporated on top of a previously evaporated Cr layer (100 Å thick) as a successful technique for producing electrodes.

2. Triggering modes

Conventionally, the trigger voltage for inducing electron emission was supplied to a ferroelectric sample by a high voltage pulse generator. Fast rising (rise time within the range 10^{-8}–10^{-7} s) trigger voltage pulses (the typical amplitude is 1–8 kV for 1-mm-thick samples, that implies the electric field of several tens of kV/cm) were applied across the sample. Trigger voltage pulse duration usually varied within the range (0.1–1) μs. The anode (or collector) was maintained at a positive potential (pulsed or constant) with respect to the cathode by a separate anode circuit in order to accelerate the emitted electrons. The accelerating anode (collector) voltage varied within a wide range of amplitude values up to 250 kV. Some researchers measured considerable electron emission with no accelerating voltage applied (Gundel *et al.*,[81] Benedek *et al.*,[90] Shannon *et al.*,[86] Asano *et al.*,[74] Shur *et al.*,[91] Rosenman *et al.*[84]).

The trigger voltage (either positive or negative) was applied to the rear electrode with the front (emitting) electrode grounded in a majority of the previous studies.[9–11,81,92] In a few studies,[12,90] the trigger voltage was also applied to a grid (front, emitting) electrode of the sample. A comparative experimental study of different modes of the trigger voltage application was conducted by Shur *et al.*[91] with ceramics PLZT 12/65/35. It was found that the best values of parameters for ferroelectric cathodes, such as the energy spectrum of the electron beam, total electron current, and perveance, are achieved when a negative triggering pulsed voltage is applied to the front patterned electrode. Also, in experiments by Krasik *et al.*[87] and by Dunaevsky *et al.*[88] different modes of applying the trigger voltage (of either positive or negative polarity) were studied for differently poled ceramic samples.

Gundel *et al.*[93,94,81] used monopolar negative trigger HV pulses applied to the rear (solid) electrode of the prepoled ceramic samples (PLZT 2/95/5 and PLZT X/65/35 with $X = 7,8,9,10$). The grid electrode was grounded. A pulsed power technique was used to generate fast rising high voltage pulses inducing the electron emission. For instance, Gundel *et al.*[81] used an electrical circuit consisting of four 2 nF capacitors linked to the ceramic sample via separate fast transistor switches. This circuit allowed the authors to control the rise time of the pulses. A high repetition rate operation was achieved by applying high voltage pulse bursts of up to 50 pulses to the samples. A Faraday cup with a graphite collector was used to measure emission current.

In experimental studies by Ivers *et al.*[9] and Flechtner *et al.*,[95] positive HV pulses with the electric field in the range of (10–20) kV/cm were applied to the rear surface of the ferroelectric PZT ceramic sample. The high voltage pulses were applied to the sample by a krytron switch through a 10 Ω impedance transmission line. A planar graphite anode located several millimeters from the emission surface was used. The anode (collector) was maintained at a positive potential with respect to the cathode by a transmission line charged up to 500 V.

Benedek *et al.*[90,96] used the Pierce design for the cathode-anode electrodes with un-prepoled PLZT 4/95/5, PLZT 8/65/35, and PZTN. The measurements were performed with a positive trigger pulse (HV trigger pulse) applied to the rear electrode (nonemitting, solid one), or a negative trigger pulse applied to the front electrode (emitting, patterned one). In the former case an accelerating voltage at the anode was used, while in the latter case the trigger voltage accelerated the electrons.

Pleyber *et al.*[92] used a 50 Hz ac electric field to induce the emission from PLZT 9.4/65/35. A high current density emission current was measured with a Faraday cup, while weak electron emission was measured with an electron channel multiplier and a pulse counting system. Almost the same experimental setup was used by Okuyama *et al.*[14] with prepoled PZT ceramic samples. To induce polarization reversal, double (bipolar) pulses were used that consisted of a negative pulse of 10 μs duration following a positive pulse of 10 μs applied to the rear electrode.

Jiang *et al.*[10] used an electron gun geometry originally designed for a thermionic cathode. They kept the same electrode geometry, but replaced the thermionic cathode with a ferroelectric one in order to compare basic parameters of the cathodes.

Bipolar trigger voltage pulses[74] or monopolar voltage pulses causing an electric field direction opposite to that of the spontaneous polarization vector[17] were used to induce the polarization reversal. It is interesting to note that Asano *et al.*[74] studied thin PZT ceramic (30–45 μm thick) samples without prepoling, while Miyake *et al.*[17] investigated the samples of 190 μm thick with and without prepoling.

Sampayan *et al.*[11] used the trigger voltage pulses coupled to the rear electrode of the ferroelectric cathodes. High accelerating anode–cathode voltages up to 60 kV were applied. Cavazos *et al.*[12] used a bias voltage (according to the authors this voltage induces a preset dipole moment) applied to the grid electrode, together with the pulsed trigger voltage by use of a coupling capacitor.

3. Measured and controlled parameters

Several basic parameters were controlled in the abovementioned experiments. The electron emission current was usually measured by a plane collector[9,74] or the Faraday cup.[81,91,88] Shur *et al.*[16] and Shannon *et al.*[86] used a grid collector which allowed the emitting surface to be viewed and photographed. The emitted electron charge was controlled by the use of *RC* integrating circuit.[81,90]

Several authors measured a current in the sample circuit,[9,96,17,88] which may be a switching current in the case of a true ferroelectric material if the direction of the electric field applied allows polarization reversal. Polarization reversal was continuously monitored by a hysteresis loop and switching current measurements in the studies by Shur *et al.*[82,83] and Rosenman *et al.*[84]

Electron energies were measured by the retarding potential method[81,95,91] or CMA of the Auger electron spectrometer.[75] The study of electron energy spectra in different triggering modes was conducted by Shur *et al.*[91]

The ion current component was measured by use of a negatively biased collimated Faraday cup.[91,83,84,88] Recently, energy spectra of emitted charged particles (both electrons and ions) were investigated by use of a temporally and spatially resolving electrostatic spectrometer.[97,21] Basic parameters of the plasma created on the ferroelectric surface, such as plasma electron density and plasma electron temperature, were studied by single and double floating probes (Dunaevsky *et al.*[88]). The authors[88] also studied parameters of neutral flow generated during the electron emission by use of an array of fast Penning probes. Visible light emission ascribed to the surface plasma formation was recorded by a fast frame camera 4QUICK05A, with a frame exposure of 5–10 ns.[87] Dunaevsky *et al.*[97] also studied uniformity of the extracted electron beam as a temporally resolved soft x-ray image of the anode and spatial potential distribution inside the anode–cathode gap. A radial distribution of the extracted electron beam was measured by an array of collimated Faraday cups.[97]

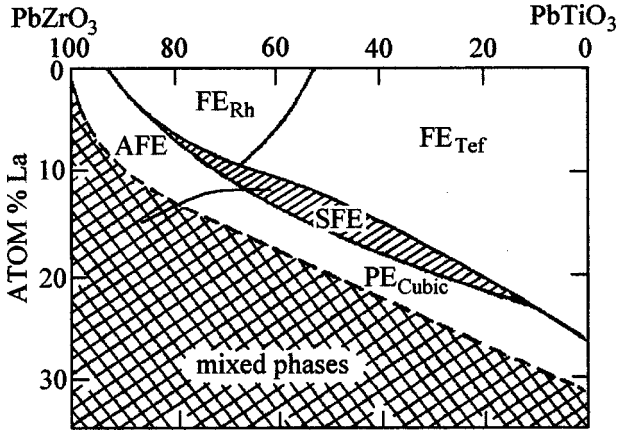

FIG. 14. A room temperature phase diagram of the PLZT system.

B. Materials and phase diagram

1. Brief survey of materials studied

As one could see in the previous paragraph, PZT (lead zirconate titanate) and PLZT (lead lanthanum zirconate titanate) ceramics of different compositions were widely used as ferroelectric cathodes. Comprehensive reviews of PZT[$Pb(Zr, Ti)O_3$] and PLZT[$(Pb, La)(Zr, Ti)O_3$] ceramic materials, used in most of the above referred ferroelectric cathode studies, can be found elsewhere.[98–100]

The room temperature phase diagram[99] of the PLZT system is shown in Fig. 14. PLZT of X/65/35 composition, where X is the atom percent of La and 65/35 is the ratio of $PbZrO_3$ to $PbTiO_3$, was typically used (Fig. 14). For $X \leqslant 8$ PLZT X/65/35 is a ferroelectric composition at room temperature (Fig. 14). If $X \geqslant 8$, the X/65/35 composition is nonferroelectric (relaxor), and cubic in its virgin state[99] (Fig. 14).

A variety of PLZT compositions, including relaxor compositions 9/65/35, 9.4/65/35, and 10/65/35, antiferroelectric composition 2/95/5, as well as ferroelectric compositions 7/65/35, 8/65/35 (Fig. 14) were used in the ferroelectric cathode studies referred to previously. It is worth noting that relaxor and antiferroelectric materials do not possess a macroscopic spontaneous polarization. These materials, demonstrating good electron emission characteristics, may exhibit macroscopic polarization only, being subjected to a high external electric field.[99] Furthermore, strong electron emission was also observed from the PLZT 12/65/35 ceramic composition related to the paraelectric phase.[16] It should be noted that all used ceramic compositions (PZT and PLZT) possess a very high relative dielectric permittivity ($\varepsilon \geqslant 2000-3000$). The ferroelectric compositions have spontaneous polarization of tens of $\mu C/cm^2$.[99]

Some experiments were conducted with TGS (triglycine sulfate) ferroelectric single crystals.[101,13,82,84] The ''model'' TGS crystal, which is among the most investigated ferroelectrics,[102,103] can be switched easily in electric fields as low as several hundreds of V/cm (430 V/cm is a typical coercive field at room temperature). The most important properties of the TGS ferroelectric crystals is a low (in 50–100 times compared to PZT and PLZT ceramics) dielectric permittivity $\varepsilon = 30$ along the polar axis and an easily achievable Curie temperature $T_c = 49\,^{\circ}\mathrm{C}$. Spontaneous polarization of the TGS crystals is $P_s = 2.8\,\mu\mathrm{C/cm}^2$, which is about one order of magnitude lower than typical values for PZT and PLZT ceramics.

2. Materials science aspects

Thus, various PZT and PLZT ceramic compositions used for development of ferroelectric cathodes are related to different phase states (Fig. 14). Application of a high electric field to a ceramic sample may cause diverse field-induced phenomena, such as reversal of spontaneous polarization P_s, field-enforced phase transition, or conventional dielectric polarization. The observed effects in the studied ferroelectric ceramics depend on their original phase state, which in turn is determined by the ceramics composition. It should be emphasized that physical properties of the considered PLZT and PZT ceramics were intensively studied for development of a new generation of electro-optic,[104–106] piezoelectric, and electrostrictive devices.[107]

Analysis of the published papers shows that ferroelectric emission was investigated from almost all known phase states in PLZT ceramics. According to the phase diagram presented in the Fig. 14, the investigated ceramic compositions are related to four phase states: ferroelectric rhombohedral, relaxor, antiferroelectric, and paraelectric phase. Let us recount peculiarities of field-induced effects in these phase states.

(1) The ferroelectric phase possesses stable macroscopic spontaneous polarization P_s without any external electric field. The main feature of this state is the possibility to reorient the direction of P_s by applying an external electric field. In the ferroelectric phase, the reversal of spontaneous polarization occurs when several experimental conditions are satisfied.

(a) The direction of the applied field E_{sw} should be opposite to the direction of the polar axis P_s. In order to achieve polarization reversal, a normal electric field component between the rear and front electrodes is required, that is ideally realized with two continuous metal electrodes. It will be shown in this review later that patterned electrode deposition drastically changes electric field distribution within the sample and, as a result, the polarization reversal kinetics. Unipolar voltage pulses may cause only a onefold reversal of P_s. Any periodic regime of the electron emission in the reversal mode needs bipolar high voltage pulses for the periodic reversal of spontaneous polarization.

(b) The field E_{sw} should exceed a definite threshold field which is called the coercive field E_c. The field E_c varies within a wide range depending on the composition and temperature of a material. For ferroelectric ceramics PLZT $X/65/35$ $(X = 6,7,8)$ related to the ferroelectric rhombohedral phase, the coercive field E_c is about 6.8–13 kV/cm at $T = 300\,\mathrm{K}$,[98] which implies the application of 1–2 kV voltage stress to 1-mm-thick samples.

(c) A complete reversal of P_s is performed under the definite condition $\tau_{dur} \geqslant \tau_{sw}$, where τ_{dur} is the duration of the applied voltage pulse, and τ_{sw} is the polarization switching time.[108] Ferroelectric polarization switching can be considered as a phase transition of the first order.[64,109] The applied electric field causes displacement of ions or polar groups in the ferroelectric crystal matrix along a specific crystallographic direction that is a polar axis. This field-induced effect represents a three-stage process consisting of nucleation of domains with opposite polarity, domain propagation into the crystal bulk, and subsequent sideways domain wall motion. The switching time τ_{sw} strongly depends on the value of applied field which also determines the polarization reversal stage limiting the switching time (either by the domain nucleation rate or the domain wall velocity). For instance, in weak electric fields the forward growth velocity of needlelike domains limits the switching time. In a recently published review[110] on ferroelectric thin films, the switching kinetics was considered in detail. The presented experimental data on switching time (τ_{sw}) in ferroelectric PZT thin films demonstrate[110] τ_{sw} within the range of tens of nanoseconds (20–40 ns) for applied electric fields as high as (200–1200) kV/cm. These fields are 10–100 times higher than those used for excitation of ferroelectric cathodes. This allows one to classify the field applied to ferroelectric cathodes as weak or intermediate fields from a polarization reversal viewpoint. In this case, the minimal switching time, which may be achieved, is roughly determined as the sample thickness divided by the velocity of sound. It should be noted that even in the higher switching fields used, for instance, with ferroelectric thin films, supersonic domain wall velocity remains a problematic issue. Therefore, the polarization switching time τ_{sw} of ferroelectrics should be limited by the sound velocity, which is of the order of 10^5 cm/s for PZT ceramics.[111] One can roughly estimate that for conventionally used ferroelectric samples 1 mm thick the switching time cannot be shorter than 1 μs. In the case of short voltage pulses with $\tau_{dur} < \tau_{sw}$ a partial polarization switching occurs.[108] The ferroelectric sample demonstrates two stages of polarization reversal: direct conventional switching of P_s and backreversal to the initial polarization state. In this mode ($\tau_{dur} < \tau_{sw}$) the ferroelectric cathode may be driven by unipolar pulses with limited repetition rate which is determined by the duration of the direct and backreversal switching process also occurring on a microsecond time scale.

(d) Complete polarization reversal occurs when the switched polarization charge $\Delta\rho = 2P_s$ is totally compensated by charges supplied by the switching current via an external circuit.[109] It is known that polarization inversion is strongly influenced by electrical properties of the interface. Early studies of polarization switching in $BaTiO_3$ (Refs. 112 and 113) demonstrated that the sidewise motion velocity of domain walls, measured with crystals having metal electrodes, is several orders of magnitude less than that found for the same switching field with liquid LiCl electrodes. An

asymmetric switching current was obtained by Kugel in TGS crystals when they were inverted through the gap between the switching electrode and the polar surface of the ferroelectric.[114] The effect of nonidentical electrodes was studied by Wurfel in Refs. 115 and 116 where one of the polar surfaces of TGS crystals was coated by the *n*-type Si electrode. Dielectric hysteresis loops, showing polarization switching in an alternative electric field, were greatly distorted because of the unipolar conductivity of the semiconductor properties of the Si switching electrode. Studies of polarization switching in different ferroelectrics that used the method of nematic liquid crystals (see Ref. 117), led to the conclusion that the switching time is defined by the conductivity of the liquid crystal which was inserted between the metal electrode and the ferroelectric surface. Detailed studies of the influence of the interface conditions implemented for TGS crystals[118] showed that a thin 1 μm dielectric film between the switching electrode and the polar ferroelectric face totally suppresses the polarization switching process.

The problem of polarization switching is especially important for ferroelectric cathodes. The experimental setup, which is used for the cathodes (Fig. 13), shows that polarization inversion occurs with a deposited patterned metal electrode. However the electron emission is generated from the uncoated polar surface (Fig. 13) where the mechanism of compensation of the depolarization field is not clear at all. This results in the fact that polarization switching in this region is considered to be very problematic.

(2) The relaxor phase (Fig. 14) has a macroscopic symmetry of the paraelectric nonpolar cubic phase with zero macroscopic spontaneous polarization P_s. Extremely high dispersion of the dielectric permittivity within an extremely wide temperature range allowed one to assume the existence of microscopic spontaneously polarized regions (domains) of nanometer size dimensions. The PLZT relaxor materials have nearly nonhysteretic polarization as a function of the electric field. A comprehensive review of relaxor PLZT and other relaxor ceramic compositions was published by Cross.[119] Application of a high electric field E_{sw} leads to a field-enforced phase transition from a macroscopically nonpolar relaxor phase to a ferroelectric phase state (tetragonal or rhombohedral symmetry) possessing macroscopic polarization. Field-induced phase transitions in these compositions was widely studied by Haertling and Land,[98] and Lang,[120] who proposed diverse electro-optic gates and shutters based on electrically controlled birefringence. According to the experimental data observed, the applied electric field needed for on/off optical switching, based on the phase transition relaxor–ferroelectric for these PLZT compositions, varied in the interval of $E_{sw}=10-30$ kV/cm. Switching times required for an on/off transition of the PLZT 10/65/35 ceramic sample 0.25 mm thick was as long as 10 μs.[121] Studies of PLZT 9.4/65/35, motivated by the application for flashblindless goggles,[106] also demonstrated a microsecond range time of the transition for a glasslike state to a macroscopic ferroelectric ordering under an electric field of 33.2 kV/cm. It should be noted that ferroelectric cathodes based on relaxor materials may be operated in a repetitive mode by application of a monopolar switching field.

(3) The antiferroelectric phase (Fig. 14) also does not possess macroscopic polarization. The applied high voltage stress induces a field-enforced phase transition to the ferroelectric phase. Upon inversion into the antiferroelectric phase a poled ferroelectric ceramic releases all polarization charges and therefore can supply a great amount of energy. Thorough studies of this type of phase transition in pulsed switching fields were performed by Pan *et al.*[122] for ferroelectric ceramics $(Pb_{0.97}La_{0.02})(Sn, Ti, Zr)O_3$. The measured switching current via deposited metal electrodes from a sample 0.6 $\times 0.4$ mm was as high as 5 A in an electric field of 32.5 kV/cm. The phase transition from the antiferroelectric to the ferroelectric phase was not abrupt. The switching time for samples 0.15–0.3 mm thick was within the range 1–2 μs under the field of 30 kV/cm.[122] Park *et al.*[123] observed a very important phenomenon of the irreversibility of the field-enforced phase transition. When a sample of PLZTS ceramic was exposed enough to the electric field for inducing the AFE-FE transition, the ceramic did not return to its virgin state. The effect of the irreversibility was confirmed in a recent study by Pokharel and Pandey.[124]

This transition from the antiferroelectric to the ferroelectric phase was thoroughly studied and proposed for use in digital displacement transducers.[125] The response time for the antiferroelectric–ferroelectric phase transition induced by the electric field was as high as 100 ms.[126] In these experiments the sample returned to the initial state when the field was switched off. Thus ferroelectric cathodes based on the antiferroelectric–ferroelectric field-induced transition may be operated in the repetitive mode by monopolar switching fields, as well as in the case of the relaxor materials.

(4) Paraelectric phase compositions (Fig. 14) have a centrosymmetric cubic structure which does not permit any spontaneous polarization. A ferroelectric state cannot be induced by an electric field, as it occurs in relaxor or antiferroelectric phase compositions. The only field-induced effect in this phase is a dielectric polarization occurring in all dielectrics. The described ceramics are related to ionic media. Therefore, the electric field application causes an ionic polarization. The response time of the ionic polarization is very short, being determined by the frequency of ionic oscillations $(10^{13}$ Hz). Ceramic cathodes based on paraelectric compositions may be activated by monopolar voltage pulses.

As was mentioned previously, strong electron emission was also studied from ferroelectric TGS crystals.[82,84] This ferroelectric possesses, at room temperature, a spontaneous polarization of $P_s=2.8\,\mu$C/cm^2. The ferroelectric state occurs in a limited temperature interval. At the temperature $T=322$ K (Curie temperature) the TGS crystal passes the phase transition ferroelectric–paraelectric. This crystal represents a very simple and comfortable model for studies of the influence of the spontaneously polarized state on electron emission generation. The coercive field for pure TGS crystals is as low as $E_c=0.5-1$ kV/cm. The switching time depends on the applied field, and it varies within the interval from microseconds to milliseconds.[102]

Thus, the short review of various phase states of ferroelectric ceramic compositions and crystals used in ferroelectric cathodes shows that they have quite different crystallo-

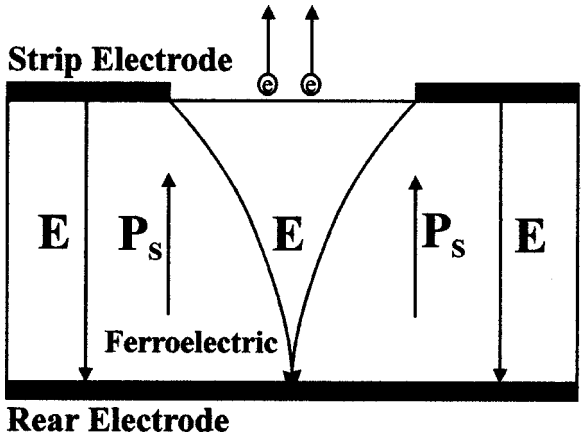

FIG. 15. A schematic drawing of electric field lines in a typical setup for the investigation of strong electron emission from ferroelectrics.

graphic symmetries and physical properties. This analysis allows the estimation of important features of ferroelectric cathodes as a function of the material's phase state. Any field-enforced phase transition, such as ferroelectric domain switching, relaxor–ferroelectric, or antiferroelectric–ferroelectric phase transition has a time response limited to the microsecond (or even millisecond) time scale. A very short response time should be observed in the nonreversal mode for ferroelectric and paraelectric phase compositions when conventional dielectric polarization occurs.

Basic modes of the strong electron emission from ferroelectric materials should be summarized here on the basis of material science considerations. Polarization reversal mode of electron emission may be realized with materials related to the ferroelectric state only if all conditions stated previously in item (1) are satisfied. Bipolar voltage pulses with a microsecond pulse duration are a required (but not sufficient) condition for this mode. The field-induced phase transitions mode may be realized with either a relaxor or an antiferroelectric material, providing conditions of items (2) or (3) are satisfied. Field-induced transitions can be achieved by monopolar voltage pulses, but the time characteristic remains critical for realizing this mode. A nonreversal mode is realized with paraelectric material [see item (4)]. Furthermore, this mode may be realized with any other material (ferroelectric, antiferroelectric, or relaxor) when the applied voltage pulse does not cause spontaneous polarization reversal.

One can see that a variety of ferroelectric, relaxor, antiferroelectric, and paraelectric ceramic compositions, as well as TGS ferroelectric crystals, were used for strong electron emission studies. Basic parameters of the electron emission observed will be reviewed in Part B, Sec. D (emission current density, current pulse width, etc.) in order to understand their dependence on the material used.

C. Electrode configuration and electric field distribution in ferroelectric cathodes

In the majority of papers dedicated to strong electron emission from ferroelectric ceramics (Ivers *et al.* (Ref. 9), Jiang *et al.* (Ref. 10), Gundel *et al.* (Ref. 81), Sampayan *et al.* (Ref. 11), Okuyama *et al.* (Ref. 14), Riege (Ref. 127)) an electrode was attached to a ceramic sample, as shown schematically in Fig. 15. The emitting polar surface of a ferroelectric was patterned with a metal grid electrode, while a solid metal contact was deposited on the rear side (Fig. 15). The schematic qualitative drawing of electric field lines of Fig. 15 tentatively shows that polarization switching, or any field-induced phase transition, occurring due to a normal component of the electric field, can take place under grid electrodes and, probably, in adjacent regions due to fringing fields. However, electron emission occurs from bare (without an electrode) regions of the ferroelectric (Fig. 15), where the normal (switching) field component is negligible near the emitting surface and appears in the ferroelectric bulk only. It should be stressed that weak electron emission, considered earlier in this paper, was observed in a ''plane-to-plane'' geometry without the strip patterned electrode. Hence, one can assume that the specific geometry of the front electrode may be a key factor leading to the drastic emission current increase observed in numerous studies referred to previously. This motivates a study of electric field distribution in a typical ferroelectric cathode experimental setup with a grid (strip) patterned front electrode.

Distribution of the applied electric field in ferroelectric cathodes was also simulated by Gundel,[128] who used MAFIA (Maxwell's equations using a finite integration algorithm) codes. It was shown that the electric field between the strips underneath the ferroelectric's surface is oriented parallel to the material/vacuum interface, rather than perpendicular to it. Furthermore, it was found that the electric field below the material's surface decreases with increasing distance to the electrode stripes.[128]

The simulation of the static electric field distribution was performed later by Rosenman *et al.*[84] in order to study a possibility of domain switching in the vicinity of the free surface, which according to the traditional interpretation, causes the electron emission from ferroelectrics. Calculations were done assuming the ferroelectric to be a dielectric medium with a dielectric constant of $\varepsilon = 1000$. Calculation results presented in this chapter were obtained for typical geometric parameters: both strip width and distance between the strips are 200 μm, the thickness of the sample is $d = 1$ mm.

Simulation results are presented in Figs. 16 and 17. The applied electric field $E_a = V/d$ (where V is the potential difference applied between the electrodes) was taken as a reference. The applied (reference) field E_a was of the same order of magnitude as the coercive one E_c (see Refs. 98 and 99) in most of the studies on the strong electron emission from the ferroelectrics referred to at the beginning of Part B, Sec. I. The Y axis (Fig. 16) is parallel to the spontaneous polarization P_s. E_Y denotes the normal electric field component causing polarization switching if $E_Y > E_c$ ($E_Y > E_a$). Figure 16 demonstrates that for all points within the area confined between the plane $Y = 0$ and the calculated curve (in normalized coordinates Y/L vs X/L for $L = 400\,\mu$m) of the normal electric field E_Y is less than the reference value $E_A = V/d$. The maximal depth of the region where $E_Y < E_a$ is $Y \sim 0.5L = 200\,\mu$m at $X = 0.5L$ (Fig. 16). Therefore, one can conclude that polarization reversal is problematic within the

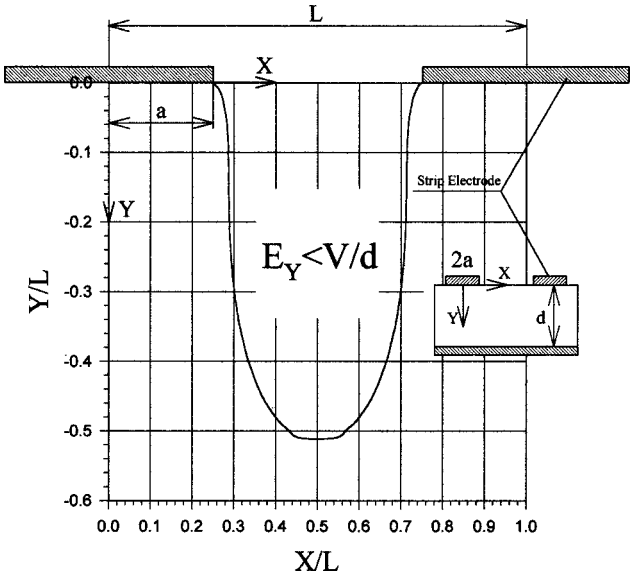

FIG. 16. An equal value line of the normal electric field $E_Y = V/d$ in the normalized coordinate system Y/L vs X/L. X is the horizontal coordinate, Y is the vertical coordinate, $2a$ is the strip width, L is the strip's period, V is the applied potential difference, d is the crystal thickness.

region where the normal electric field is less than the coercive one.

This conclusion is confirmed by the data in Fig. 17. In this figure the normal electric field component (E_Y), calculated for depth values $Y = 10$ Å and $Y = 50$ Å, is plotted as a function of a distance from the electrode edge ($X-a$). The normal component of the electric field E_Y decreases drastically in the vicinity of the electrode edge. For instance, the field E_Y becomes five times less compared to the applied field V/d at the distance $X < 100$ nm for 10 Å depth and at $X < 200$ nm for 50 Å depth.

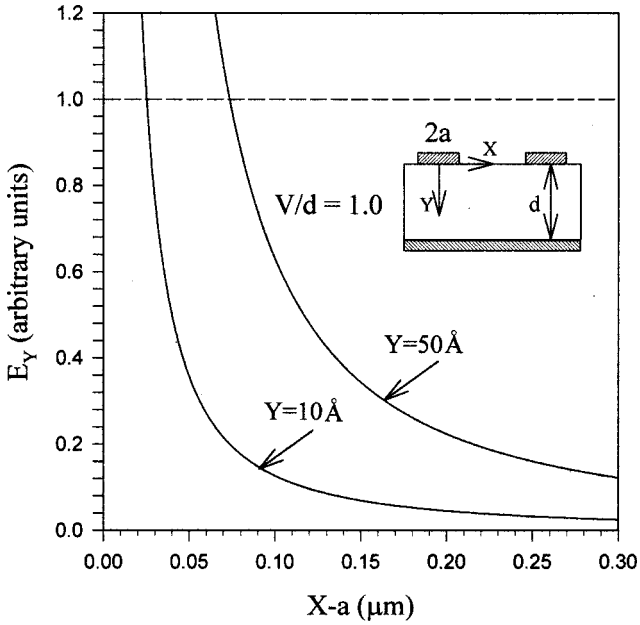

FIG. 17. The normal electric field, E_Y, as a function of the distance from the electrode ($X-a$) for two different depths $Y = 10$ Å and $Y = 50$ Å. The field $E_Y = V/d$ corresponds to unity on the vertical axis.

The following conclusions can be made on the basis of the above-mentioned simulation.

(1) Using the patterned electrode configuration in ferroelectric cathodes causes drastic changes in the applied field distribution, in comparison with plane-to-plane geometry exploited for the generation of the weak FEE. Both normal and tangential components are induced by the patterned electrode. The normal field which may cause polarization switching or a field enforced phase transition is negligibly small in the vicinity of the polar emitting surface uncoated by the patterned electrode. Because of this we firmly believe that polarization switching or a field-induced phase transition cannot occur in the vicinity of the ferroelectric surface between patterned electrode fragments except in the region which is very close to the electrode.

(2) The tangential electric field component appears near the electrode strips[84,16,128] in a typical ferroelectric cathode geometry. The tangential electric field may cause acceleration of electrons along the ferroelectric surface with subsequent electron avalanching and surface plasma generation.[16] Besides, the tangential electric field component near the electrode strips may cause 90° domain switching in PZT (PLZT) ceramics.[85] We will be able to see in the next section how the tangential electric field component can dramatically change the physical nature of the phenomenon.

Meanwhile, one important aspect of the microscopic structure of ferroelectric dielectric materials should be briefly discussed. The electrons in ferroelectrics are in a polaron state due to a strong interaction between electrons and optical phonons in these crystals.[129,130] The mobility of the electrons in the polaron state may be as low as 10^{-8} cm^2/(V s) indicating a hopping mechanism of the conductivity.[129,131] The mean free path of the electrons is defined by a polaron radius; and, for most low conductive ferroelectrics, polarons of a small radius (''small polarons'') contribute to the conductivity.[129] The mean free path of such polarons is of the order of a lattice constant. This implies that the electrons from a polaron band are emitted from a depth of no more than 10–20 Å. Since electrons may be emitted from a shallow depth (10–20 Å) only, the switched area which may contribute to the electron emission is adjacent to the strip edges (see Figs. 16 and 17) and does not exceed 0.1% compared to the entire area without electrodes, which makes the emitting area negligible. Furthermore, if the switching process occurs in the bulk of the sample where the normal electric field seems to be sufficient for polarization switching (see Figs. 16 and 17), it will not contribute to the electron emission into the vacuum because of the strongly limited free mean path.

According to the above-mentioned polaron concept, electrons can be emitted from the regions located in the vicinity of the surface of the ferroelectric only. However, on the basis of theoretical simulations (see Figs. 16 and 17), a good question to ask is how polarization switching may be facilitated in the vicinity of the ferroelectric surface where the normal electric field is negligible. One can also ask how the electron emission is related to polarization switching in ferroelectrics in general.

D. Basic experimental results on strong electron emission

Application of a triggering high voltage pulse to a ferroelectric cathode may cause a diverse field-enforced effect depending on its phase state and mode of operation. This part of the paper reviews experimental results on the basis of the ferroelectric materials used.

1. Electron emission from materials in the ferroelectric phase

It was shown that applying fast rising monopolar (negative polarity) high voltage pulses of several kilovolts amplitude (tens of kV/cm in terms of the electric field strength) to the ferroelectric PLZT 8/65/35 (Refs. 6 and 8) ceramic samples causes electron emission currents of several A/cm^2 and emitted charges of several μC/cm^2.[93,94,81] The electron current pulse width did not exceed several hundreds of ns.[94,81] Numerous data showing the influence of the amplitude, rise time, and repetition rate of high voltage pulses on the electron current and charge density emitted from ferroelectrics were reported by Gundel *et al.*[81] Gundel *et al.*[94] also presented studies of strong electron emission from ferroelectric PLZT 7/65/35 ceramics. The currents measured from PLZT 7/65/35 ceramics were of the same order of magnitude (several A/cm^2).

Electron beam current density of up to 70 A/cm^2 (electron pulse duration about 200 ns) from PZT ferroelectric ceramics, caused by the electric field of 10–20 kV/cm (monopolar positive voltage pulses applied to the rear electrode), was reported by the Cornell research group [Ivers *et al.* (Ref. 9), Schachter *et al.* (Ref. 132), Flechtner *et al.* (Ref. 95)]. The current was found to vary linearly with the anode voltage and exceeded by two orders of magnitude that of the Child–Langmuir current.[9]

Benedek *et al.*[90] observed electron emission when the ceramic PLZT 8/65/35 is excited by a positive (monopolar) trigger voltage pulse on the rear electrode and by a negative pulse on the front (emitting) electrode (the electric field applied was of the order of tens of kV/cm also). Emission currents of less than 1 A/cm^2 were measured without an acceleration voltage. The positive trigger voltage pulse was applied to the rear electrode. Strong emission currents of tens of A/cm^2 were observed by adding the accelerating voltage in the case of positive pulsing via the rear electrode or by pulsing the front electrode with negative trigger pulses. Emission current pulse durations did not exceed several hundreds of ns except in special cases of extremely low diode impedance,[90] which should be evidence of gap closure by a plasma. Further studies of the above-mentioned PLZT ferroelectric ceramic compositions by Benedek *et al.*[96] showed a correlation between the emitted and the polarization switching current. The PLZT samples emitted only if their switching current was short and messy.[96] In a recent study by Boscolo *et al.*[89] improved stability of the strong electron emission was achieved by use of a special form front electrode consisting of unconnected metal patches contained within a metal ring.

Averty *et al.*[13] and Pleyber *et al.*[92] observed strong electron emission currents up to 10–20 A/cm^2 from ferroelectric PZT and TGS materials with a pulse duration of the order of hundreds of nanoseconds. The emission was stimulated by a periodic bipolar voltage (mostly sinusoidal) with the emission current observed during negative voltage half-period on the rear electrode. Airapetov *et al.*[15] observed peak emission current densities up to 400 A/cm^2 in tens of nanoseconds time scale from the ferroelectric PSZT (lead strontium zirconate titanate) ceramic composition. Okuyama *et al.*[14] measured up to 70 A/cm^2 from ferroelectric PZT ceramics under a bipolar switching voltage. An emission current density of up to several A/cm^2 was observed by Miyake *et al.*[17] and by Zhang and Huebner[85] from ferroelectric PZT ceramics in the same pulse duration time scale (up to 100–200 ns). The emission was stimulated by monopolar negative voltage pulses applied to the rear electrode. Miyake *et al.*,[17] who studied both poled and unprepoled ceramics, found only a slight difference (a factor of 2 in peak current density) between the poled and unprepoled ceramic states.

Jiang *et al.*[10] reported emission currents up to 36 A (10 A/cm^2) at an accelerating voltage of 22.5 kV in a submicrosecond time scale. The ferroelectric cathode emitted a one order of magnitude higher current, compared to the thermionic one in the same experimental setup. The measured brightness of the electron beam was as high as 1.2×10^7 A/cm^2 sr^{-1} (at a beam current of 15 A and an extraction voltage of 10 kV). Peak currents up to 150 A, on applying acceleration voltages up to 60 kV, were measured by Sampayan *et al.*[11] Both Jiang *et al.*[10] and Sampayan *et al.*[11] used monopolar high voltage pulses for inducing the electron emission current. The currents were above the Child–Langmuir limit.[10,11] According to Sampayan *et al.*[11] the measured electron beam brightness was $\geqslant 10^5$ A/cm^2 sr^{-1}, which is two orders of magnitude lower than that measured by Jiang *et al.*[10] The electron current (tens of A/cm^2) pulse duration was extended to several microseconds as reported in a recent paper by Flechtner *et al.*,[95] who used monopolar positive or negative high voltage pulses applied to the rear electrode. Advani *et al.*[133] showed that pulsed electron currents up to 1 kA, with a pulse width of several microseconds, can be generated with ferroelectric cathodes. These results allow one to assume that high current pulsed electron guns based on ferroelectric cathodes may be developed. It should be stressed that the emission current pulse extension in most of the papers referred to previously was achieved with monopolar trigger high voltage pulses. Obviously monopolar excitation can cause only onefold polarization inversion. However, it can induce conventional dielectric polarization.

Reversal and nonreversal modes of the emission excitation were studied by Shur and Rosenman[83] in the ferroelectric ceramics PLZT 7/65/35. In the reversal mode, with bipolar voltage pulses reversing the spontaneous polarization direction, emitting current pulses in the microsecond time scale were attained with relatively low applied voltages ($V_{ap}\geqslant 500$ V for 0.3-mm-thick PLZT 7/65/35 samples) in comparison with the voltage, which should be applied in the nonreversal mode ($V_{ap}\geqslant 1500$ V), for the electron emission generation. The reversal of spontaneous polarization was proved by measurements of the switching current. Additional evidence of P_s reversal was the fact that applying repetitive

trigger pulses of the same polarity, with an amplitude of about 500 V, did not cause any electron emission current.

Parameters of the strong emission induced by these different modes were studied. Maximal emitting current density up to 10 A/cm^2 for both modes was measured.[83] However the delay time in the reversal mode was much higher than that in the nonreversal mode. The measurements showed that the delay time in the reversal mode was about 150 ns whilst in the nonreversal mode it was 50 ns. It should be noted that recent studies of the PZT ceramics in the nonreversal mode by Krasik and Dunaevsky[88,97] allowed the observation of an extremely short delay time reaching 5 ns.

Another attempt to separately observe reversal and nonreversal modes was undertaken for TGS crystals. Instead of short voltage pulses, the authors used a sinusioudal voltage of 50 Hz frequency with $V_{ap} > 100$ V for 0.6-mm-thick TGS crystals [Shur *et al.* (Ref. 82), Rosenman *et al.* (Ref. 84)]. Such a low voltage could not cause electron emission due to a conventional dielectric polarization, and it was not observed, either at the temperatures above the Curie point (in the paraelectric phase) or under monopolar trigger voltage pulses (amplitude $|V_{tr}| \leqslant 2.5$ kV, pulse width $100\,\text{ns} \leqslant \tau_{tr} \leqslant 100\,\mu$s) eliminating polarization reversal.[82,134] These results will be considered in detail in the next section.

Summarizing the paragraph the following points should be stressed.

(a) Typical electron emission current density observed from ceramic materials in the ferroelectric phase varied from several A/cm^2 up to tens of A/cm^2. Usually, higher currents (up to 100 A/cm^2) were observed with an accelerating voltage applied.

(b) The triggering voltage pulse in the polarization reversal mode may be much lower in comparison with the nonreversal mode.

(c) In the reversal mode the delay time is much longer that that in the nonreversal mode, which may be several nanoseconds.

2. Antiferroelectric materials

Gundel *et al.*[6,81] also observed electron emission from PLZT 2/95/5 ceramics belonging to the antiferroelectric phase in experimental conditions identical to those for the ferroelectric PLZT 8/65/35. Electron emission currents of the order of several A/cm^2 (pulse duration up to several hundreds of nanoseconds) were induced by use of monopolar negative high voltage trigger pulses (several kV scale) applied to the rear solid electrode. However, in contrast to PLZT 8/65/35, high repetition rates of the electron emission current (up to 2 MHz) have been achieved by use of the antiferroelectric PLZT 2/95/5.[81]

According to Benedek *et al.*,[90] the antiferroelectric PLZT 4/95/5 material was much less effective than the ferroelectric PLZT 8/65/35. In this case a monopolar positive trigger voltage was applied to the rear electrode without an accelerating voltage or a negative trigger voltage was applied to the front electrode. Only at higher temperatures $T > 130\,^\circ$C the parameters of the electron emission from the PLZT 4/95/5 were improved to be comparable to those with PLZT 8/65/35.[90] In a recent paper by Boscolo *et al.*,[89] comparing two types of front electrode, basic parameters of electron emission from PLZT 4/95/5 (emission current density up to several A/cm^2, pulse duration up to several hundreds of nanoseconds) were confirmed. In order to make PLZT 4/95/5 show electron emission parameters comparable to those of PLZT 8/65/35 higher electric fields were applied to the samples. The higher electric field was required to induce the antiferroelectric–ferroelectric phase transition.[89] Furthermore, the electron emission current observed from the PLZT 4/95/5 possessed two peaks ascribed by Boscolo *et al.*[89] to the fast buildup of spontaneous polarization (the first peak) and to the slower relaxation of spontaneous polarization (the second peak).

An emission current density of the order of 100 mA/cm^2 was observed by Shannon *et al.*[86] from the antiferroelectric PLZT 2/95/5 without an accelerating voltage by applying bipolar voltage pulses to the rear electrode. In the ''bright'' emission mode (ascribed to plasma-assisted emission) the electron emission pulse width was as short as about 100 ns, while in the so-called ''dark'' mode (ascribed to polarization switching) the pulse duration approached the microsecond time scale.

3. Relaxor materials

Gundel *et al.*[94] presented studies of strong electron emission from PLZT X/65/35 ($X = 9,10$) ceramic compositions which relate to the relaxor phase. The currents measured from PLZT X/65/35 ceramics under monopolar voltage pulses were of the order of several A/cm^2. The authors observed that relaxor ceramics PLZT 9/65/35 and PLZT 10/65/35 emitted a much higher electron charge compared to that emitted by ferroelectric PLZT 8/65/35.[94] Averty *et al.*[13] and Benedek *et al.*[90] observed strong electron emission currents up to 10–20 A/cm^2 with a pulse duration of up to several hundreds of nanoseconds from relaxor PLZT 9.4/65/35 ceramic composition by applying a bipolar sinusoidal trigger voltage.

4. Paraelectric materials

A strong electron emission current up to tens of A/cm^2 with a pulse duration up to hundreds of nanoseconds from the paraelectric PLZT 12/65/35 ceramic was observed by Shur *et al.*[16,91] under applied electric fields of 10–25 kV/cm. Electron emission was induced by either monopolar or bipolar voltage pulses[16] applied to either a rear or front (patterned) electrode.[91] An electron emission with a high repetition rate (up to 100 kHz) was demonstrated.[16] In contrast, the experimental results by Shur *et al.*[82,134] and Rosenman *et al.*[84] showed that the electron emission effect from TGS crystals vanishes above the Curie point ($T_C = 49\,^\circ$C) indicating that low applied voltages ($\geqslant$100 V for 0.5- to 1-mm-thick TGS crystals) required for polarization reversal in TGS were insufficient to induce the emission in the paraelectric phase, as was observed in the case of PLZT 12/65/35.[16] This issue will be discussed in detail in the next section.

TABLE III. Basic studies of strong electron emission from ferroelectric, antiferroelectric, relaxor, and paraelectric materials.

Phase state	Composition	Selected references	Emission current density	Pulse duration
Ferroelectric	PLZT 7/65/35	81, 94	Several A/cm^2	Hundreds of ns
	PLZT 8/65/35	90, 96		
	PZT (LTZ-2)	9–11	Tens of A/cm^2	Hundreds of ns
	PZT	14, 95		Several μs
		133		Several μs
	PZT	17, 85	Several A/cm^2	Hundreds of ns
	PZT, TGS	13	Tens of A/cm^2	Hundreds of ns
Ferroelectric	PLZT 7/65/35	83	Tens of A/cm^2	Several μs
	PSZT	15	Hundreds of A/cm^2	Tens of ns
Antiferroelectric	PLZT 2/95/5	81, 86	Several A/cm^2	Hundreds of ns
		84		up to 1 μs
	PLZT 4/95/5	90, 96	Tens of A/cm^2	Hundreds of ns
Relaxor	PLZT 9/65/35	94	Several A/cm^2	Hundreds of ns
	PLZT 10/65/35			
	PLZT 9.4/65/35	92	Tens of A/cm^2	Hundreds of ns
Paraelectric	PLZT 12/65/35	16, 91	Tens of A/cm^2	Hundreds of ns

5. Brief summary

Thus, strong electron emission was measured from ferroelectric materials PZT and PLZT (7, 8)/65/35 ceramics, TGS ferroelectric crystals, relaxor PLZT (9, 10)/65/35, paraelectric PLZT 12/65/35, as well as antiferroelectric PLZT (2, 4)/95/5 ceramics. It should be stressed that for the variety of ferroelectric compositions used, some parameters of the electron emission observed (current density, pulse width, etc.) are comparable. Keeping in mind the importance of the material aspect we can definitely state that emission current densities observed from ferroelectric, antiferroelectric, relaxor, and paraelectric phases are all of the same order of magnitude. Table III summarizes the data of the materials studied, their phase states, and the parameters of measured electron emission current densities. One can find that, regardless of the phase state, the measured electron emission current density varied from units to dozens of A/cm^2. Higher currents were measured with high accelerating voltages,[15,10,11] while lower currents (several A/cm^2 and less than 1 A/cm^2) were observed with modest ones and without an accelerating voltage at all.[81,90,86]

Experimental results on the electron emission from ferroelectric thin films stand apart from the results reported for bulk materials. For this reason they are presented separately in Sec. III B 5. We would like to note here that only a few studies dedicated to the subject have been published to date. The first publication is that of Auciello *et al.*,[75] who observed electron emission from PZT thin films $\leqslant 1$ μm thick. Comparative studies of electron emission from ferroelectric samples of different thickness (from 6 μm to 1 mm) were conducted by Averty *et al.*[13] Recently, Sviridov *et al.*[76] also observed electron emission from several μm thick PZT films.

E. Nonplasma interpretations

Two quite different interpretations of strong electron emission from ferroelectric materials have been proposed to date. Historically, the first one is based on specific properties of ferroelectric materials such as polarization reversal and various field-induced phase transitions, while the second one ascribes electron emission to surface plasma formation followed by electron extraction from the plasma. In the next paragraph, the first approach, referred to also as nonplasma interpretations, will be considered.

1. Fast polarization switching and fast field-induced phase transition

The high electron emission current densities observed were ascribed to a fast nanosecond polarization reversal of ferroelectric domains, a fast change of a polarization state of the ferroelectric, or a fast field-induced phase transition from the antiferroelectric or the relaxor state, to the ferroelectric phase of specific ceramic compositions.[81,14,127,90,96,11,13,74] These interpretations, first proposed by Rosenman,[3] rely on a fast change of spontaneous polarization in order to minimize the relaxation within the material.[127] It is assumed that both the field-induced phase transition and polarization reversal may be realized on a nanosecond time scale, thereby inducing the electron emission on the same time scale. A negative pulse applied to the rear electrode induces polarization switching or a phase transition and, as a result, a negative potential at the emitting surface repulsing the electrons is achieved.[127] Subsequently, a strong internal field in the surface layer, due to a rapid change of spontaneous polarization, leads to a copious electron emission from ferroelectric ceramics into the vacuum. According to Gundel,[93] the electrons were liberated from local donor levels created by La doping in PLZT ceramics or from a valence band. The concentration

of donor centers should be especially high near the surface layer of the prepoled ceramic sample from where the electrons are liberated during ferroelectric domain switching.[94,81]

Gundel *et al.*[93,94,81] investigated both PLZT 2/95/5 and PLZT 8/65/35 ceramics. The former composition demonstrates a phase sequence AFE–FE–PE (antiferroelectric–ferroelectric–paraelectric) when the temperature is increased, while the latter shows a FE–PE (ferroelectric–paraelectric) phase sequence.[81] For both compositions the authors assumed the coexistence of different phase transition regions (AFE–FE and FE–PE) and high donor-center concentration to be responsible for the electron emission process. The PLZT 2/95/5 composition is in the AFE phase at room temperature. This state can be transformed to the FE phase when the material is subjected to an external electric field of several dozens of kV/cm. Gundel *et al.*[81] proposed that electron emission from this composition occurs due to an abrupt return of the material to the AFE phase when the electric field is switched off. This fast return of the material to the nonpolar state was assumed to be responsible for the high repetition rates of the electron emission current that were obtained from this ceramic composition.[81]

Twin ferroelectric domains were assumed to be responsible for the fast polarization reversal in PLZT 8/65/35 (see Ref. 81). According to the authors, the fast reversal of one half of the twin domains can explain a negligible time delay between the HV pulse rise and the electron emission. Some of the reversed domains are fixed by the internal electric field within the surface layer hindering the fast relaxation of the material, as was assumed in the case of the PLZT 2/95/5. This allows one only low repetition rate (1 Hz) excitation for obtaining stable electron emission from the PLZT 2/95/5 ceramic composition.[81]

Benedek *et al.*[90,96] also used a model of fast polarization switching for PLZT 8/65/35 and a fast field-induced AFE–FE phase transition for PLZT 4/95/5. The authors assume that the excitation field directed from the rear surface toward the patterned surface of the sample with no accelerating field applied causes electron emission due to polarization switching. The authors also assume that some electrons acquire high energies due to the Auger process.[90]

Benedek *et al.*[96] assumed that relaxor properties of PLZT ceramics may be important in the strong electron emission induced by these effects. The change of polarization can be extremely fast in PLZT relaxors.[90] The authors assume that the small size (of the order of 10 nm) ferroelectric domains should be responsible for the fast switching (Benedek *et al.*, Ref. 96).

In a recent paper Boscolo *et al.*[89] improved the stability of electron emission from PLZT 8/65/35 and PLZT 4/95/5 by use of the front electrode, due to a pattern of unconnected patches contained within a ring. The authors assumed that the pattern of disconnected metal islands allows all surface domains to switch back and forth. Therefore, according to Boscolo *et al.*,[89] the domains of the uncovered portion of the surface can attract and push the electrons away from the surface.

Sampayan *et al.*,[11] Okuyama *et al.*,[14] Averty *et al.*,[13] and Asano *et al.*,[74] also agree with this model of fast polarization switching.

2. Fast change of the polarization state of a ferroelectric (experiment and model)

Ivers *et al.*[9] from Cornell University explained their experimental results by a theoretical model which assumed the surface screening charge to be injected into the vacuum gap of the electron diode as the polarization state of the ferroelectric changes (Schächter *et al.*, Ref. 132). According to the authors, the local electric field on the ferroelectric surface can be as large as 4×10^7 V/cm, which is sufficient for field emission from either the ferroelectric or the metal grid electrode.[9,132] When a positive voltage pulse is applied to the rear electrode of ferroelectric cathodes[9] there is an increase in the electron charge in the vicinity of the grid electrode due to the field emission from the grid. The above-mentioned field can cause a field emission current of the order of 20 A/cm^2 (Ref. 9). Moreover, both the electric field and the emitted current can be enhanced close to the grid edges. The authors assumed that the free electron charge is redistributed on the ferroelectric surface by a flow of electrons in the vacuum from the gridded (metal) regions to the bare ceramic ones, rather than by a surface flashover.[9]

Subsequently, electrons emitted from either the ferroelectric surface or the metal grid may form an electron cloud close to the cathode surface, thereby reducing the local potential.[9] The model supposes that the current through the diode consists of two parts: the flow into the cloud from the ferroelectric and the flow through the remaining part of the diode. According to the authors, the energy of the emitted electrons (for a positive voltage pulse applied to the rear electrode) are insufficient to account for the high currents measured. However, the theoretical model proposed by Schächter *et al.*[132] predicted electron emission currents and linear $I-V$ characteristics of the gap in good agreement with the experimental results. According to the model, the dependence of the current on the voltage is linear rather than $V^{3/2}$ (Child–Langmuir law) with the gap resistance R_{gap} given by[132]

$$R_{\mathrm{gap}}\equiv\frac{V_{\mathrm{AN}}}{I_{\mathrm{AN}}}=\eta\frac{1}{36}\frac{g^2}{A}\gamma_0^2\sqrt{(\gamma_0+1)/(\gamma_0-1)}, \tag{21}$$

where g and A are the vacuum gap and the diode surface area, respectively, and $\eta=377\,\Omega$. The parameter γ_0 is expressed as follows[132]:

$$\gamma_0=1+\frac{1}{36}\overline{Q},\quad \overline{Q}\equiv\frac{eQ_{\mathrm{gap}}g}{\varepsilon_0 Amc^2}, \tag{22}$$

where Q_{gap} is the total amount of charge in the gap. On the basis of quantitative analysis, the authors concluded that the presence of an electron cloud in the gap is directly responsible for the linear $I-V$ characteristics observed experimentally. This theory virtually explains the discrepancy with the Child–Langmuir law for diodes with ferroelectric cathodes.

A fast change of the polarization state of the ferroelectric was also used by Jiang *et al.*[10] to interpret their experimental

results. Recently, Sviridov *et al.*[76] introduced the so-called dielectric electron emission which, according to the author's opinion, may occur without polarization reversal. This interpretation is similar to the model of fast polarization change described previously.

3. Other interpretations

The model briefly described previously[132] is the only quantitative description of strong electron emission from ferroelectrics available to date. Other models (mostly qualitative) of strong electron emission were proposed by Rosenman and Rez,[72] Ivanchik,[135] and Wang *et al.*[136]

Assuming strong electron emission to be of a solid state origin, one can expect a huge conductivity current flowing within the ferroelectric (dielectric) surface layer in order to provide the copious electron current into the vacuum. However, most of the ferroelectrics tested for emission properties are very good insulators with a typical electric conductivity within the range of $(10^{-14}-10^{-10})\ \Omega^{-1}\,\mathrm{cm}^{-1}$. The explanation was proposed by Rosenman and Rez,[72] who assumed that at high electric fields the electric conductivity in the surface layer may be enhanced due to the Poole–Frenkel effect. According to the authors' estimation, ten orders of magnitude conductivity increase may occur in fields of the order of 10^7 V/cm. This drastic conductivity increase (that is actually due to multiplication of charge carriers at high electric fields) may be responsible for the high conductivity current within the surface layer, and it may lead to the hot electrons' appearance followed by overbarrier electron emission.[72]

Incomplete polarization reversal in ferroelectric materials was assumed to be responsible for strong electron emission by Airapetov *et al.*[15] The authors argued that in high internal fields, caused by uncompensated charges during fast polarization reversal, the bounded uncompensated charge can be screened by intrinsic electrons and holes due to Zener breakdown. Airapetov *et al.*[15] introduced two processes to be responsible for strong electron emission from ferroelectrics. According to the hypothesis, the first one is tunneling through a low wedge-shaped energy barrier, which is formed due to a high external electric field and huge (comparable to the band gap of a material) band bending inside ferroelectric materials. This emission process causes the appearance of uncompensated positive bound charges on an emitting surface that cease the emission when their electric field is equal to the external one. In the crystal bulk the field of the uncompensated charge is antiparallel to the initial polarization (for a monodomain sample), which leads to a formation of crystalline seeds with opposite polarization direction and subsequent ''second process'' responsible for the effect. The crystalline seeds cannot grow through the crystal because of the applied short electric field pulses. According to the authors, the second process occurs when the external field is switched off and the crystal returns to its initial state. It is assumed that the seeds are pushed to the surface and collapse, leading to the emission of electrons screening the polarization within the seeds. According to the experimental data presented by the authors, a second process of the crystalline seeds collapse predominates, which leads to an emission current density as high as 400 A/cm^2. Subsequently this hypothesis was extended to a qualitative theory based on physical estimations. [135]

On the basis of the experimental result, which shows considerable electron emission from a ferroelectric above the Curie point, Okuyama *et al.*[14] proposed an abrupt change of dielectric flux as an alternative to polarization switching. Pleyber *et al.*[92] assumed that electron emission from ferroelectrics is tunnel electron emission at low current densities, and it becomes plasma induced field emission at high emission currents. Shannon *et al.*[86] divided the electron emission into two modes: the plasma-assisted bright mode and the so-called dark mode induced by polarization reversal. Miyake *et al.*[17] ascribed strong electron emission to both emission of screening electrons during polarization switching and plasma formation on the ceramic surface. A similar interpretation of simultaneous ferroelectric and plasma emission was proposed by Zhang and Huebner.[85] Detailed studies of plasma-assisted emission in both reversal (Shur *et al.*,[82,83] Rosenman *et al.*,[84]) and nonreversal (Shur and co-workers,[16,91,83] Krasik *et al.*,[21,87] and Dunaevsky *et al.*,[88,97]) modes have been conducted. The next section will present features and basic physics of plasma-assisted electron emission from ferroelectric materials.

F. Laser-induced electron emission from ferroelectrics

The first observation of the intense laser-induced electron emission from PLZT 9/65/35 (up to 2 A/cm^2, 20 nC/cm^2) was reported by Geissler *et al.*[137] The electron emission was induced by 6-ns-long UV laser pulses (266 nm wavelength) with an output power density on the sample of 5×10^5 W/cm^2. Electron emission from the ferroelectric started only with extraction voltages of several kV. The electron current pulse time coincided with the laser pulse time. Illumination by green laser light ($\lambda = 532$ nm) did not cause emission, despite higher light intensity and extraction voltage.

The experimental setup was similar to that used for strong electron emission induced by high voltage pulses. A quartz window and a special Faraday cup design allowed the laser beam to illuminate the gridded ferroelectric surface (gold stripes of 200 μm width separated by a bare surface of the same width). A negative dc extraction potential up to 10 kV was applied to the grid electrode. An opposite surface of the sample was coated with a solid electrode.

The laser-induced emission observed from the PLZT 9/65/35 was interpreted as a photoeffectlike emission.[137] It was assumed that either a spontaneous polarization change (due to a pyroelectric effect, for instance) or the liberation of electrons from donor levels (or even from the valence band through the band gap of about 3.4 eV) was responsible for the electron emission.[136]

Strong enhancement of the laser-induced electron emission and intense laser induced self-emission of electrons were demonstrated subsequently.[138,139] Both effects were induced by previous high voltage pulsing of PLZT samples. The energy of the self-emitted electrons was as high as 10 keV. An extended study of these effects was conducted by Geissler *et al.*[140] using pulsed laser radiation of 266, 355,

and 532 nm wavelength (energy density of 13 mJ/cm^2, 5 ns pulse width). PLZT 2/94.5/5.5 samples with an identical electrode configuration were employed.

According to Geissler *et al.*[140] there are three different models of the laser induced electron emission:

(a) pure laser-induced emission with no high voltage pulsing of the samples used (only an extraction potential is applied);
(b) enhancement of the pure effect by subsequent high voltage and laser pulse application to the PLZT cathode (a laser pulse is accompanied by an extraction voltage);
(c) self-emission of electrons measured in the condition of (b) without any extraction potential (laser pulses are applied after pulsing the cathode with high voltage).

The effects (b) and (c) were assumed to occur due to laser-induced macroscopic polarization change in the ferroelectric. Both effects were characterized by a threshold dependence of the emission efficiency on the energy density of the incident light and a high energy of emitted electrons. Photoassisted domain switching was proposed as a possible mechanism of the enhanced laser-induced emission (b) and self-emission (c) of electrons.[140]

Both self-emission and enhanced laser-induced emission decayed as function of the number of laser pulses without further electrical pulsing of the cathode.[140,141] Hence, the effect (a) was classified as a ''normal steady state'' emission in the presence of a constant extraction field, while the effects (b) and (c) were referred to as a ''transient mode,'' after a high voltage pulsing of the ferroelectric cathode.[141]

Using ultrashort femtosecond laser pulses was found to be favorable for ferroelectric photocathodes.[141] Hence, the laser-induced emission efficiency of the ferroelectric photocathodes surpassed that of metallic photocathodes by at least one order of magnitude.[141] Geissler *et al.*[141] stated that ferroelectric photocathodes can work properly in a gas or a plasma atmosphere, and they are superior to most of metallic photocathodes in reliability and lifetime. Therefore, ferroelectric photocathodes may be used in free-electron lasers, electron accelerators, and high power linear colliders.[141] The first demonstration of a ferroelectric laser photocathode operating in an acceleratorlike structure was presented by Gundel *et al.*[142]

Laser-induced electron emission from PLZT ceramics was recently studied by Benedek and Boscolo.[143] Their results confirmed those described previously. In addition, the authors observed electron emission induced by laser wavelengths as long as 1064 nm with a corresponding increase of laser pulse energies. In general, it was stated that the higher the energy of the incident photons, the higher the efficiency. Furthermore, it was found that the ferroelectric material PLZT 8/65/35 is much more efficient than the antiferroelectric PLZT 4/95/5.

Benedek and Boscolo[143] proposed a new model based on the Auger process in a high density sheet of electrons that screen the macroscopic spontaneous polarization near the front surface of the ferroelectric ceramic. According to the authors, an electron density of $n<10^{20}\,\mathrm{cm}^{-3}$ in the vicinity of the emitting ferroelectric surface should make the Auger process very effective. Electrons exit the ferroelectric ceramic due to a Coulomb repulsion as a result of polarization switching within the surface layer.[140,141] The laser-induced electron emission under normal steady state operation (without high voltage pulsing) at short wavelengths was ascribed to a conventional photoemission process as was initially proposed by Geissler *et al.*[137]

A more detailed review of laser-induced electron emission from ferroelectrics can be found in the paper by Riege *et al.*[18]

II. PLASMA-ASSISTED ELECTRON EMISSION FROM FERROELECTRIC MATERIALS

The review of the experimental results presented in the previous section showed that various ferroelectric materials related to quite different phase states (ferroelectric, antiferroelectric, relaxor, paraelectric) demonstrate strong electron emission currents. Application of high voltage stress to the ferroelectric cathodes may cause diverse field-induced effects, including spontaneous polarization inversion of the materials in the ferroelectric state, field-enforced phase transitions such as antiferroelectric–ferroelectric and relaxor–ferroelectric. In these cases strong emission was observed. It was also shown that high density electron emission is generated also in the paraelectric phase PLZT 12/65/35,[16,91] which is a linear dielectric with very high dielectric permittivity and the only field-induced effect occurring in this material is dielectric polarization.

Analysis of numerous experimental results revealed that the studied ferroelectric crystals and ceramics with various compositions, in different phase states and excited in different modes, demonstrated similar values of the electron emission currents. This allows the assumption of a common mechanism for all studied ferroelectric materials. In some research papers it was assumed (Pleyber *et al.*,[92] Riege[127]) that a surface plasma may be formed at a ferroelectric cathode surface, and it contributes to the strong electron emission. In the article by Shannon *et al.*[86] the emission was divided into two modes: a plasma-assisted ''bright'' mode and the so-called ''dark'' mode, induced by spontaneous polarization switching of a ferroelectric. A similar interpretation that considered simultaneous true ferroelectric emission and plasma emission was recently proposed by Zhang and Huebner.[85] The authors claim that plasma-assisted electron emission follows the emission induced by polarization switching.[144] Dorfman *et al.*[145] disagree with this assumption; and, on the basis of their experimental results, they argue that the surface plasma appears in the first few nanoseconds and can only be the source of electrons for the strong emission. Benedek *et al.*[90] assume that a so-called ferroelectric current pulse appears about 50 ns after the end of the switching pulse, while plasma formation starts at the end of the rise of the driving pulse. This hypothesis also contradicts that of Zhang *et al.*[144] Flechtner *et al.*[95] interpreted their results assuming that in the first $\approx 1\ \mu$s the ferroelectric cathode controls the electron flow, while beyond this time plasma effects dominate. Shur *et al.*[82] observed plasma-assisted electron emission of a ferroelectric origin existing in

the ferroelectric phase only. In a later paper [83] the authors found two different modes of excitation of the surface flashover plasma, initiated by either weak electron emission under polarization reversal (true ferroelectric emission) or field emission at triple points.

In this section we will consider the plasma interpretation of strong electron emission from ferroelectric cathodes. We will review various methods of surface plasma initiation, including plasma ignition by classical field emission and by weak ferroelectric emission when the generated plasma is of a ferroelectric origin.

A. Plasma-assisted electron emission from ferroelectric cathodes in the nonreversal (nonswitching) mode

Direct evidence of a plasma-assisted character of ''strong'' electron emission from the ferroelectric ceramics PLZT 12/65/35 in the paraelectric phase was presented by Shur *et al.*[16] The idea to use the PLZT 12/65/35 ceramic was to completely eliminate spontaneous polarization reversal as a possible mechanism of electron emission generation. A ferroelectric material in the paraelectric phase does not possess spontaneous polarization. The experimental evidence, presented by Shur *et al.*,[16] showed that despite the lack of polarization reversal, as well as any field-induced phase transition, strong electron emission with typical current densities of tens of A/cm^2 was observed. Plasma generation was observed by direct observation of surface flashover and by measurements of both electron and ion currents. Subsequently, detailed studies of parameters of the plasma generated on a PZT and a $BaTiO_3$ ceramic surface were presented by Krasik *et al.*[87] and by Dunaevsky *et al.*[88,97]

Ferroelectrics are well-known dielectric materials. Some ferroelectric materials, such as various ferroelectric ceramics, possess a high dielectric permittivity $\varepsilon_r \approx 10^2 - 10^4$. High dielectric permittivity of ferroelectric ceramic materials made them attractive for use as metal-dielectric cathodes that have been known for more than 30 years.[146–152] Operation of metal–dielectric cathodes is based on plasma formation that results from a noncompleted surface discharge (in equivalent terms dielectric surface flashover) followed by the extraction of an electron beam from the surface plasma. It should be stressed that the experimental setup (electrode configuration) used in these early investigations was very similar to the experimental setup used at the present time in studies of ferroelectric cathodes (see the previous section).

The severe lowering of the breakdown voltage for vacuum gaps with dielectric is known from the pioneering work of Kofoid.[146] The primary phenomenon is attributed to extremely high electric fields produced in the unavoidable very small gaps at the metal-to-dielectric contact. The effect is especially pronounced for ceramics with high dielectric permittivity such as barium titanate.[146] It was proposed that surface flashover starts at a negative metal–dielectric junction, due to the initial release of electrons by the field emission process.[146]

In a triple junction region where metal, vacuum, and dielectric meet the electric field can be roughly estimated as follows:

$$E = \frac{E_0 \varepsilon}{(\delta_0 \varepsilon / \delta) + 1}, \tag{23}$$

where E_0, ε, and δ are the applied electric field ($E_0 = V/\delta$), dielectric constant, and dielectric thickness, respectively, δ_0 is the microgap between the dielectric and metal. If $\delta_0 \varepsilon / \delta \ll 1$, the electric field in the triple junction is approximately increased by a factor of ε. According to Schachter[153] the current emitted via field emission at triple junctions is also proportional to the dielectric constant.

Bugaev *et al.*[148,149] conducted detailed investigations of a surface flashover mechanism at a dielectric–vacuum interface. High voltage pulses (up to 40 kV for 2-mm-thick samples) with a very short rise time ($\sim$1 ns) were used to cause the flashover on forsterite and steatite ($\varepsilon_r \approx 7$) ceramics. The dominant role of the metal–dielectric contact in the process of the flashover initiation was confirmed by Bugaev *et al.*[148] Using fast frame photographing and visible light spectroscopy, Bugaev *et al.*[151] showed that intense electron emission starts almost simultaneously with the appearance of light emission at triple junctions on a $BaTiO_3$ surface. This result was obtained for any polarity of the applied trigger voltage. However, it was shown that plasma channel velocity along the ceramic surface depends on the polarity and amplitude of the trigger voltage applied. The light emission observation and spectroscopy data (spectral lines of ceramic components as well as electrode material were observed) allowed the authors to propose a concept of explosive electron emission at triple junctions (Bugaev *et al.*;[151] Mesyats[154]).

Metal–dielectric cathodes were successfully used as electron sources for nanosecond high current accelerators. High density pulsed electron emission currents of up to $10^3 - 10^4$ A/cm^2 with a current pulse width up to 100 ns were obtained from barium titanate with $\varepsilon = 1500$ by applying high voltage trigger pulses with an amplitude of 1–4 kV (typical sample thickness was 1–2 mm).[150]

A barium titanate cathode with a wire grid on the emitting surface was recently analyzed by Puchkarev and Mesyats[152] on the basis of their previous studies referred to earlier. They noted that triple junctions formed at the grid–dielectric contact played a fundamental role. It was also assumed that the flashover was initiated as a result of an explosive electron emission at the triple junctions. The discrepancy with the Child–Langmuir law was explained by the prefilling of a vacuum diode with the flashover plasma.[152,154]

At the present time there is no comprehensive and precise theory describing the dielectric surface flashover. However, there are some generally accepted points related to a qualitative scenario of the flashover process. According to the review of dielectric surface flashover phenomenon by Miller,[155] the surface flashover of insulators in a vacuum is initiated by the emission of electrons from the cathode triple junction. These electrons then usually multiply (avalanching process) as they traverse the insulator surface due to the tangential electric field component, either as a surface secondary electron emission avalanche, or as an electron cascade in a thin surface layer, causing desorption of gas which had been absorbed at the insulator surface. This desorbed gas is

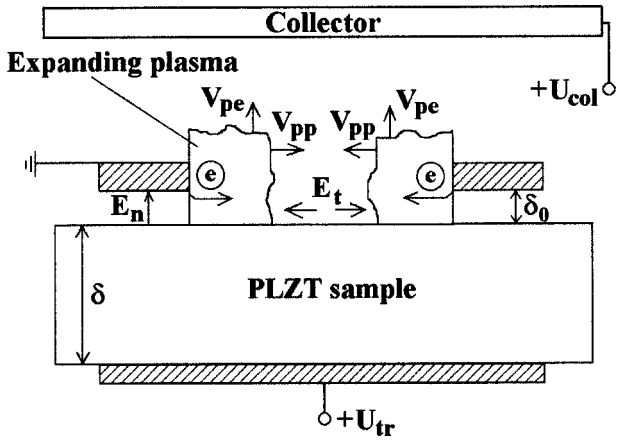

FIG. 18. A possible mechanism of surface flashover plasma formation when polarization reversal is eliminated (nonreversal mode). v_{pe}, v_{pp}, E_t, and E_n are the plasma expansion velocities into the vacuum gap, plasma propagation velocity along the dielectric surface, and tangential, and normal component of the electric field.

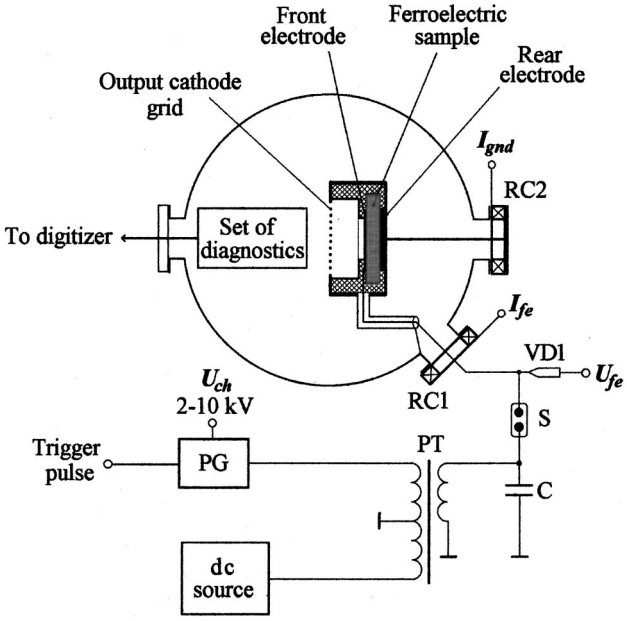

FIG. 19. A schematic drawing of the experimental setup used for surface plasma diagnostics.

then ionized, which leads to the surface flashover of the insulator.[155] In other words, the final stage of the surface flashover is thought to occur in desorbed surface gas and/or in vaporized insulator material.[155,156] Another possible flashover mechanism has been proposed by LeGressus *et al.*[157,158] and Blaise.[159] The surface flashover was ascribed to a relaxation of the crystal lattice initiated by a charge detrapping process.

A possible scenario of the surface plasma formation in the typical ferroelectric cathode geometry is shown schematically in Fig. 18,[16] and the qualitative mechanism of the strong electron emission[16,87,88] will be briefly discussed in the following in terms of the dielectric surface flashover.[160,154] If a positive voltage pulse is applied to the rear contact of the sample and the grid electrode is grounded (Fig. 18), the metal grid–dielectric contact represents a cathode triple junction; i.e., a region where a metal (cathode), insulator, and vacuum meet.[155,156] The field is enhanced in unavoidable small gaps (see Fig. 18) at triple junctions by a factor ε_r (relative permittivity of a dielectric).[146] Field electron emission at the triple junctions occurs as a result of the above-mentioned field enhancement of the normal electric field component E_n. Field electron emission at the triple junctions is a priming electron emission required for further surface flashover development. Emitted electrons then multiply as an avalanche traversing the dielectric surface, due to a tangential electric field component E_t (see Fig. 18). Several models of this flashover development process are available to data (Anderson and Brainard,[161] Pillai and Hackam,[162]; Avdienko and Malev,[163,164] LeGressus *et al.*,[157,158] Bommakanti and Sudarshan[165]). It should be stressed that both priming electron emission and the tangential electric field E_t are prerequisites required for the surface flashover initiation.

A detailed investigation of ferroelectric cathodes in the nonreversal mode was conducted recently by Krasik *et al.*[87,166] and Dunaevsky *et al.*[88] The experimental setup is shown in Fig. 19. A PZT, $BaTiO_3$ and a linear dielectric printed circuit board (according to the producer Walter Lemmen Ltd. made of fiber glass reinforced with epoxy) with a very low dielectric permittivity ($\varepsilon_r \approx 3$) were studied. The samples were placed inside a cylindrical aluminum box with an output window covered by a stainless steel grid. The cathodes were operated by applying a driving pulse of either positive or negative polarity to the front or to the rear electrode of the ferroelectric sample. The driving pulse ($V_{\mathrm{fe}} = 2-10\,\mathrm{kV}$, $\tau_p = 500\,\mathrm{ns}-50\,\mu\mathrm{s}$) was produced by a pulse generator. All experiments were carried out at a repetition rate of (0.5–2) Hz in a vacuum of 2×10^{-5} Torr. The plasma ion and electron saturation currents were measured simultaneously by an array of biased CFCs in one shot. The electron temperature of the plasma and the plasma electron density were estimated by use of single and double floating probes. The driving voltage and current through the sample were measured by a HV divider (VD1) and Pearson Rogovsky coils (RC1 and RC2). The parameters of the neutral flow were studied by fast Penning probes and the light emission of the plasma was studied by a fast framing camera 4Quik05A with frames $\geqslant$4 ns.

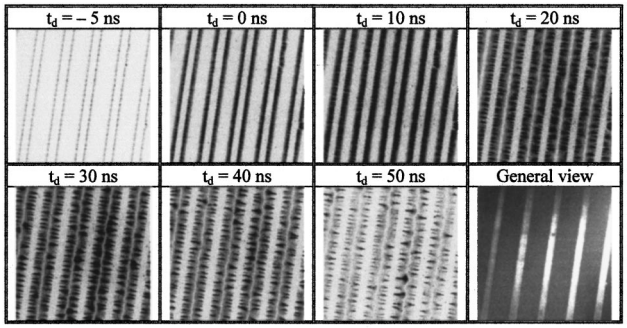

FIG. 20. Typical frames (frame duration $\tau = 10$ ns) of visible light emitted from the surface of the PCB material formed by a surface plasma with a different delay τ_d from the start of the trigger pulse (trigger pulse, 10 kV with duration of 100 ns applied to the rear electrode of the sample).

Typical frames of the visible light emitted by the surface plasma formed at the surface of the PCB are presented in Fig. 20. One can see that the individual surface discharges start within the first 5 ns from the start of the high-voltage pulse at the edges of the strips. Furthermore, these discharges propagate toward each other with a velocity of $V_{pl} \approx 10^7$ cm/s. Already after 35–40 ns from the start of the HV driving pulse, the plasma covers the space between the strips leaving a narrow ($\leqslant 1$ mm) width space in the middle. The decay of the light starts at 50 ns and at $t > 80$ ns no visible light is observed. The temporal evolution of an individual discharge shows that it has a conic spatial structure with the apex at the edge of the strip. Experiments with PZT and $BaTiO_3$ samples showed the plasma formation to be also almost simultaneous with the beginning of the trigger pulse (a few kV).

An interesting feature of the observed noncomplete surface discharge is that the plasma streamers, which are formed at the edges of opposite strips, do not cross each other, leaving a small narrow gap. This is a typical feature of a noncomplete discharge when the discharge current is closed to the displacement current through the sample and the plasma has the same potential as the grounded electrode. Since the leading front of the surface discharge consists of electron flow (avalanching process), it will stop at a certain distance due to the Coulomb repulsive force.

On placing the printed circuit board dielectric in a vacuum at the same voltage amplitude, only a few sporadically appearing discharges were observed. Increasing the voltage amplitude to 20 kV led to an increase in the number of discharges, but still the uniformity and reproducibility of the discharges were poor. A further increase of the HV amplitude caused a breakdown of the circuit board.

The plasma formation should be accompanied by desorption of surface atoms and molecules. It was found that an increase of the amplitude of the driving pulse from 4 to 6 kV led to an almost three times increase of the Penning signal. The pressure in the regions where the probes were located (1 and 3 cm from the front surface of the PZT sample) increased slightly (from 1 to 2×10^{-5} Torr). The neutral density according to the geometrical factor and measured velocity of the neutral flow ($\approx 1\times10^5$ cm/s) is about $n_n \approx 10^{15}\,\mathrm{cm}^{-3}$ in the vicinity (within a 0.1-mm-thick layer) of the front electrode. Thus, the Penning probe measurements showed that application of the driving pulse to the ferroelectric sample leads to neutral flow formation, which may spoil the vacuum in the system.

The measurement of the parameters of the plasma which was produced on the surface of the $BaTiO_3$ and PZT samples showed that the amplitude and duration of the ion and electron plasma saturation currents depend strongly on the amplitude and polarity of the driving pulse, as well as on the method of its application and the polarization state of the samples used. Detailed data are presented in the paper by Dunaevsky *et al.*[88] Here only the main results will be presented.

Electron and ion flows were observed for all tested samples. Moreover, ion and electron flows appeared almost simultaneously, indicating a charge compensated flow (plasma) which propagates outward from the ceramic surface. Time-of-flight measurements show that this plasma flow consists of two components: fast and slow. The fast one has a velocity of up to $(1-2)\times10^7$ cm/s, while the slow one has a velocity of about 0.5×10^6 cm/s. The electron plasma density of the fast and slow plasma flows was estimated as $\leqslant 10^{11}$ and $\leqslant 10^{12}\,\mathrm{cm}^{-3}$, respectively, at a distance of ≈ 2 cm from the front electrode of the sample. The electron plasma temperature of the slow plasma flow was estimated to be about 3 eV. Taking into account the measured divergence of the plasma flow, one can estimate the plasma density in the vicinity of the front electrode (1- to 10-μm thick plasma layer) as $\leqslant (10^{13}-10^{14})\,\mathrm{cm}^{-3}$.

Papers dedicated to the subject showed that a surface flashover plasma can be initiated by either field electron emission (Puchkarev and Mesyats,[152] Shur *et al.*,[16,91]) due to electric field enhancement at triple junctions (nonreversal mode), or ferroelectric electron emission (FEE) induced by a noncompensated charge arising on a polar ferroelectric surface (reversal mode) during polarization reversal (Rosenman *et al.*,[84] Shur and Rosenman[82,83]). A high current density electron beam can be extracted from the surface plasma formed at a free ferroelectric surface by either of the above-mentioned processes (Puchkarev and Mesyats,[152] Advani *et al.*,[133] Shur *et al.*,[82] Shur and Rosenman[83]).

Almost all studies published during the last few years somehow involve plasma generation on a ferroelectric surface (Riege,[127] Pleyber *et al.*,[92]; Shur *et al.*,[16,91,82,83] Rosenman *et al.*,[84] Shannon *et al.*,[86] Benedek *et al.*,[90,96] Flechtner *et al.*,[95] Zhang and Huebner[85]). As a matter of fact, surface plasma can serve as an almost unlimited source of electrons for a strong electron beam current.

The surface plasma can be initiated by the field enhancement in triple junctions according to the above-described mechanism. This mechanism does not involve any ferroelectric properties of materials except a high dielectric constant of PLZT (PZT) ceramics used. The electron emission, according to this scenario, was referred to as a nonreversal mode of plasma-assisted electron emission from ferroelectric. Nevertheless, another plasma initiation mechanism, involving spontaneous polarization reversal and existing in the ferroelectric phase only, has been revealed recently (reversal mode). This new plasma initiation mechanism in the so-called reversal mode will be discussed in the next paragraph.

B. Electron emission from a surface plasma of ferroelectric origin

In the previous paragraph experimental evidence of the plasma-assisted character of strong electron emission in the nonreversal mode from the ferroelectric ceramic PLZT 12/65/35 related to the paraelectric phase and linear dielectric printed circuit board was demonstrated. It was clearly proved that a surface flashover plasma can be the source of electrons for strong electron emission. However, it is still unclear how basic ferroelectric properties of materials may be involved in strong electron emission. So far it is necessary to find a suitable experimental situation and to choose a suitable ferroelectric material which allows the separation of reversal and

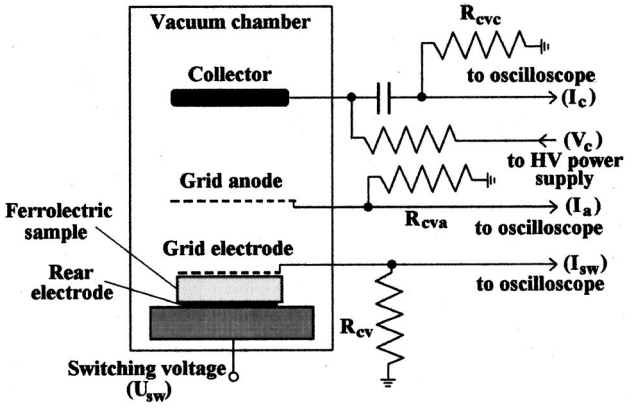

FIG. 21. A schematic diagram of the experimental setup showing a grid anode and solid collector (''anode-collector'' setup).

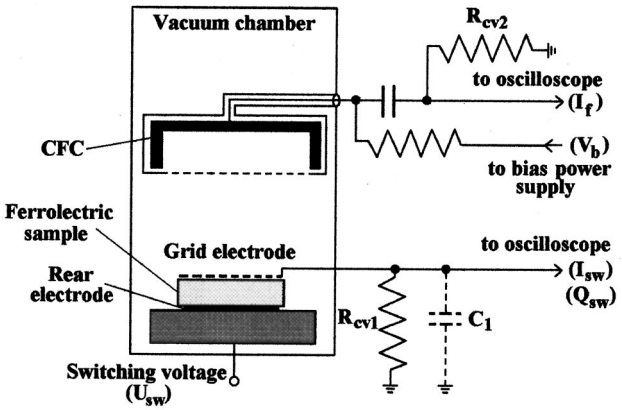

FIG. 22. A schematic diagram of the experimental setup with a collimated Faraday cup (CFC).

nonreversal modes; in other words, induce strong electron emission by spontaneous polarization inversion.

Here, the role of polarization switching in surface plasma formation and subsequent electron emission will be considered by the use of ''model'' (''classic'') TGS crystals[82] which are among the most investigated ferroelectrics.[102,103] The ferroelectric TGS crystal (spontaneous polarization $P_s = 2.8\ \mu C/cm^2$) is easily switched in electric fields of several hundreds of V/cm, facilitating studying basic physical principles of the phenomenon. Furthermore, it can be easily heated up to the paraelectric phase due to the low Curie temperature $T_C = 49\ ^\circ C$ of this crystal.

For studying emission properties of the TGS samples, the following procedure was carried out. One polar surface of the sample was coated with a silver paint to form a rear contact. A copper fine grid (4 μm wire diameter, 16 μm period) was pressed onto another polar surface of the crystals to form a grid electrode. The TGS samples were mounted on a copper holder with an internal heater by gluing the rear contact of the samples to the holder (Fig. 21) with silver paint.

The experimental setup using grid anode and solid collector electrodes for measuring charged particle fluxes is shown in Fig. 21. This setup is similar to the double probe system,[167,168] which results in avoiding a large difference between electron and ion currents. By using this setup, a plasma separation into electrons and ions (if any) should be observed. Either a rectangular switching voltage pulse V_{sw} (amplitude and pulse width were $100\ V \leqslant V_{sw} \leqslant 900\ V$ and $150\ \mu s \leqslant \tau_{pulse} \leqslant 500\ \mu s$, respectively) or a sinusoidal (ac) voltage ($100\ V \leqslant V_{sw} \leqslant 1000\ V$, $20\ Hz \leqslant f \leqslant 1000\ Hz$) was applied to the rear contact of the TGS samples (Fig. 21). The grid was grounded through a current viewing resistor $R_{cv}(10-100\ \Omega)$, in order to measure the switching current by the Merz method.[169,108] The switched charge (Q_{sw}) was measured by an integrating *RC* circuit (charging time constant 10 ms) which replaced R_{cv}. In the case of an ac switching voltage, a hysteresis loop was continuously monitored by the Sawyer–Tower method.[169]

Spontaneous polarization was reversed by applying a switching voltage to the rear contact. Subsequently, the initial polarization direction may be restored by applying a switching voltage of opposite polarity to the rear contact. In the case of the ac switching voltage each period of the sinusoidal wave caused a forward and a subsequent backward polarization switching.

A stainless steel grid (52 μm wire diameter, 460 μm period) was used as an anode placed at a distance of 3 mm from the sample. The anode was grounded through a current viewing resistor $R_{cv}(10\ \Omega - 10\ k\Omega)$. A solid copper collector electrode was placed 2 mm behind the grid anode. The collector was biased by a positive dc voltage V_A (Fig. 21) varied within the range (0–2) kV by using a bypass capacitor (0.1 μF). The collector current I_C was measured by using the current viewing resistor $R_{cv}(10\ \Omega - 100\ k\Omega)$. Both anode ($I_A$) and collector ($I_C$) current wave forms were measured by a digital storage oscilloscope.

Another experimental setup used for charged particles diagnostics is shown in Fig. 22 where a collimated Faraday cup (CFC) replaces the anode and collector electrodes.[84] One can see from Fig. 22 that it is actually a single probe system. From a current–voltage characteristic ($I-V$) of the single probe some plasma parameters can be estimated.[167,168] The circuit for measuring the switching current (I_{sw}), the switched charge (Q_{sw}), and the ferroelectric hysteresis loop (Fig. 22) was the same as that described previously for the ''anode-collector'' setup (Fig. 21). The CFC was biased by a dc voltage (V_b) in the range from -1 to 1 kV. The CFC current (I_{CFC}) was measured by using the same measuring circuit as that for the collector current (I_c) in the ''anode-collector'' setup. The distance between the CFC and the sample surface (Fig. 22) was about 4 mm. All experiments were implemented in a vacuum of 10^{-6} Torr. The temperature of the samples varied within the range of (20–100) °C.

Various analytic tools were used to determine whether a plasma is formed at the surface of the TGS samples. Particularly, optical microscopy, scanning electron microscopy (SEM), and x-ray photoelectron spectroscopy (XPS) techniques were used for a surface analysis of the TGS samples after periodic polarization reversal.[84]

Recorded ion and electron currents (Fig. 23) as well as a surface analysis (Fig. 24; Rosenman *et al.*)[84] showed that a plasma appears on the TGS ferroelectric surface despite the low external voltage applied ($\geqslant 100$ V).

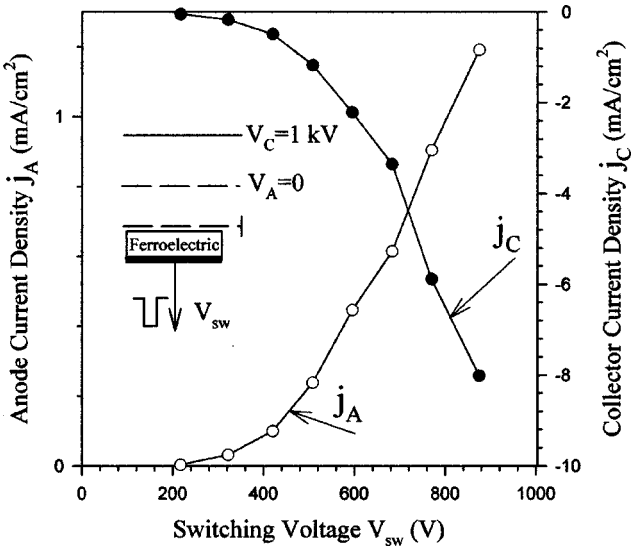

FIG. 23. Anode (j_A) and collector (j_c) current densities (peak values) vs the switching voltage (V_{sw}) for TGS crystals at room temperature.

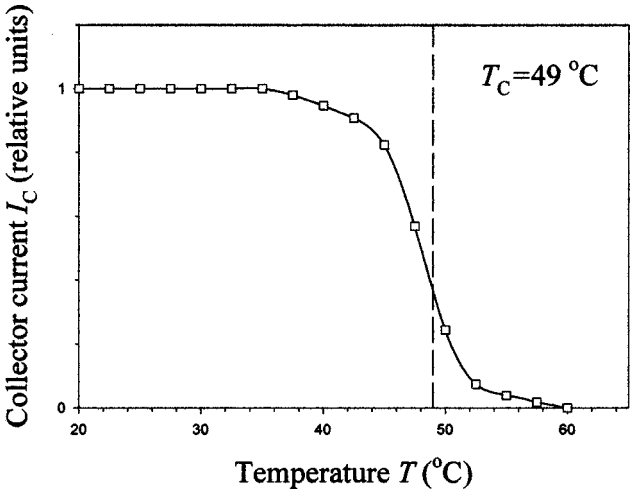

FIG. 25. A typical plot of the collector current (peak value) vs temperature for TGS crystals. The switching voltage is $|V_{sw}| \approx 600$ V (polarization vector is always reversed), while the collector bias voltage is $V_C = 1$ kV.

Figure 25 shows that the electron emission, which can be interpreted as a plasma-assisted effect, is observed in the ferroelectric phase only. The phenomenon disappears above the Curie point (Fig. 25); that is, after the phase transition ferroelectric–paraelectric. We believe that the observed plasma is created due to spontaneous polarization switching occurring in the ferroelectric.[82–84]

Figures 23 and 24, and other experimental data presented in the papers by Shur *et al.*[82] and Rosenman *et al.*,[84] show that the external voltage required to cause polarization reversal in the TGS sample and plasma formation on its free polar surface ($V_{th} \geqslant 100$ V) is one order of magnitude lower than that required to form the plasma on PLZT 12/65/35, which possesses a high dielectric constant ceramic surface without the polarization reversal.[16] This voltage is also one order of magnitude lower than those used to cause strong electron emission from ferroelectrics in basic experimental studies (Gundel *et al.*,[81] Ivers *et al.*,[9] Jiang *et al.*,[10] Sampayan *et al.*,[11] Shannon *et al.*).[86] The surface flashover mechanism described previously (Miller,[155,156] Anderson and Brainard,[161] Avdienko and Malev,[163] Bugaev and Mesyats,[170] Bugaev *et al.*,[171] Brainard and Jensen,[172]) fails to explain the vanishing of the effect in the paraelectric phase, as well as of the drastic decrease of plasma initiation voltages despite the low dielectric constant of the TGS samples ($\varepsilon_{TGS} \ll \varepsilon_{PLZT}$). The above-mentioned considerations imply that a new mechanism of surface plasma initiation on a free ferroelectric surface should be formulated.

The following qualitative mechanism was proposed (Shur *et al.*)[82,83] for surface plasma initiation in the reversal polarization switching mode. It is based on understanding that primary electrons and the high tangential electric field accelerating them along a dielectric surface are required for surface plasma generation. A schematic sketch of the pro-

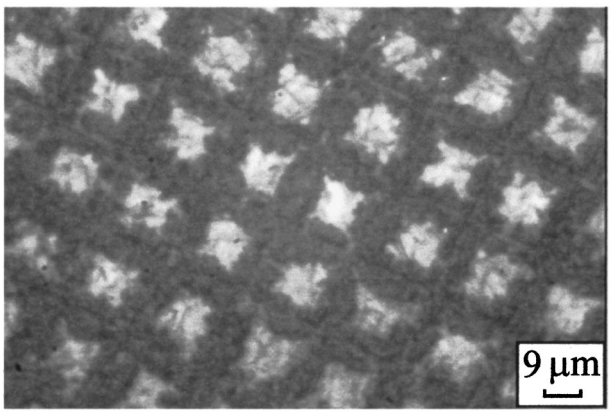

FIG. 24. An optical image of a TGS polar surface after periodic switching by a sinusoidal ac voltage for 30 min ($V_{sw} = 255$ V, $f = 100$ Hz). The image is obtained by a reflected light microscope.

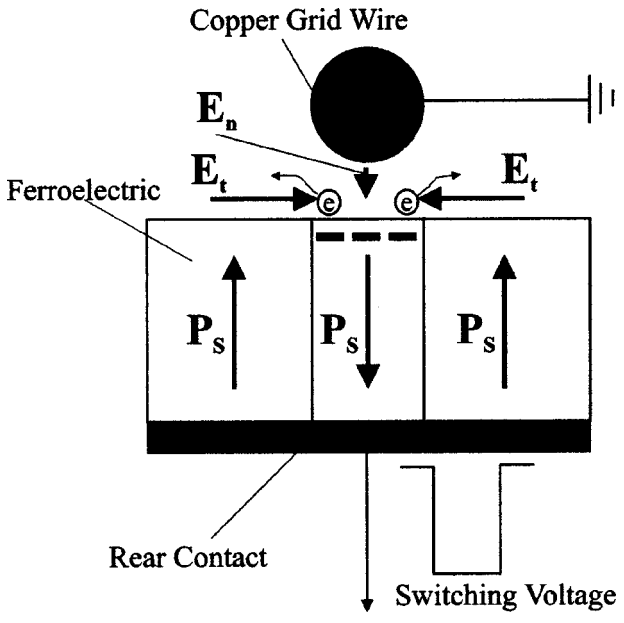

FIG. 26. A simplified schematic drawing of the surface plasma formation mechanism. P_s, E_t, and E_n denote the spontaneous polarization, tangential electric field component, and normal electric field component, respectively.

posed mechanism is shown in Fig. 26. Polarization switching starts under the grid wires and an electron emission current, screening uncompensated polarization charge, begins (Fig. 26). This is the weak electron emission which should be FEE.[3,173] It acts as a priming electron emission current which is required to initiate the surface flashover. Subsequently, the inhomogeneous distribution of noncompensated surface charges may cause a high local potential gradient along the surface (tangential electric field). This tangential field between switched and nonswitched, yet adjacent regions, leads to electron avalanching followed by plasma covering the crystal surface. Fast propagating plasma (the plasma velocity 10^6 cm/s) coats the free polar surface between the strips of the electrodes in a very short time. From this moment the plasma serves as a dynamic electrode for polarization switching in this region.

One can conclude that the initial electrons for the initiation flashover process, as well as the tangential electric field component required for electron avalanching, are of a ferroelectric origin. An avalanche may be triggered by an emission current as low as $\approx$1 nA.[172] The FEE current density from TGS crystals was found to be of the order of 10^{-7} A/cm^2.[72] One can conclude that it is sufficient for the surface flashover initiation.

Optical microscopy (Fig. 25), as well as SEM and XPS analysis indicate that grid evaporation or sputtering occurs in the vicinity of the crystal surface. We believe that this process takes place due to high local current densities from/to the grid electrode when the surface plasma is generated.

A good question to ask is: can the electron current from the TGS cathode be increased up to current densities of several dozens of A/cm^2 as was observed from PLZT 12/65/35 without polarization switching? In order to verify this point, some additional experiments were conducted. We examined the emission from a TGS cathode with either a ring or a grid front electrode. Either positive or negative trigger voltage pulses with an amplitude of $|V_{tr}| \leqslant 2.5$ kV and pulse width within the range 100 ns$\leqslant \tau_{tr} \leqslant 100$ μs were applied to the rear contact of the TGS cathodes. All trigger voltage pulses applied were monopolar in order to eliminate polarization reversal. The experimental setup shown in Fig. 21 was used for the experiments, and all results were verified by using the CFC setup of Fig. 22. All experimental conditions were the same as previously described. It should be stressed that neither electron emission nor plasma formation was observed in these experiments.

The lack of electron emission in the above-described conditions indicates that in the given range of applied voltages ($|V_{tr}| \leqslant 2.5$ kV), a surface plasma followed by electron emission can be induced by polarization reversal only. TGS has a much lower dielectric constant ($\varepsilon \approx 50$) compared to that of PLZT 12/65/35 ceramic ($\varepsilon \approx 3400$). According to Suzuki,[174] for an electrode spacing of 1 mm (typical dimension in our experimental conditions) a dielectric surface flashover voltage of TiO_2 ($\varepsilon \approx 60$) in a vacuum was about 12–14 kV, while the flashover voltage of $BaTiO_3$ ceramic ($\varepsilon \approx 6000$) was only 2–3 kV.

Thus, in contrast to PLZT 12/65/35 ceramics, a voltage of several kV is insufficient for initiating a flashover plasma on a TGS surface in the nonreversal mode by the conventional scenario[156] because of the low dielectric constant. However, a drastic decrease of the flashover voltage can be achieved by involving polarization reversal in surface flashover initiation according to the above-proposed mechanism.

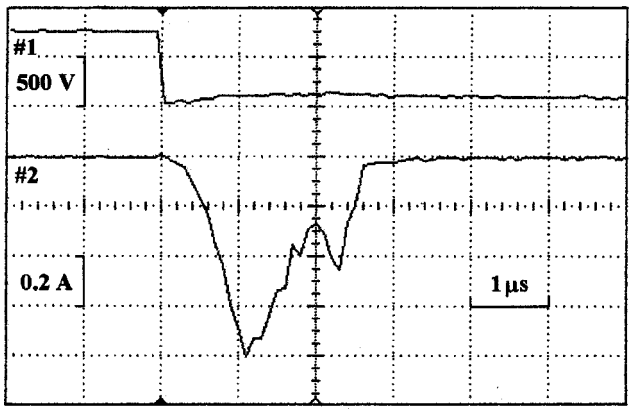

FIG. 27. Traces of the electron emission current (0.2 A/div, lower trace) and the applied voltage (500 V/div, upper trace) in the reversal mode (PLZT 7/65/35). The CFC bias voltage and the emitting area are $V_b = 100$ V and $A_e \approx 0.1$ cm^2, respectively.

C. Reversal and nonreversal modes of plasma assisted electron emission from ferroelectric ceramics

Electron emission properties of PLZT 7/65/35 ceramics should be of interest for a comparative study of electron emission when spontaneous polarization is reversed (reversal mode) and without polarization reversal (nonreversal mode).[83] As was described previously, TGS crystals represent a good ferroelectric material for experimental modeling of strong electron emission from ferroelectrics. However, it has been shown that the strong electron emission cannot be observed in the nonreversal mode from a TGS crystal, due to the rather low dielectric constant of this crystal. This restriction should be avoided in the case of PLZT 7/65/35 ferroelectric ceramics. On the one hand, this composition possesses a high dielectric constant comparable to that of the PLZT 12/65/35 ceramic composition.[99] On the other hand, the PLZT 7/65/35 composition is a ferroelectric one possessing a high spontaneous polarization of several dozens of μC/cm^2.[99] Hence, strong electron emission can be studied by the comparison of the reversal and nonreversal modes realized by using the same PLZT 7/65/35 ferroelectric ceramics. Thus, this study should summarize all plasma-assisted processes which can be involved in strong electron emission from ferroelectric cathodes based on PLZT ceramics. One more interesting effect to be considered is a partial polarization switching followed by backswitching of ferroelectric domains. This was proposed early as a possible explanation of electron emission from ferroelectric ceramics,[81,15] and will be included.

In the reversal mode, the polarization switching current (I_{sw}) and the electron emission current (I_e) are generated by the first (reversing) applied voltage pulse only. Consequent pulses of the same polarity and amplitude cause neither a polarization switching current nor an emission current.

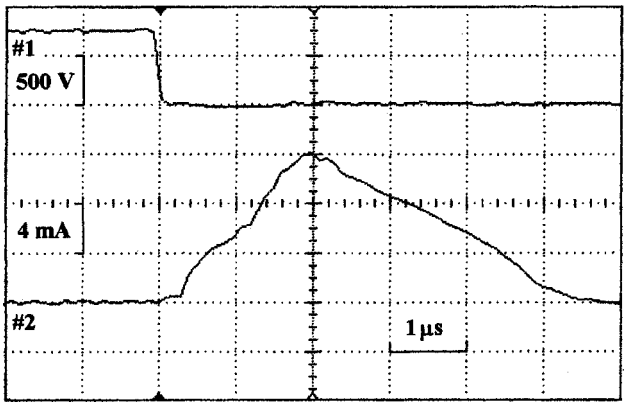

FIG. 28. Traces of the ion emission current (4 mA/div, lower trace) and the applied voltage (500 V/div, upper trace) in the reversal mode (PLZT 7/65/35). The CFC bias voltage and the emitting area are $V_b=-1000$ V and $A_e\approx 0.1$ cm^2, respectively.

Sometimes the second shot induced a much weaker emission current compared to the first one. In this mode the electron emission can be induced only by rather wide applied voltage pulses ($\tau>300$ ns) which are higher than the threshold voltage $V_{\text{thr}}=500$ V.[83]

The polarization switching current and switched charge were measured simultaneously with the electron (ion) emission current. The peak value of the polarization switching current density for an applied voltage of $V_{\text{ap}}=-750$ V was about $j_{\text{sw}}\approx(14\pm 2)$ A/cm^2, and the measured switched charge was about $Q_{\text{sw}}\approx(15\pm 3)\ \mu$C/cm^2.

A typical trace of the electron (the CFC bias voltage $V_B=100$ V) emission current in the reversal mode for an applied voltage $V_{\text{ap}}=-750$ V (pulse width $\tau_{\text{ap}}=100\ \mu$s) is shown in Fig. 27. For the given applied voltage, a peak value of the electron current density was $I_e\approx(7\pm 2)$ A/cm^2, while the electron current pulse width was $\tau_e\approx(0.8\pm 0.2)\ \mu$s (Fig. 27). A rather low negative (retarding) bias voltage ($40\text{ V}\leqslant V_B\leqslant 70$ V) was required in order to cancel the electron current ($I_e=0$). For higher negative CFC bias voltages (V_B) the ion current (I_+) was observed (Fig. 28). The delay time

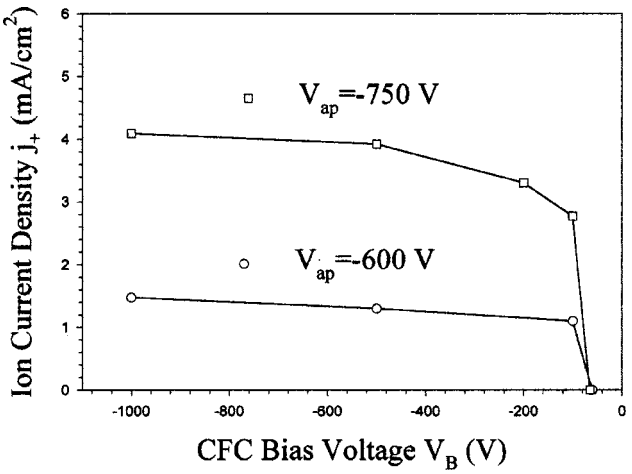

FIG. 29. The ion current density j_+ (peak value) in the reversal mode vs the CFC bias voltage V_b for two different negative applied voltages V_{ap} (PLZT 7/65/35).

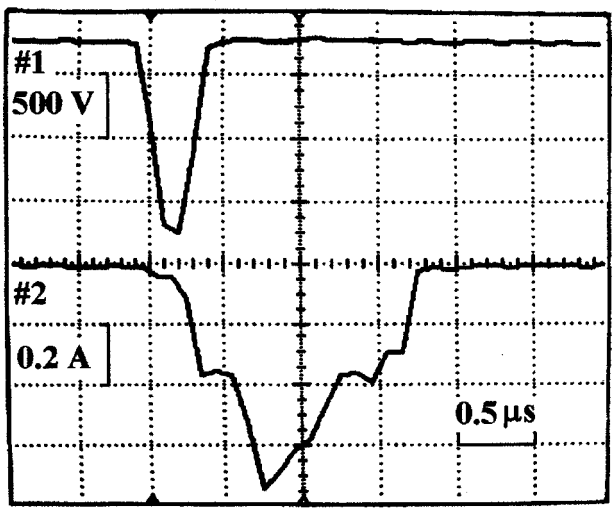

FIG. 30. Traces of the electron emission current (0.2 A/div, lower trace) and the applied voltage (500 V/div, upper trace) in the nonreversal mode (PLZT 7/65/35). The CFC bias voltage is $V_B=100$ V. The applied voltage amplitude is $|V_{\text{ap}}|=1550$ V, the pulse width is $\tau_{\text{ap}}\approx 300$ ns.

of the ion signal with reference to the starting point of the switching voltage pulse was $t_d\approx(460\pm 20)$ ns. The ion current pulse width was $\tau_+\approx(2.3\pm 0.7)\ \mu$s (Fig. 28). A typical trace of the ion ($V_B=-1000$ V) emission current in the reversal mode for applied voltage parameters the same as mentioned previously ($V_{\text{ap}}=-750$ V, pulse width $\tau_{\text{ap}}=100\ \mu$s) is shown in Fig. 29.

The ion current peak value is plotted versus the CFC bias voltage for two different switching voltages ($V_{\text{ap}}=-600$ V and $V_{\text{ap}}=-750$ V) in Fig. 29. One can see that both plots tend to saturate at $|V_B|>100$ V. The saturation ion current density (peak value) was $j_+\approx 1.48$ mA/cm^2 at $V_{\text{ap}}=-600$ V, and $j_+\approx 4.09$ mA/cm^2 at $V_{\text{ap}}=-750$ V.

The result obtained in the nonreversal mode is shown in Fig. 30, which demonstrates typical oscilloscope traces of the applied voltage and the electron emission current. A considerable increase of the applied voltage amplitude ($|V_{\text{ap}}|\geqslant 1500$ V) was required in order to obtain electron emission in the nonreversal mode. Emission current was observed in each shot regardless of polarization reversal. The switching current transient in the nonreversal mode represented a charging current of the capacitor (capacitance of the PLZT 7/65/35 sample). The peak value of the electron current density was $I_e\approx(8\pm 3)$ A/cm^2, while the electron current pulse width was $\tau_e\approx(0.8\pm 0.2)\ \mu$s. It can be seen that the parameters of the electron/ion emission obtained in the nonreversal mode were close to those of the reversal mode regardless of severe differences in applied voltages and delay times.

The experimental results show that a threshold voltage required for electron emission is three times higher in the nonreversal mode ($V_{\text{nr}}\approx 1500$ V) than in the reversal mode ($V_r\approx 500$ V). Moreover, in the nonreversal mode electron emission can be induced by short duration voltage pulses ($\tau_{\text{ap}}<300$ ns) as well as by wider ones. In contrast, in the reversal mode the electron emission current vanishes for short duration voltage pulses ($\tau_{\text{ap}}<300$ ns).

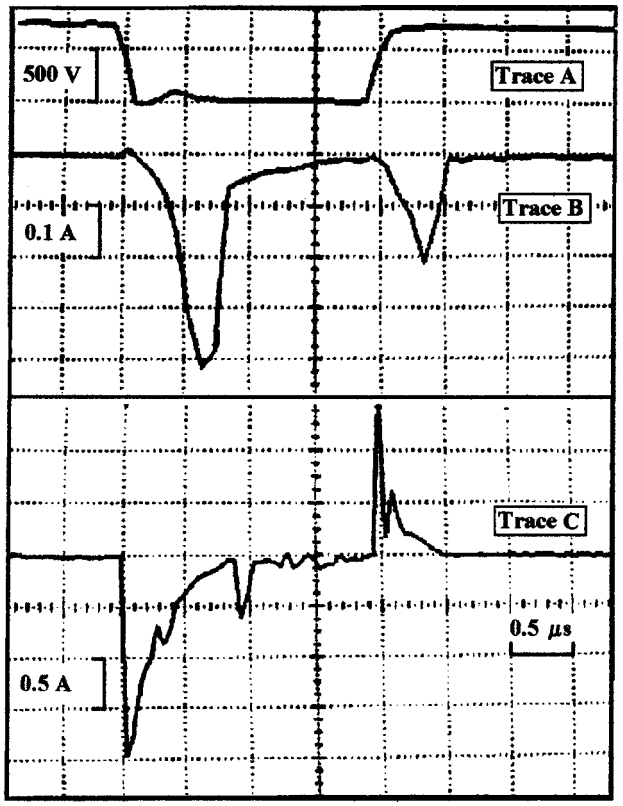

FIG. 31. Traces of the applied voltage (trace A), the electron emission current (trace B), and the switching current (trace C) in the reversal mode (PLZT 7/65/35). The applied voltage amplitude is $|V_{ap}| \approx 750$ V, the pulse width is $\tau_{ap} \approx 2\ \mu$s. The CFC bias voltage is $V_B = 100$ V. The emitting area is $A_e \approx 0.08\ \text{cm}^2$.

Special measurements of the delay time of the electron emission current, with respect to the applied voltage, were carried out with an oscilloscope time scale of 50 ns. They showed that in the reversal mode the delay time was (150 ± 10) ns. In contrast, in the nonreversal mode the delay time was as short as (50 ± 5) ns.

Figure 31 shows typical traces of the applied voltage (trace A), the electron emission current (trace B), and the polarization switching current (trace C) in the reversal mode when the applied voltage pulse is as narrow as $\tau_{ap} = 2\ \mu$s ($V_{ap} = -750$ V). Two electron emission pulses (Fig. 31, trace B) were observed if the applied voltage pulse width was approximately within the range of $1\ \mu\text{s} \leqslant \tau \leqslant 2\ \mu$s. The backswitching current at the falling edge of the applied voltage pulse is opposite in sign to that of the forward polarization switching current (Fig. 31, trace C). The second electron emission current pulse (Fig. 31, trace B) coincided with the backswitching current transient (Fig. 31, trace C) on the time scale. When the applied voltage was within the approximate range of $1.1\ \mu\text{s} \leqslant \tau \leqslant 1.6\ \mu$s, the amplitude of the second electron emission pulse became much higher than that of the first one, which remained the same as that shown in Fig. 31 (trace B). For a pulse width $\tau \leqslant 1\ \mu$s of the applied voltage two emission pulses merged, and a single electron emission current pulse with rather high amplitude and pulse width was observed, as depicted in Fig. 32.

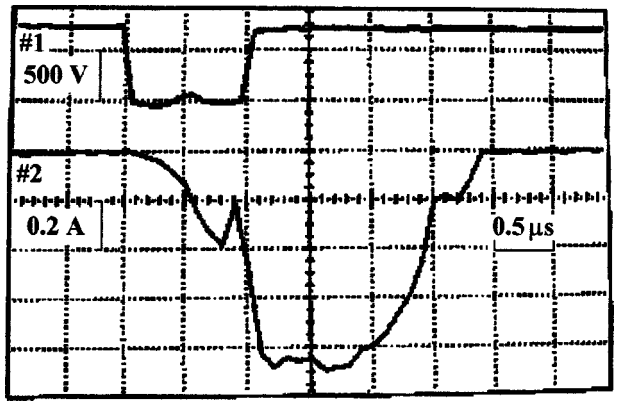

FIG. 32. Traces of the electron emission current (0.2 A/div, bottom trace) and the applied voltage (500 V/div, top trace) in the reversal mode (PLZT 7/65/35). The CFC bias voltage is $V_B = 100$ V. The applied voltage amplitude is $|V_{ap}| \approx 750$ V, the pulse width is $\tau_{ap} \approx 1\ \mu$s. The CFC bias voltage is $V_B = 100$ V. The emitting area is $A_e \approx 0.08\ \text{cm}^2$.

The appearance of the second electron emission current pulse induced by a single applied voltage pulse (Figs. 31 and 32) leads to a severe increase of a total emitted charge. Figure 33 demonstrates that the total emitted charge increases significantly (about 7 times) within the pulse width interval of $0.6\ \mu\text{s} \leqslant \tau \leqslant 2\ \mu$s. The emission (emitted charge) in the reversal mode vanishes for applied voltages with a pulse width of $\tau \leqslant 300$ ns (Fig. 33). As was mentioned at the beginning of this section, in the nonreversal mode electron emission can be obtained by such short pulses ($\tau \leqslant 300$ ns) by using much higher applied voltages.

A physical interpretation of the effects observed may be given on the basis of the ion current component measured in each experiment by biasing the CFC with a negative bias voltage. The ion current recorded in both reversal and nonreversal modes is direct evidence of a surface plasma formation. We believe, however, that regardless of the common plasma-assisted character of the emission, the surface plasma may be initiated by two quite different mechanisms.

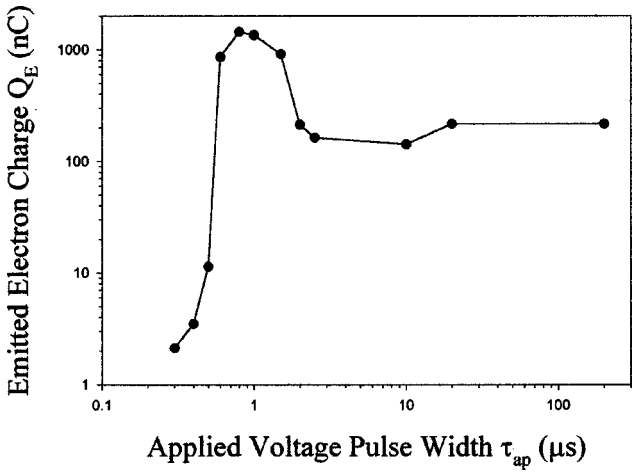

FIG. 33. Total emitted electron charge Q_E vs applied voltage pulse width τ_{ap} in the reversal mode (PLZT 7/65/35). The applied voltage amplitude is $|V_{ap}| \approx 750$ V, the CFC bias voltage is $V_B = 100$ V, and the emitting area is $A_e \approx 0.08\ \text{cm}^2$.

The first one does not require polarization reversal and may also be observed in the paraelectric phase. This is confirmed by the experimental results showing that in the nonreversal mode, electron emission is observed during each applied voltage pulse of the same polarity regardless of polarization reversal. The observed delay of 50 ns is a typical plasma formation delay for the given experimental conditions.[16] The surface plasma and consequent electron emission may be induced by narrow ($\tau_{ap} \leqslant 300$ ns) pulses of rather high voltage ($|V_{ap}| \geqslant 1500$ V). These applied voltage parameters and electron emission current (Fig. 30) characteristics (peak current density and pulse width) are typical for PLZT ceramics, including the particular PLZT 12/65/35 composition (Sec. I E 2). The high dielectric constant of PLZT ceramics ($\varepsilon \approx 1600$ for the PLZT 7/65/35 ceramic studied) causes a considerable field enhancement at triple junctions.[147,152] Therefore, we believe that in the nonreversal mode the plasma formation followed by electron/ion emission should be ascribed to the above-described mechanism.

Surface flashover can also be induced in the reversal mode by an alternative mechanism due to spontaneous polarization reversal.[82,83] This assumption is based on the experimental results for ferroelectric TGS crystals demonstrating that polarization reversal is required in this mode in order to obtain both electron and ion emission currents.

Comparing reversible polarization of PLZT 7/65/35 ($2P_R \approx 63.4\ \mu$C/cm^2 with metal contacts) to the measured switched charge ($Q_{sw} \approx 15.3\ \mu$C/cm^2), one can see that the polarization switching is partial. To this end, it should be noted that an insufficient compensating current decreases the switchable spontaneous polarization.[175] In line with this, two remarks about the compensation process with a dynamic plasma electrode should be given. First, a surface plasma is a finite source of compensating charges (the density of charged particles is incomparable to that of metals). Second, plasma initiation is followed by its expansion into the vacuum, and the plasma density degrades gradually as a function of time. This makes the compensation process at the free ferroelectric surface less effective compared to that at a surface covered with a metal electrode, and as a result leading to partial polarization switching. Nevertheless, we believe that one can approach complete polarization switching by increasing the surface plasma density under higher switching voltages.

One can see from Fig. 31 that the polarization switching (backswitching) current and the first (second) electron emission current are of the same duration. Therefore, we believe that the electron emission pulses shown in Fig. 31 are due to double surface plasma formation caused by partial forward polarization switching (the first pulse) and by backswitching of ferroelectric domains (the second pulse). The backswitching causes the appearance of a second noncompensated charge (opposite sign with respect to the forward reversal) positive in our experimental conditions during the same applied voltage pulse. Therefore, the conditions for surface plasma generation may be achieved twice during the single applied voltage pulse. The rather high electron emission current (Fig. 31) is attributed to emission from the surface plasma. The double plasma formation leads to the drastic increase of the total emitted electron charge (Fig. 31) in the backswitching region ($0.6\ \mu s \leqslant \tau_{ap} \leqslant 2\ \mu$s).

Figure 33 demonstrates that electron emission in the reversal mode vanishes if the applied voltage pulse is narrow ($\tau < 300$ ns). The abrupt decrease of the emitted electron charge for the narrow applied voltage pulses (Fig. 33) should indicate a lack of plasma during both forward polarization reversal and backswitching of ferroelectric domains. This assumption is based on the experimental result showing that neither forward polarization reversal current nor backswitching current was observed for the narrow applied voltage pulses. One can assume that the short time of reversing field application allows only a few spikelike ferroelectric domains (if any) to grow through the crystal. The electric field of noncompensated charges, generated by this process at the free ferroelectric surface, is insufficient for the priming electron emission from the ferroelectric or metal electrode initiating the surface plasma.

The conclusions of the present section can be summarized as follows

(1) Strong electron emission from ferroelectric PLZT 7/65/35 ceramics is a plasma-assisted effect. The surface flashover plasma may be initiated by either field electron emission at triple junctions (nonreversal mode) or ferroelectric electron emission induced by a noncompensated charge arising on the polar ferroelectric surface during polarization reversal (reversal mode).

(2) In the reversal mode a surface plasma may be generated due to both forward polarization reversal and backswitching of ferroelectric domains. This leads to a drastic increase of the emitted electron charge compared to that caused only by polarization reversal.

(3) The difference in activation parameters of ferroelectric cathodes is as follows. In the nonreversal mode the trigger voltage is unipolar whilst the reversal mode is realized only by bipolar pulses. The amplitude of the applied voltage pulse for the ceramics PLZT 7/65/35 in the reversal mode is several times less than that of the nonreversal mode. (Other ferroelectric crystals and ceramics compositions may be found with a very high coercive field that exceeds the voltage needed for the plasma ignition from the tripple points.)

(4) The emission current densities for the reversal and the nonreversal modes of the studied PLZT 7/65/35 composition are comparable. The delay times in the observed modes strongly differ. The delay time in the reversal mode is much longer than that in the nonreversal mode. This property is the principal one which should be observed for any ferroelectric cathode. It is explained by the limited velocity of the ferroelectric domain forward growth.

The important result of this study is a plasma-assisted character of strong electron emission from ferroelectric cathodes in both modes. The electron beam is extracted from the surface plasma by either the external or the surface potential of the ferroelectric cathode. Basic features of ferroelectric cathodes in both the reversal and the nonreversal modes are summarized in Table IV for the different materials used (according to Shur *et al.*,[16,91,82] Rosenman *et al.*,[84] Shur and Rosenman[83]).

TABLE IV. Basic features of ferroelectric cathodes based on different materials in the reversal and nonreversal modes.

	Reversal mode	Nonreversal mode
Ferroelectric material	TGS	PLZT 12/65/35
	PLZT 7/65/35	PLZT 7/65/35
Phase	Ferroelectric only, $T<T_C$	No restriction
Dielectric constant	No restriction	As high as possible
Operating voltage (Applied field)		
(i) Polarity	(i) Bipolar	No restriction
(ii) Field intensity applied	(ii) $E>E_C$	As high as possible
(iii) Rise time of applied voltage pulse	(iii) Any rise time	As short as possible

III. APPLICATIONS OF ELECTRON EMISSION FROM FERROELECTRICS

The previous chapter considered two sorts of electron emission from ferroelectrics. Weak ferroelectric electron emission is an unconventional effect in which the crystal emits electrons as a result of a small variation of temperature (pyroelectric effect), mechanical stress (piezoelectric effect), or polarization inversion. The distinguishing feature of ferroelectrics is a very low conductivity. This allows the preservation of the local surface distribution of induced uncompensated charges of pyroelectric or piezoelectric origin, corresponding to the distribution of the temperature or applied mechanical stresses. In the case of polarization switching, the individual operation of ferroelectric domains also gives rise to a corresponding distribution of uncompensated surface charges. Ferroelectric emission allows conversion of these charges[1] distribution to electron emission flux. The applied technique of position sensitive electron detection to ferroelectrics[1,3] resulted in the visualization of the electron flux by the corresponding optical image. It makes it possible to develop a new generation of devices, such as thermal and x-ray converters. The most attractive application is a ferroelectric flat panel display.

The second phenomenon is a strong emission effect,[6,7,18] which resulted in immense efforts to develop and use high density electron cathodes for microwave generation, gas spark switches, etc.

Here we will present some examples of this new generation of devices based on electron emission from ferroelectrics.

A. Ferroelectric electron emission devices

1. Ferroelectric emissive flat panel displays

Use of ferroelectric materials is rather promising for flat panel display technology. Electrically addressed light valves may be used as a basis for flat panel display.[169] Display devices that are comprised of ferroelectric materials in combination with other active (electroluminescent or photoconductive) materials have also been proposed.[176] An emissive flat display[74,127,75,177,178,5] based on electron emission from ferroelectrics potentially combines the best attributes of cathode ray tubes, such as high efficiency, brightness, and a wide viewing angle, and flat panel displays such as thinness and low weight.

An idea to develop an emissive flat panel display on the basis of ferroelectric thin films $\leqslant 1$ μm thick or bulk ferroelectric materials thinned down to tens of microns was proposed by Auciello *et al.*,[75] Averty *et al.*,[13] Le Bihan *et al.*,[177] Asano *et al.*[74]). In the first demonstration of PZT thin film emission by Auciello *et al.*[75] an emission current density of 10^{-7} A/cm^2 was measured. However, according to Sampayan *et al.*[179] and Gundel[178] a charge density of the order of 1 μC/cm^2 per frame is required for generating a mid-gray scale over the entire screen. A charge density of about only 0.1 nC/cm^2 is available per pulse according to Auciello *et al.*[75] This implies that 10^4 pulses per 10 ms (assuming 100 Hz TV frame rate) should be emitted (1 MHz repetition rate) from a ferroelectric. The high repetition rate of 1 MHz allows one to assume that ferroelectric material fatigue, causing a reduction in the device lifetime, will be a serious problem in developmening a ferroelectric flat panel display.

An experimental model of ferroelectric electron emission demonstrating feasibility of the device concept was developed by Rosenman *et al.*[5] To illustrate FEE display feasibility we used ferroelectric TGS plates of *Y*-polar cut ($10\times1\times10$ mm). A 50 Hz sinusoidal switching voltage was applied between two electrodes. The front electrode was an electron detector—a microchannel plate placed in front of an emitting surface of a TGS sample (Fig. 34). It should be noted that this front electrode which is also a switching electrode should be transparent to electrons, such as a fine grid or a conductive plate with numerous small channels. The second switching electrode, patterned with a required shape,

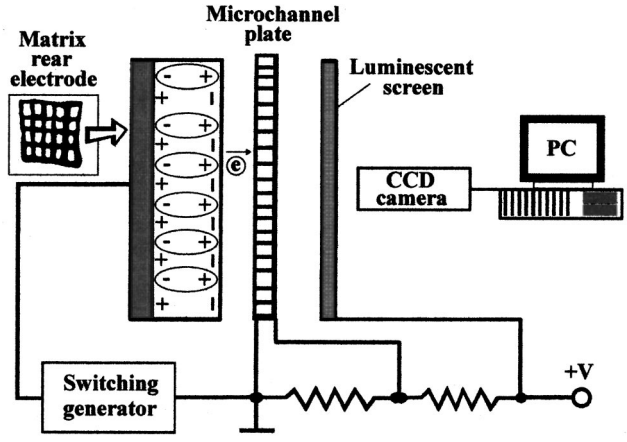

FIG. 34. An experimental setup of a ferroelectric electron emission flat panel display.

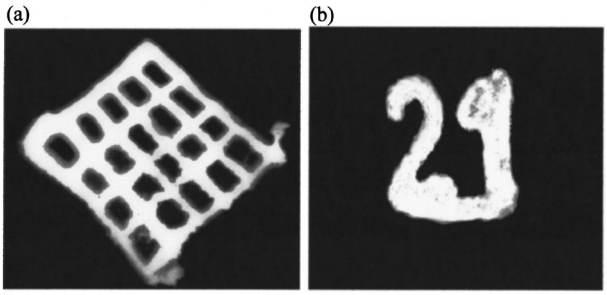

FIG. 35. Ferroelectric electron emission images for different shapes of the rear switching electrode.

was deposited on the rear nonemitting polar surface of the sample (Fig. 34).

Three different types of silver paint electrodes were used as rear electrodes. The first sample was coated with a uniform electrode. A grid-shape electrode was deposited on the rear surface of the second sample and the electrode of the third sample had a ''21'' shape. The electron emission flux was imaged by the use of a phosphor screen. The optical image emerging on the phosphor screen was recorded by a charge-coupled device camera (Fig. 34). The dielectric hysteresis loop was measured by the Sawyer–Tower method in order to analyze the polarization switching process.

Application of a switching voltage larger than 75 V caused the appearance of several bright emission points. Increasing the voltage gradually up to 300 V resulted in observing the images shown in Fig. 35. In the first sample, electron emission was observed from the entire polar front surface. Electron images of the second and third samples [Figs. 35(a) and 35(b)] reproduced the above-mentioned rear electrode shapes, respectively. The dielectric hysteresis loop measured simultaneously with the image was almost saturated, indicating complete switching. The experimental results demonstrate that the electron flux possesses a spatial distribution coinciding with the rear electrode form.

The electron emission current density depends strongly on many parameters such as switching time, crystal work function, sample thickness along the polar axis, etc.[72] An emission current of the order of 10^{-7} A/cm^2 was measured under similar experimental conditions by the use of TGS crystals.[73] The low conductivity of ferroelectrics makes it possible to retain an uncompensated switching charge $\Delta\sigma_s$ on a free polar ferroelectric surface, exactly at the regions where switching occurs (display pixels). Hence, the obtained distribution $\Delta P_s(x,y)$ (x, y are the surface coordinates) corresponds to a distribution of the switching field applied, i.e., to the shape of the rear switching electrode (Fig. 35). If the resulting electric field E is sufficient for the ferroelectric electron emission, the switched crystal regions (domains) will represent themselves as local electron emission cathodes. These cathodes may be individually operated by local domain switching. A pixel shrinking limitation should be related to a minimal electron emission current which can activate the phosphor screen. We believe that this will be the main parameter restricting the display resolution.

The observed results show that the FEE display is flat and that the dielectric properties of the employed ferroelectric material allow one to build it in a ''plane-to-plane'' geometry. Certainly, the data presented demonstrate a static electron display. Clearly, an array of local ferroelectric cathodes (pixels) should be operated by an active electrode matrix deposited on the rear ferroelectric surface.

2. FEE imaging and memory devices

The developed ferroelectric display demonstrates an important ability of ferroelectrics to generate electron emission from individually operated ferroelectric domains or domain clusters. It implies a homogeneous coercive field in the ferroelectric plate used. Here a specific property of ferroelectrics to alter a spatial distribution of the coercive field will be exploited to visualize a hidden x-ray image and neutron flux. Another example of a potential application of the electron emission effect is FEE thermal imaging based on pyroelectrically induced FEE.

X-ray or neutron irradiation of dielectric crystals gives rise to the generation of point defects. The damage-produced mechanism includes both the displacement and the ionization of atoms. In these cases the radiation defects bring about local mechanical strains in the ferroelectric crystal matrix. Unlike linear nonpiezoelectric dielectrics, ferroelectric crystals are media without a center of symmetry. Structural defects in ferroelectrics possess their own dipole moment $\Delta\mu$.[168] For monodomain ferroelectrics, all dipole moments formed by the defects are oriented in the same direction and macroscopic ''defect'' polarization $\Delta P = N\Delta\mu$ (N is the defect concentration) arises.[180] This polarization ΔP is opposite to the spontaneous polarization P_s and causes ferroelectric domain clamping. Experimentally observed hysteresis loops for irradiated ferroelectrics show the existence of an internal bias field. As a result the coercive field in irradiated ferroelectrics increases.[181]

The coercive field and the FEE effect of irradiated ferroelectric TGS crystals were studied.[182] Two sorts of x-ray irradiation were used. Continuous 30 keV x-ray radiation was employed from a conventional x-ray tube. A pulsed x-ray source had the following parameters: energy 500 eV, pulse duration $\tau = 10^{-9}$ s. The estimation of the coercive field E_c from measured hysteresis loops for crystals irradiated by a continuous x-ray flux showed that E_c was enhanced three times (from 0.25 to 0.75 kV/cm) with increasing irradiation exposure doses in the region 0.8×10^3–6.3×10^5 R.

A FEE image was studied from samples preliminarily irradiated through a lead protected mask of a specific form. As a result of the irradiation, a part of the sample was damaged, whilst the other parts were totally protected by the mask. This gives rise to a corresponding distribution of the coercive field when it was larger in the irradiated region than in the nondamaged region. The FEE image was induced by a periodic inversion of the spontaneous polarization of the TGS crystal in a 50 Hz periodic switching field. The experimental setup was identical to that previously described. Figure 36 demonstrates the FEE image of a sample subjected to an exposure dose of 2.3×10^5 R. The applied switching field

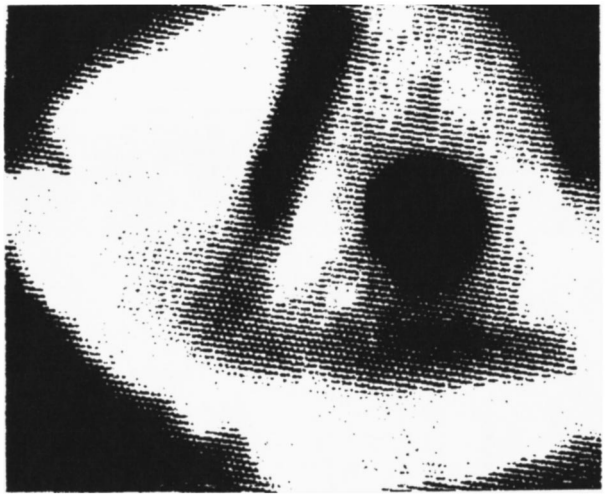

FIG. 36. Ferroelectric electron emission of a hidden x-ray image in a ferroelectric TGS crystal.

was $E_{sw}=0.5\,\mathrm{kV/cm}$, which was twice as much as that for the virgin TGS sample, but it was less than that for the irradiated sample. The FEE image completely duplicated the form of the protected mask, namely the irradiated central part did not emit electrons (it is dark) whilst the nondamaged region of the sample emitted electrons. This method may be used to visualize x-ray hidden images. One of the problems which should be solved is the limited resolution of the position-sensitive electron detector-microchannel plate used, which is about 40 lines/mm.

Similar results were observed with a neutron irradiated TGS sample.[183] The sample was irradiated from a Cf-neutron source. This isotope has a complicated spectrum of the radioactive decay including γ rays and slow and fast neutrons. A special screen protected from γ rays and slow neutrons was used and mainly fast neutrons with a flux of $1.1\times10^{10}\,\mathrm{n/cm^2}$ irradiated the sample. The FEE image demonstrates a distinct contrast where a dark spot is the neutron damaged region (Fig. 37).

The article[183] also reported on FEE visualization of infrared radiation from a CO_2 laser (10.6 μm). In this experiment FEE was induced by the pyroelectric effect. Samples of polar cut monodomain crystals of $LiTaO_3$ 50 μm thick were used. The FEE effect was measured from a C^+ polar face, whilst the opposite C^- face was subjected to irradiation from a CO_2 laser ($P=10\,\mathrm{mW/cm^2}$) through a germanium window in a vacuum chamber. Figure 38 illustrates three photographs taken every 120 ms. The first photograph shows the FEE image corresponding to the profile of the laser beam. The next segment demonstrates fast broadening of the thermal flux along the $LiTaO_3$ pyroelectric target. The third photo shows the process of sample cooling when the laser was switched off. It was shown that a detectivity of the proposed FEE method of IR radiation visualization was $0.1\,\mathrm{mW/cm^2}$.

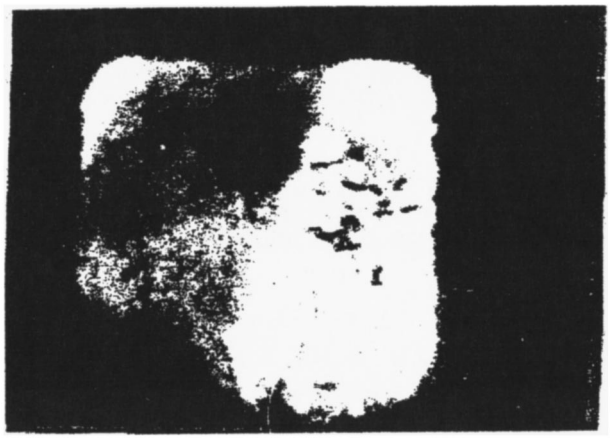

FIG. 37. A ferroelectric electron emission image of a neutron-irradiated TGS crystal.

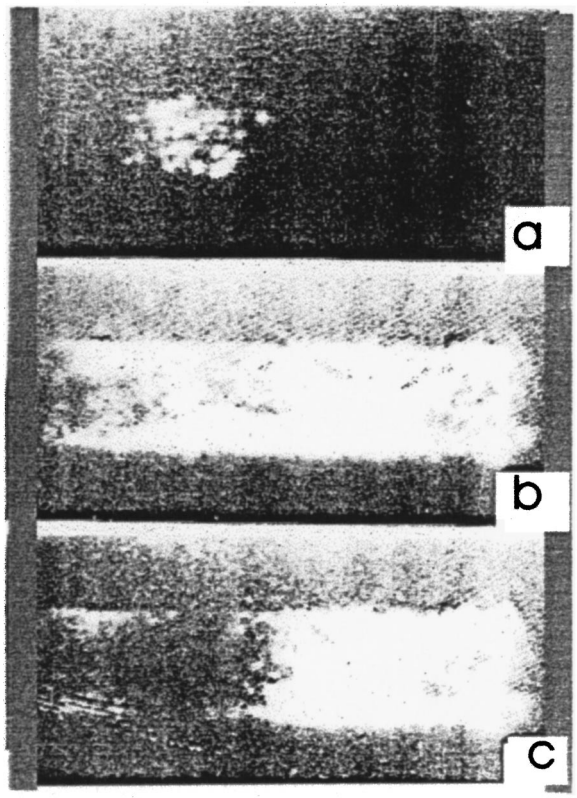

FIG. 38. A ferroelectric electron emission image of an infrared CO_2 laser beam.

B. Ferroelectric cathodes and electron guns

1. Basic parameters

The first observation of high electron current density up to $10^2\,\mathrm{A/cm^2}$ (Gundel *et al.*[6,7]) from ferroelectric materials stimulated the development of ferroelectric cathodes by several research groups (Ivers *et al.*,[9] Jiang *et al.*,[10] Sampayan *et al.*,[11] Cavazos *et al.*,[12] Averty *et al.*,[13] Okuyama *et al.*,[14] Airapetov *et al.*,[15] Benedek *et al.*,[90] Boscolo *et al.*,[89] Shur and Rosenman,[16,91] Advani *et al.*,[133] Krasik *et al.*,[166] Dunaevsky *et al.*,[88,97] Nation *et al.*[184]). A ferroelectric cathode was compared to a thermionic one in the same gun structure by Jiang *et al.*[10] In the same experimental conditions the ferroelectric cathode was able to supply one order of magnitude higher current compared to the thermionic one. Current densities up to $10\,\mathrm{A/cm^2}$ (total current up to 36 A) were obtained

by use of the ferroelectric cathode. A beam brightness (measured at a beam current of 15 A and an extraction voltage of 10 kV) was 1.23×10^{11} A/m^2 sr. By comparing this value with corresponding parameters of conventional cathodes (see the previous text), one can see that such high brightness values can be achieved by Schottky and field emission cathodes only.[185,186] It should be stressed, however, that generating a high total current is not achievable with single field emission cathodes. In contrast, extremely high total currents are available with ferroelectric cathodes. In fact, Advani *et al.*[133] showed that total electron currents with a peak value of up to 1 kA (pulse width of several microseconds) can be generated by ferroelectric cathodes. Thus, despite a current density of hundreds of A/cm^2 available from ferroelectric cathodes (approximately the level of Schottky cathodes), none of the above-mentioned conventional cathodes can achieve very high total currents generated by the use of ferroelectrics.

According to Sampayan *et al.*[11] the measured electron beam brightness was $\sim10^9$ A/m^2 sr (beam current from 6 A at 11 kV up to 42 A at 21 kV), which is two orders of magnitude lower than that measured by Jiang *et al.*[10] This implies considerable scattering in brightness values for different ferroelectric electron guns. Obviously, additional experimental studies are needed to determine the typical electron beam brightness that ferroelectric cathodes can demonstrate.

In the early papers devoted to the strong electron emission from ferroelectrics (see, e.g., papers by Gundel *et al.*,[81] Ivers *et al.*,[9] Airapetov *et al.*[15]) the electron current pulse duration did not exceed several hundreds of ns. Recently, electron current pulse duration was extended to a microsecond time scale.[90,95,133,83] Generating long (microsecond time scale) and flattop current pulses is a matter of importance for high power microwave devices.[187]

The triggering mode of ferroelectric cathodes includes the polarity and application technique of the voltage applied to a ferroelectric cathode. The latter implies that the trigger voltage can be applied to either the rear (solid) or the emitting (grid or strip) electrode. Dependencies of emission current[90] and electron energy[95] on the triggering mode were studied. A study conducted by Shur *et al.*[91] showed a crucial role of the cathode triggering mode in broadening the electron energy spectra and cathode perveance. The perveance P, defined by the relation $P=I/V^{3/2}$, where I is the gun current and V is the voltage,[188] is one of the basic parameters of electron guns. The perveance reached by a gun with a negative trigger voltage applied to the front electrode[91] was as high as 67 μP, while with the same trigger voltage applied to the rear electrode the perveance was only 11 μP. Nevertheless, both of these values exceed by more than one order of magnitude a typical perveance for thermoinic cathodes.[188] However, a perveance of about 280 μP has been achieved in an electron gun with a plasma cathode based on the extraction of electrons from a hollow cathode discharge.[189] One can conclude that a high perveance, which is a typical feature for plasma cathodes, can also be reached by ferroelectric cathodes based on the extraction of the electrons from a surface flashover plasma. It is interesting to note that a perveance of 10–15 μP with a negative trigger voltage applied to the rear electrode has also been achieved by Jiang *et al.*[10] and Sampayan *et al.*[11]

Relative timing between the trigger voltage pulse applied to a ferroelectric sample and application of the accelerating cathode-collector voltage appears to be an important factor influencing ferroelectric cathode parameters. The delayed gap voltage application, which has been studied by several investigators (Sampayan *et al.*,[11] Flechtner *et al.*,[95] Advani *et al.*[133]), showed the existence of an optimal delay time allowing a maximum current density to be generated by the ferroelectric cathode. The experimental optimal delay time was found to be within the range 0.4–5.0 μs. Beyond this time interval the current drops and consequently vanishes.

Recently Dunaevsky *et al.*[88,97,190] studied the operation of an electron diode based on a ferroelectric cathode under the application of high voltage anode–cathode pulses ($\leqslant$45 kV with a repetition rate of 5 Hz and $\leqslant$250 kV in a single shot mode). The obtained results indicate that the source of charged particles is a plasma which is formed on the front electrode of the ferroelectric due to an incomplete surface discharge. Unpoled ferroelectric PZT samples with the front surface covered by copper strips were used. The solid rear electrode was made of copper. The samples were placed inside a cylindrical aluminum box with or without covering the output window by a stainless steel grid. In these experiments, besides the commonly controlled $I-V$ characteristics of electron diode, studies of electron beam uniformity (by use of an array of CFCs and a soft x-ray image of the electron beam) and potential distribution inside the anode–cathode gap (by use of HV floating probes) were carried out. In addition, light emission from the anode–cathode gap was studied by a fast framing camera.

In the experiments with framing photos, a nonpoled PZT sample was placed at a distance of 10 mm from the output cathode grid. A negative driving pulse ($V_{fe}=3$ kV, $t_{dr}\approx10\,\mu$s) was applied to the rear electrode of the sample. An anode–cathode gap of 20 mm was used in this set of experiments. Framing photos (20 ns frame) were taken with a time delay of 200 ns from the start of the driving pulse. When the PFN (pulse forming network) pulse ($V_a=35$ kV, pulse duration $\approx20\,\mu$s) was applied prior to the driving pulse, the observed electron current in the diode was $I_e\approx80$ A ($j_e\approx10$ A/cm^2, $t_e\approx500$ ns). This current started almost simultaneously with the application of the driving pulse. When the driving pulse was applied, light emission appeared at the anode surface and later weak light emission was observed at the surface of the output cathode grid (see photo 1 in Fig. 39). After 200 ns the anode and the cathode light-emitting regions had a width of a few mm with a smooth boundary. The light intensity in these regions decayed almost simultaneously with the end of the electron beam current in the diode. The weak intensity and the fast decay of the light emission indicated the absence of an explosive emission plasma.

The light emission changed when the PFN pulse was applied with $\tau_d\approx1.5\,\mu$s (see photo 2 in Fig. 39). In this regime electron emission started simultaneously with the application of the PFN pulse with the diode current amplitude

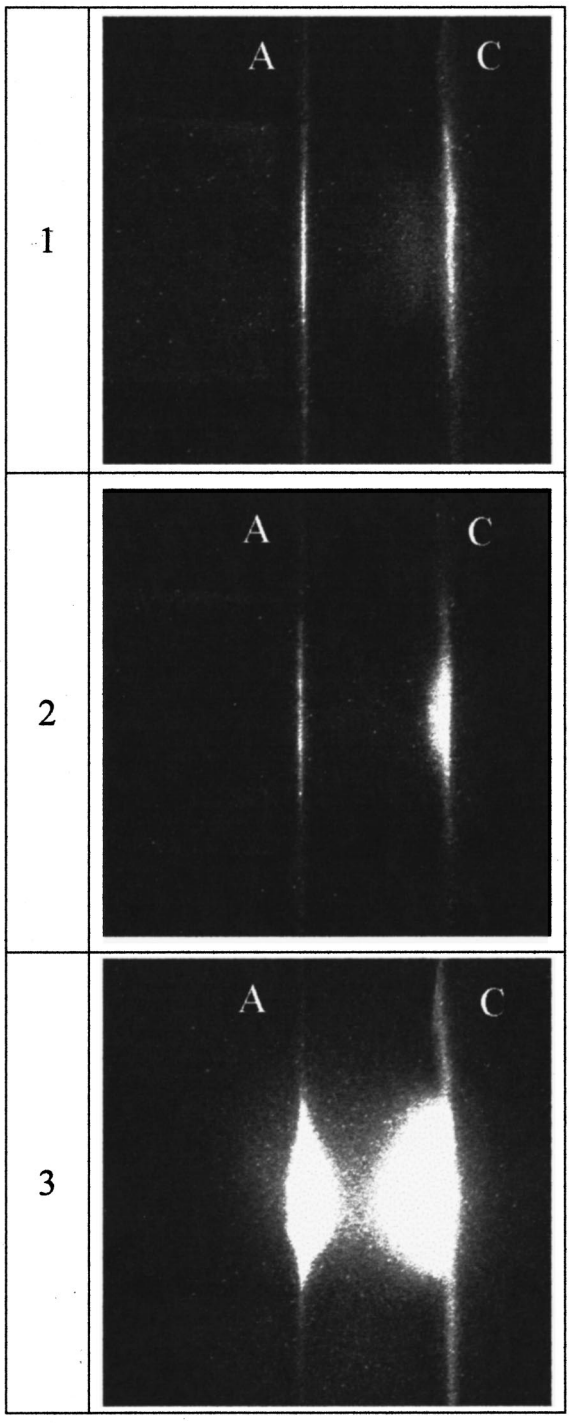

FIG. 39. Framing photos of the visible light emission observed from the planar diode for two different cases: accelerating voltage is applied prior (frame 1) to and after the start of the driving pulse (frames 2 and 3, were taken with a time delay $\tau_d = 1.5\ \mu$s). Frame 2 was taken at 200 ns from the start of the driving pulse, and frame 3 at 750 ns. The frame duration is 20 ns. A—anode; C—cathode.

increasing in time. In this case, a bright layer, which appeared at the output cathode grid at the beginning of the PFN accelerating pulse, was observed. Further, this layer spread with a velocity of $(1-2)\times 10^6$ cm/s and intersected with the anode plasma (see photo 3 in Fig. 39). At this instant a fast increase of the diode current accompanied by a fast decrease of the accelerating voltage were observed. We think that this regime is related to the plasma prefilled operation of the electron diode with the formation and expansion of the explosive plasma.

The plasma nature of a ferroelectric electron source was shown in experiments with an electron diode. It was shown that the temporal behavior of the diode impedance strongly depends on the time delay between the application of the driving pulse and the beginning of the accelerating pulse. Without the plasma prefilling of the anode gap the diode impedance decreases within the accelerating pulse due to the explosive emission plasma expansion. In the case of the absence of the explosive emission plasma and an infinite source of electrons, the diode impedance Z_d should be proportional to $V_a^{-1/2}$. However, in the experiment a rising or quasiconstant impedance was observed that can be associated only with the preliminary plasma prefilling of the anode–cathode gap.

It was found that in the plasma prefilled regime, electron beam generation with a current density of several hundreds of A/cm^2 is possible (with an applied accelerating voltage of several tens of kV). By properly adjusting τ_d, $V_{\rm fe}$, V_a, and $d_{\rm ac}$, an electron beam with duration of several hundreds of nanoseconds was obtained. In addition, depending on the values of τ_d, $V_{\rm fe}$, V_a, and $d_{\rm ac}$, diode operation with or without the formation of an explosive emission plasma was observed. Besides, we obtained diode operation with a quasistationary boundary of the plasma which provides almost a constant diode impedance.

According to the results, it is evident that the diode operation as well as the characteristics of the extracted electron beam depend strongly on the parameters of the driving pulse, the parameters of the accelerating voltage source, and the cathode geometry. The large divergence in the amplitude and duration of the extracted electron beams observed in previous studies can be explained by differences in the abovementioned experimental conditions. The present research shows that plasma cathodes, based on ferroelectric materials, can be successfully used in an electron diode configuration to generate high-current electron beams. Extensive experimental data dedicated to the subject have been presented in the paper by Dunaevsky *et al.*[88]

Recently an electron gun device supplying a few hundred amperes at 500 keV and based on a ferroelectric cathode was developed.[191] The gun should be used to generate high power microwaves by the use of a TWT amplifier. The ferroelectric cathode was based on PZT prepoled ferroelectric ceramics 1 mm thick with an exposed cathode area of 2.8 cm^2. A thin grid consisting of a number of 200 μm width silver strips, spaced 200 μm from each other was deposited on the front ferroelectric surface. The grid was grounded and a positive trigger voltage pulse of 1 kV was applied to the rear surface of the ferroelectric sample. Emission was observed as 250 ns width pulses in a repetitive mode (1 Hz repetition rate). An electron current density as high as 125 A/cm^2 was observed. The rise time of the electron beam current was less than 20 ns. The authors assumed that field emission from triple points may lead to plasma formation at the ferroelectric surface.

The above-considered results show that high quality pulsed electron guns based on the ferroelectric cathodes can be developed for use in high power microwave generation. According to Thumm,[192] in high power cw (or long pulse) gyro-devices thermionic impregnated dispenser cathodes or thermionic lanthanum hexaboride are mostly used. Short pulse high power gyro-devices also use cold cathode explosive emission guns.[192] High current ferroelectric cathodes have a potential to change the situation in this field after preliminary results demonstrating the use of such cathodes for CRM (gyrotron) microwave oscillators.[19,193] Besides high total current and brightness, basic advantages of the ferroelectric cathodes for microwave applications are their ruggedness, absence of high vacuum requirements, instant turn-on capabilities, ease in manufacturing, and low cost.

2. Electron energy spectra of ferroelectric cathodes

The electron energy spread is an important quality factor for electron sources and may play a crucial role for applications of these cathodes, especially in microwave tubes. Electron energies were measured by the retarding potential method by Gundel *et al.*,[81] Ivers *et al.*,[9] and Flechtner *et al.*[95] Gundel *et al.*[93] measured the emitted charge versus decelerating voltage on a retarding grid in order to estimate the energy spectrum of the electrons emitted from the ferroelectric cathodes. The emitted charge decreased gradually with increasing the retarding potential, thereby demonstrating two different slopes of the resulting emitted charge—decelerating voltage plot.[93] The plots showed that the electron energy spans from 0 up to several kV corresponding to the amplitude of the negative trigger voltage applied to the rear electrode of the cathode. Thus, the measurements by Gundel *et al.*[93] showed a rather wide electron energy distribution from zero energies up to values slightly higher than the negative trigger voltage applied to the rear electrode of the ferroelectric cathode.

Qualitatively similar results for negative pulses applied to the rear electrode were presented by Flechtner *et al.*[95] Furthermore, Flechtner *et al.*[95] showed that the electron energies were much higher with a negative trigger voltage compared to a positive one. Applying positive trigger pulses to the rear electrode, Ivers *et al.*[9] measured low energies of the emitted electrons (up to 60 eV). However, Flechtner *et al.*[95] found that one can increase the electron energies up to about the trigger voltage value ($\geqslant$1 keV) by applying a negative trigger voltage pulse to the rear electrode.

Auciello *et al.*[75] measured emitted electron energies using the CMA of an Auger electron spectrometer. A sharp electron energy distribution (full width at half maximum $\approx$30 eV) was observed by exciting a 110-μm-thick ferroelectric cathode with a negative trigger pulse via the rear electrode (after restoring the polarization vector by a positive pulse). A sharp energy distribution centered around 265 eV remained the same for excitation (trigger) voltages within the 300–400 V range.[75]

A detailed study of the electron energy spectrum as a function of the triggering mode was conducted by Shur *et al.*[91] Figure 40 shows an electron energy spectrum of a PLZT ceramic cathode, triggered by negative voltage pulses

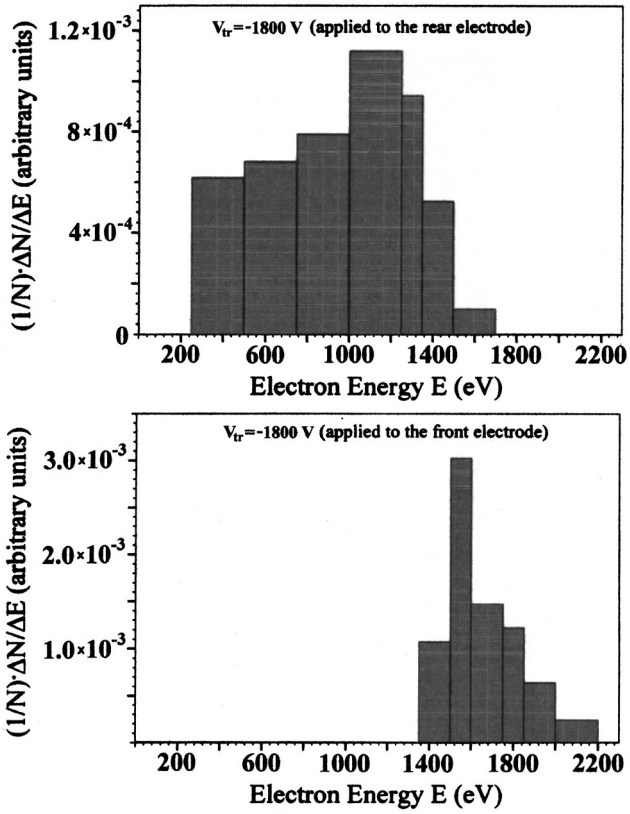

FIG. 40. Experimental electron energy spectra for the same negative trigger voltage ($|V_{tr}| = 1800$ V) applied to the rear electrode (upper graph) and to the front (ring) electrode (lower graph).

applied to the front electrode, compared to the same voltage applied to the rear one. The energy spectra are quite different. The latter electron energy spectrum (the cathode triggered via the rear electrode) is much wider with a full width at half maximum of about 1100 eV, while the former one (the cathode triggered via the front electrode) is about 100 eV. Moreover, in the case of triggering via the front electrode, the maximum of the spectral distribution is shifted toward higher energies by $\approx$400 eV.

To interpret the electron energy spectra, a static potential distribution at the cathode surface was simulated [Figs. 41(a) and 41(b)] for both triggering modes. The partial differential equation TOOLBOX for MATLAB, utilizing the finite element numerical technique was used. One can see that in the case of triggering via the front electrode (mode *B*), at the initial stage of the surface flashover the electric field E_n is retarding for plasma electrons [Fig. 41(b)]. Therefore, the electrons together with ions may reach the expander grid where charge separation occurs [Fig. 41(b)] due to the plasma expansion gradient. If the plasma inside the expander has a negative potential close to the applied trigger voltage V_{tr}, the electrons will be pushed out of the plasma by the accelerating potential difference between the grounded intermediate grid and the negative plasma potential [Fig. 41(b)]. The experimental electron energy spectrum (Fig. 40) is rather narrow in mode *B*, and it probably corresponds to the potential distribution in the plasma, which should be narrower than that of the dielectric surface [Fig. 41(a)].

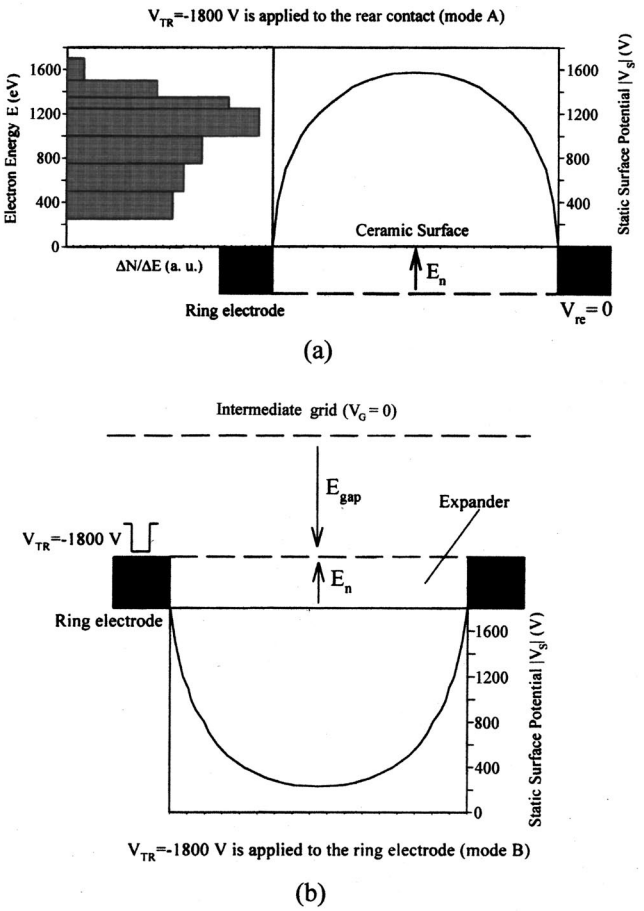

FIG. 41. (a) Calculated static potential distribution at the ceramic cathode surface for the triggering mode A ($V_{tr}=-1800$ V is applied to the rear contact) compared to the energy spectrum of the emitted electrons. (b) Calculated static potential distribution at the cathode surface for the triggering mode B ($V_{tr}=-1800$ V is applied to the ring electrode) with a simplified electric field diagram.

One can see from Fig. 41(a) that there is reasonable agreement between the wide electron energy spectrum measured and the calculated surface potential distribution in the case of the triggering via the rear electrode (mode *A*). In mode *A* the electric field E_n is accelerating for electrons. Therefore, electrons already in the vicinity of the ceramic surface may be extracted from the plasma due to a low plasma density in mode *A*. Hence, one can assume that in mode *A* the electron energies should follow a rather wide surface potential distribution [Fig. 41(a)].

Estimations of the expanded plasma density in mode *B* from the measured ion current showed that it is of the order $n_{pl}\approx 3\times 10^9\,\mathrm{cm}^{-3}$. Additional estimations showed that the plasma density near the cathode surface could be as high as $n_{pl}\approx 10^{12}\,\mathrm{cm}^{-3}$.

Examining the literature related to surface flashover physics, one can see that desorption of adsorbed gases occurs prior to surface flashover (Bugaev *et al.*,[148]) Avdienko and Malev,[163] Gray[194]). According to these studies molecules can travel (1–5) μm after being desorbed before flashover begins. This implies that the initial ionization occurs in a very thin layer of desorbed gas (1–5) μm adjacent to the dielectric surface, which may be considered as the initial plasma layer thickness. For the above-estimated plasma density near the cathode surface ($n_{pl}\approx 10^{12}\,\mathrm{cm}^{-3}$) and a typical electron temperature of 1 eV, the Debye length is $L_D\approx 7.4\,\mu$m, which is rather close to the range of (1–5) μm. This implies that during plasma generation the plasma density is also influenced by the potential of the ceramic surface [Figs. 41(a) and 41(b)].

Thus, the ionization process within the streamer is accompanied by charge separation due to the charged dielectric surface. It should be noted that this qualitative explanation and diagrams of Fig. 41 may not be applicable for further stages of the flashover characterized by dense plasma generation.

Studies of temporally and spatially resolved energy spectra of charged particles emitted from ferroelectric cathodes were recently conducted by Dunaevsky *et al.*[195,190] Ferroelectric cathodes based on unpoled and poled PZT-856 ($\varnothing=40$ mm, $\delta=2$ mm, $\varepsilon_r\approx 4000$) were used in this research. The front electrode consisted of a structure of interconnected 1.5 mm width strips with a 1.5–2 mm spacing between the strips. The cathodes were operated by applying a driving pulse ($V_{fc}=2-10$ kV, $\tau_p=500$ ns) of either positive or negative polarity to the front or to the rear electrode of the ferroelectric samples.

For measuring the energy of the emitted charged particles an electrostatic spectrometer was used. A system of diaphragms limited the divergence of the microbeam to about 3 mrad. Deflection of the microbeam occurs when it passes the region between two parallel electrodes with a dc electric field between them. To analyze the deflected charged particles a gated (700–1000 V, 60 ns) MCP with a phosphor screen placed behind it was used. A framing camera 4Quick05A was used to observe the electron pattern on the phosphor screen. It was determined that the sensitivity of the spectrometer is $\leqslant 20\ \mu\mathrm{A/cm}^2$. For aligning the spectrometer opposite different regions of the cathode, a HeNe laser was used.

With a positively poled PZT sample, electrons with an energy of $\leqslant 2$ keV were obtained when the amplitude of the positive driving pulse applied to the rear electrode was $\leqslant 6$ kV. For the case of a negative driving pulse applied to the rear electrode, no deflected electron microbeam patterns were observed. A similar situation was realized for the negatively poled PZT sample, i.e., no electron microbeam patterns were observed for the positive driving pulse applied to the rear electrode. In the case of a negative driving pulse applied to the rear electrode, the energy of electrons was found to be $\leqslant 1.3$ keV when the amplitude of the driving pulse was 4 kV.

For unpoled PZT samples the energy of the emitted electrons also does not exceed 1.4 keV when the amplitude of the negative driving pulse applied to the rear electrode was $\leqslant 4.5$ kV. Energetic electrons and ions ($E_{e,I}\leqslant 4.2$ keV) were observed when a positive driving pulse was applied to the front electrode of both unpoled and poled PZT samples.

Thus, the same qualitative results concerning the energy of the emitted electrons and ions were observed with poled and nonpoled PZT samples. Namely, the authors observed neither electrons nor ions with energies exceeding the driv-

ing pulse amplitude when it was applied to either a rear or front electrode.

The variation in energy of electrons emitted from different regions of the ferroelectric cathode surface can be explained if one assumes that the plasma density decreases from the strip electrode edge toward the middle point of the space between the strips. A part of the plasma ions are attracted to the ferroelectric surface in order to compensate the negative surface charge. In this case the plasma may have a noncompensated negative potential which increases toward the middle point between the two strips. This negative potential leads to the emission of electrons with increased energy from the plasma. Certainly, this explanation needs additional proof; for instance, by nondisturbing spectroscopic measurements of the temporal and spatial distributions of the surface potential.

When a negative driving pulse was applied to the front electrode, the energy of the emitted electrons was almost equal to the amplitude of the driving pulse. This result is consistent with the plasma model because in this case the simple diode configuration was realized. Indeed, the entrance diaphragm of the spectrometer serves as a grounded anode with respect to the ferroelectric plasma cathode. This suggestion is consistent also with the observation of energetic ions when a positive polarity driving pulse was applied to the front electrode. Taking into account the time of flight which ions need in order to pass from the cathode to the MCP, one can conclude that the ion emission begins within the first 10–20 ns of the positive driving pulse. We believe that only a plasma formation model can explain the observation of ions with energies determined by the driving pulse amplitude.

The existence of the energetic charge particle flux emitted by the ferroelectric cathode, together with plasma prefilling the electron diode, virtually explain numerous experimental results where a considerable increase of the emission current above the space charge limited value was demonstrated. Indeed, it is well known that the comparison of the observed electron current density with a space charge limited one can be valid only in the case of a vacuum diode with zero initial electron velocity. The data above-mentioned show that this is not the case when ferroelectric cathodes are used.

3. Lifetime of ferroelectric cathodes

Some basic parameters of ferroelectric cathodes such as electron current density, brightness, perveance, and energy spectra have been studied by M. Einat. These studies demonstrated fairly good figures of merit compared to classical electron sources. It was shown previously that regardless of the phase state and modes of the initial electron emission excitation (ferroelectric electron emission under polarization reversal, field-induced phase transition, or field emission from triple junctions), the strong emission from ferroelectric cathodes is a plasma-assisted effect. One may assume that the surface flashover plasma should cause damage to the cathode surface, influence reproducibility of the emission current, and limit the cathode lifetime. Recent publications reported observations of erosion of deposited front patterned electrodes and the ferroelectric surface itself.[92,82,85]

In this paragraph an experimental study of the lifetime and the reproducibility of ferroelectric cathodes, which is extremely important for predicting future applications, will be presented. This study was conducted with ferroelectrics of different crystal structures, different phase states, and in different modes of electron emission excitation (with and without polarization reversal). The ferroelectric ceramics PLZT 12/65/35, PZT (APC-856),[196] and TGS ferroelectric single crystals were investigated. These materials are related to different phase states: TGS crystals and poled PZT (APC-856) ceramics possess macroscopic spontaneous polarization (ferroelectric state), whilst PLZT 12/65/35 composition is in the paraelectric phase, and it represents a linear dielectric with high dielectric permittivity of $\varepsilon_r \approx 3400$.

The experimental setup was traditional for ferroelectric cathode studies. A continuous electrode was applied to the rear surface of the sample (rear electrode). Different patterned electrodes (strip, grid, or ring) were deposited on the front emitting surface (front electrode). In the experiments with TGS crystals a fine copper grid (4 μm wire diameter, 16 μm period) was used. A brass washer with internal diameter of 3.4 mm served as the front electrode. TGS monodomain crystals 0.5 mm thick were tested in the reversal mode with a continuous sinusoidal (ac) voltage ($V_{\mathrm{rms}} = 250$ V) of 100 Hz frequency, applied to the rear electrode for 30 min. The PLZT 12/65/35 ceramic samples were subjected via the front electrode to negative rectangular high voltage pulses with the following parameters: $1.5\,\mathrm{kV} \leqslant |V_{\mathrm{tr}}| \leqslant 2.5\,\mathrm{kV}$, pulse width of $\tau_{\mathrm{tr}} = 150$ ns, and repetition rate of up to 10 kHz. In both the TGS and PLZT 12/65/35 experiments mentioned previously, ion and electron emission currents were measured by a collimated Faraday cup (CFC). The surface damage was inspected by reflected light optical microscopy. All experiments were conducted in a vacuum of $\sim 10^{-5}$ Torr.

A lifetime test was performed on a PZT (APC-856) $10 \times 10 \times 1$ ceramic sample using a nonreversal mode of the emission excitation. The cathode was subjected to monopolar negative rectangular voltage pulses (<1 kV with a repetition rate of 100–200 Hz and a rise time of less than 100 ns) via the front electrode. The emission current was measured by a Faraday cup. Six consequent cycles of apparently 10 min each were performed. The reproducibility of the electron emission current was investigated after each consequent cycle and the damage to the sample was investigated after 20, 40, and 45 min of the cathode operation.

The lifetime test with TGS ferroelectric monocrystal cathode showed that the threshold voltage required for the emission excitation was as small as 100 V. Both ion and electron emission currents were observed.[82] The examination of the TGS crystal surface demonstrated a strong damage of the emitting surface. A grid pattern identical to the primary grid electrode was observed on the surface. XPS analysis resulted in the discovery of copper atoms implanted into the TGS crystal matrix, as a result of screening the depolarization field by ions from the plasma during polarization reversal.[82,84] The experiment showed that cathode operation

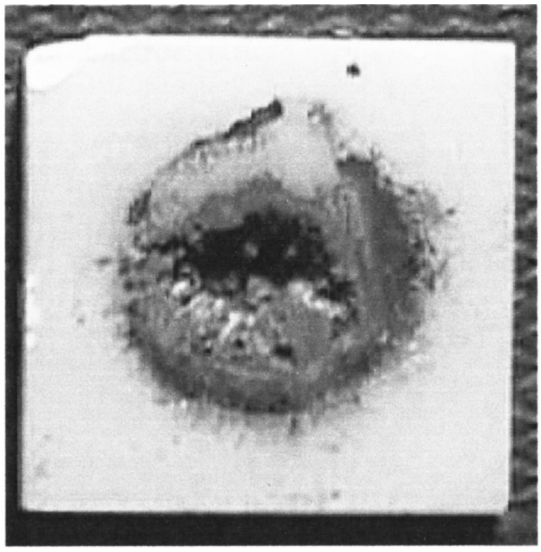

FIG. 42. Damage of the ferroelectric sample PLZT 12/65/35 after 30 min of continuous operation.

led to evaporation of the copper grid electrode.

The PLZT 12/65/35 cathode was operated at a 1 kHz repetition rate. Electron current irreproducibility was observed from the first seconds of the cathode operation. At the end of the test, the time duration of the electron current had been reduced from 100 ns at the beginning to short spikes of several nanoseconds, and the number of missed pulses was more than 50%. Severe damage was observed in the tested sample (see Fig. 42). A hole of 0.5 mm diameter completely through the center of the ring electrode was found after 30 min of continuous work.

Studies of PZT (APC 856) ceramics showed that the first high voltage pulses (applied to the cathode manually for verification of the emission current parameters) caused several stable electron emission current pulses with ≈ 5 A peak current. Periodic operation with a repetition rate of $f = 100$ Hz caused a decrease of the electron current. The maximum peak value of the electron current was $I = 3.1$ A. Subsequently testing the PZT cathode at a frequency of $f = 100$ Hz led to a gradual degradation of the electron current parameters. After 1 min of cathode operation (6×10^3 shots) two distinct peaks, instead of one peak, were observed. The maximum current decreased to $I = 2.2$ A. Subsequent testing showed that the emission current pulse duration τ_{dur} decreased from $\tau_{dur} = 200$ ns in the first 6×10^3 shots, to $\tau_{dur} = 120$ ns after 190×10^3 shots. Considerable reduction was observed in the emission charge, which characterizes a total emission capability of the cathode per pulse. The emitted charge decreased by a factor of 3 during the test, from 3.1×10^{-7} C per pulse to 0.9×10^{-7} C per pulse. Figure 43 shows the dependence of the electron emitted charge Q per pulse versus the number of shots.

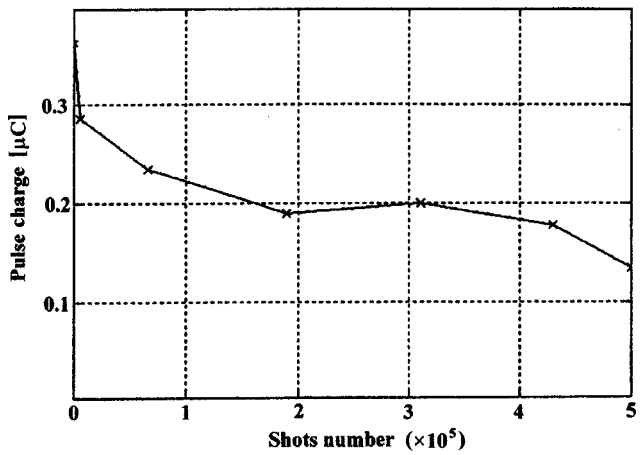

FIG. 43. The electron emission current-pulse charge degradation from PZT ceramics.

It should be noted that despite the rather low repetition rate ($f = 100$ Hz) the electron current did not appear for each applied high voltage pulse. While at the first stage of the test, a current pulse was observed for each shot; at the last stage, after 500×10^3 shots, about 20%–30% of the high voltage pulses produced a current pulse.

During the experiment, a gradually growing damage of the cathode surface was observed—from a small local damaged point on the surface at the beginning to severe damage leading finally to total destruction of the cathode bulk. The surface damage development was correlated to a reduction in the measured electron current.

It has been shown previously that ferroelectric cathodes may be operated in two different plasma-assisted modes. The first mode is a reversal mode when surface plasma followed by strong electron emission is initiated by polarization reversal. The nonreversal mode is observed when a ferroelectric material is in the paraelectric phase or when a material in the ferroelectric phase is subjected to an applied field of the same direction as that of spontaneous polarization vector, thus eliminating polarization reversal.

The studied ferroelectric cathodes relate to different phase states. The strong electron emission was excited in both of the above-mentioned modes. The TGS ferroelectric crystals were investigated in the reversal mode where an applied sinusoidal voltage causes periodic inversion of spontaneous polarization. Both ferroelectric ceramics that were associated with quite different phase states were tested in the nonreversal mode. The ceramic PLZT 12/65/35 does not possess spontaneous polarization at all. Application of repetitive unipolar high voltage pulses to PZT (APC 856) ceramics also eliminated polarization reversal. Regardless of all the above-mentioned differences between the studied ferroelectric cathodes, in both emission excitation modes, the following common features were observed: (a) strong electron emission, (b) visible light emission, (c) ion emission, (d) erosive surface damage, and (e) irreproducibility of electron current and charge at high repetition rates. The points (a)–(e) are evidence that strong electron emission is a plasma-assisted effect.

A surface plasma in a vacuum may be generated in two ways. The first one is desorption and ionization of atoms and molecules of residual gases localized on the ferroelectric surface. The second way is sputtering and evaporation of the surface atoms from the ferroelectric cathode material and electrode. The repetition rate of the applied high voltage

TABLE V. Basic parameters of conventional and ferroelectric cathodes (parameters of the conventional cathodes are according to Reimer—Refs. 198, 199).

Cathode type	Cathode temperature T_c (K)	Emission current density j_c (A/cm^2)	Brightness β, A/(cm^2 sr)	Energy spread ΔE (eV)
Thermionic (tungsten)	2500–3000	1–3	$(0.3–2)\times10^5$ for $E=20$ kV	1–2
Thermionic (LaB_6)	1400–2000	20–50	$(3–20)\times10^5$ for $E=20$ kV	1
Schottky emission (ZrO/W)	1800	500	$10^7–10^8$ for $E=20$ kV	0.8
Field emission (cold cathode)	300	2×10^5	$10^7–10^8$ for $E=20$ kV	0.2–0.4
Field emission (heated cathode)	1800	5×10^6	$10^7–10^8$ for $E=20$ kV	0.5–0.7
Ferroelectric	300	100 (total current up to 1 kA)	$10^5–10^7$ for $E=10–20$ kV	30 eV[a] $\geqslant$100 eV[b]

[a]Reference 75.
[b]Reference 91.

pulses determines which of the processes dominates. It is known that in a vacuum of 10^{-5} Torr at ambient temperature, a monolayer of air will be adsorbed on the ceramic surface in 0.2 s.[197,198] Since the lowest repetition rate used was 100 Hz, the longest time period was 0.01 s. This means that for all studied ferroelectric cathodes, plasma formation occurred as a result of the cathode and electrode materials. The observed strong damage of the cathodes is a natural effect occurring as a result of surface flashover plasma formation. Obviously, at the final stages of cathode operation when the damage becomes critical, the irreproducibility of the electron emission current from the ferroelectric cathode increases. The observed changes of the current shape and emitted charge per pulse is evidence that ferroelectric cathodes have limited reproducibility and lifetime when operated in a repetitive mode. The observed lifetime for the cathodes, based on the PZT (APC 856) ceramic and operated at the repetition rate of 100–200 Hz, was $\sim10^6$ current pulses of 0.2 μs duration.

The presented experimental data show that the lifetime of ferroelectric cathodes operated at high repetition rates is limited. Nevertheless, it can be compared to velvet and carbon-fiber cathodes, which also operate in a pulse mode, and have a limited lifetime of $\sim10^4$ and $\sim10^6$ pulses, respectively.

4. Brief summary

Basic parameters of conventional and ferroelectric cathodes are given for comparison in Table V (all data for conventional cathodes are taken from Reimer.[199,200]) One can see from Table V that ferroelectric cathodes have several advantages over conventional ones, such as high electron emission current density, high brightness, and ambient temperature operation. A typical emission current density for ferroelectric cathodes is of the order of 100 A/cm^2, which is less than that for Schottky and field emission cathodes. Nevertheless, the total emission current from the ferroelectric cathodes can be as high as 1 kA,[133] which is hardly achievable by conventional cathodes. However, the energy spread is orders of magnitude broader than that for the conventional electron cathodes. This implies that ferroelectric cathodes can be used only in devices tolerating such a large energy spread without performance degradation. Additional studies of the brightness parameter should be conducted. A brightness value of 10^5 A/(cm^2 sr) measured by Sampayan *et al.*[11] is achievable with thermionic tungsten cathodes.

5. Ferroelectric thin film cathodes

One of the most attractive applications of FEE cathodes are devices based on ferroelectric thin films. To the best of our knowledge, only three research groups have studied ferroelectric thin film cathodes (Asano *et al.*,[74] Auchello *et al.*,[75] Sviridov *et al.*[76]). As shown in Part A of this paper the ''plane-to-plane'' geometry (Fig. 12) allows one to induce in ferroelectric thin films a field $E_{d\text{out}} < 10^3–10^5$ V/cm, which is too small for FEE generation. The experimental setup used for the development of thin film ferroelectric cathodes[74–76] was identical to the setup proposed by Gundel *et al.*[6,7] where a patterned electrode was fabricated on the polar surface of a ferroelectric ceramic.

FEE from nonpoled PZT samples 30–45 μm thick in low vacuum 10^{-2} Torr was studied by Asano.[74] No details were presented on either the ceramic composition or its phase state. A field 25–75 kV/cm was applied to an evaporated strip Al electrode. A FEE current of 0.7 A/cm^2 was observed with a negative voltage pulse. It was proposed that FEE might be used in vacuum electronic devices, such as microtriodes and flat panel displays.

A low voltage triggering FEE was investigated by Auciello *et al.*[75] from PZT ferroelectric thin films 0.8 μm thick obtained by the sol-gel synthesis technique as well as from PLZT plates mechanically thinned to be $\sim$110 μm thick. A photolithography patterned Pt electrode was deposited. Polarization reversal of the studied thin film samples was thoroughly verified by measuring dielectric hysteresis loops. PLZT cathodes, excited by a switching voltage of 100–400 V, demonstrated a FEE current $j = 0.5–1.5$ mA/cm^2. The measured energy spectrum showed a sharp electron energy distribution around $W_e \sim 265$ eV (comparable with the triggering switching voltage) and a

FWHM ~30 eV. PZT thin film samples generated a weak FEE current in the range 0.07–0.15 μA/cm^2 under application of a switching voltage of 10–40 V (1.25–5.0 $\times 10^5$ V/cm). Important measurements of FEE current reproducibility showed that a stable FEE current is observed up to only 10^5 cycles of polarization switching. A fatigue test of identical samples with continuous oxide electrodes indicated that successful operation could be extended to 10^{12} cycles.[75]

A group of researchers, headed by LeBihan, studied FEE from TGS and PLZT cathodes with different thicknesses from 1 mm to 6 μm along the polar axis (Averty *et al.*,[13] Le Bihan *et al.*[177]). A patterned steplike electrode of various periodicity, as conventionally used for ferroelectric cathodes, was deposited by thermal evaporation. Two different schemes for measureming electron current were used. An electron multiplier detected weak FEE currents and a system containing a grid electrode and a collector was used for strong emission. The weak FEE current was studied under a 100 Hz sinusoidal switching field. FEE appeared at a switching field of 5 kV/cm for a TGS 1 mm thick, and this threshold excited field increased dramatically to 25 kV/cm for thinner TGS samples 40 μm thick. Simultaneous measurements of FEE and the switching current allowed the observation of a correlation between the two currents and an explanation of FEE by the polarization inversion model. A FEE current for TGS and PZT ceramics 100 μm thick was 3 and 20 A/cm^2 correspondingly. A discharge plasma and strong damage was observed for a higher FEE current. It was found that the thinner the sample, the smaller the FEE current. The observed peculiarities for samples with different thickness may be related to changes of the switching field distribution.[13] Qualitative consideration of the normal component of the switching field showed that the switched area and the FEE current increases with an increase in the sample thickness. The authors of Ref. 13 attempted to optimize the relation between the sample thickness and the width of the electrode strips. New data were recently published by Sviridov *et al.*[76] who studied the FEE current from PZT films several μm thick using an electron multiplier. The authors observed the FEE effect using an applied field in nonreversal mode-''dielectric'' electron emission. A measure of the FEE current was 10^6 counts/s, which corresponds to 10^{-12} A. FEE was highly stable for 4×10^6 cycles of the switching field. The authors believe that this method of FEE excitation eliminates the fatigue problem.[76]

C. Ferroelectric devices based on strong electron emission

1. Gas spark switches

A low pressure hollow cathode switch, triggered by a pulsed electron beam emitted from a ferroelectric cathode, was developed at CERN,[8] for the CERN Large Hadron Collider beam dumping system.[128] The electron beam was transported from the interior of a hollow cathode into the main gap of the switch for initiating (with nanosecond precision) a gas discharge with a maximum current of 45 kA.[127] The switching efficiency and long-term reliability of the device has been reported.[127]

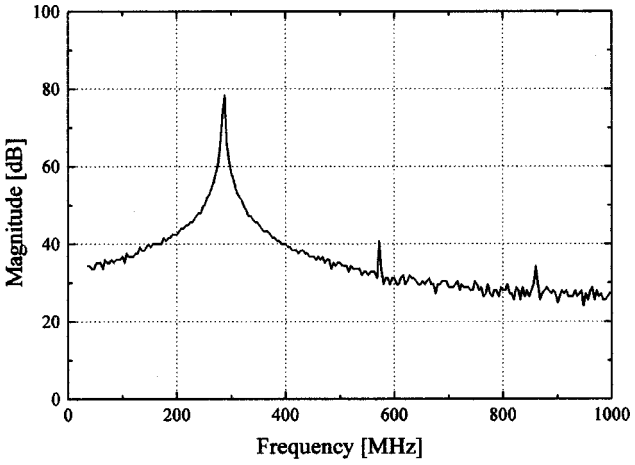

FIG. 44. Typical example of the Fourier analysis of the B-dot loop signal.

Bergmann *et al.*[201] used a cathode, based on high dielectric constant material,[152] to trigger a radial multichannel pseudospark switch. Distributing a current to several discharge channels allows one to achieve higher discharge currents. This triggering method without any restrictions for the switch geometry tolerates low working gas pressures ($<$10 Pa) that make such trigger units inefficient when using glow discharge triggering.[201]

2. High-frequency electron beam modulation

Current modulation of an electron beam, i.e., space-charge modulation, is one of the key problems in electronic devices used to generate high-frequency radiation.[202] Recently a new phenomenon related to electron beam high-frequency modulation observed in an electron diode with a plasma ferroelectric cathode has been reported.[21,203] The experimental setup was similar to that shown in Fig. 19. A positive polarity high voltage (HV) pulse (25–45 kV) was generated by a pulse forming network (PFN generator). To produce the plasma, unpoled ferroelectric samples $BaTiO_3$ and PZT were used. The front surface of the samples was covered by copper strips. The samples were placed inside an aluminum box with an output window covered by a stainless steel plate. The plasma was created by applying a driving pulse ($V_{fe}=2-8$ kV, $\tau_p=500$ ns) of either positive or negative polarity to the front electrode of the ferroelectric samples.

In addition to the diagnostics set shown in Fig. 19, the authors used a B-dot loop placed inside a vacuum chamber and microwave detectors were placed outside the chamber to measure the HF radiation. The potential distribution inside the cathode box was studied by an array of HV floating probes.

HF modulation was observed with an accelerating voltage of $\geqslant$30 kV for both $BaTiO_3$ and PZT samples. The electron beam current modulation was 60%–70%, and was 100% in some shots. It was found that the appearance of HF modulation did not depend on the polarity of the driving pulse applied to the front electrode.

It was found that HF modulation started with a delay of (1.0 ± 0.3) μs after the application of the driving pulse. HF

modulation was observed up to 35 μs when the amplitude of the quasiconstant electron current remained at a level $\geqslant 2$ A. An analysis of the low-frequency and high-frequency components of the currents allowed the authors to conclude that there is no electron emission from the output grid and that the plasma inside the cathode box supplies the electrons.

A typical example of a fast Fourier transform analysis of the oscillation frequency spectrum is presented in Fig. 44. The observed frequency peak has a narrow bandwidth ($\leqslant 5\%$ at the 20 dB level). It was found that the frequency was independent of the amplitude and the polarity of the driving pulse applied to the front electrode of the ferroelectric samples. In addition, the authors did not observe changes in frequency during the pulse of HF oscillations. Finally, it was shown that the frequency could be controlled over a broad range by changing the length of the input cable for the driving pulse.

The measurements of the plasma parameters showed that at the time of the appearance of the HF modulation the plasma density was of the order of $(5\pm 3)\times 10^{11}\,\mathrm{cm}^{-3}$, and the plasma expansion velocity was $(1.5\pm 0.2)\times 10^{6}$ cm/s. The data obtained by Penning probes showed that the neutral density in the vicinity of the ferroelectric sample is $n_n \approx 10^{14}\,\mathrm{cm}^{-3}$, and the neutral flow velocity is of the order of $(1-2)\times 10^{5}$ cm/s. The measurements of the potential distribution between the front electrode and the output cathode grid showed a significant increase in the amplitude of the negative signals from the probes when the HF oscillations started.

On the basis of the above-mentioned experimental data the authors proposed a qualitative model. According to this model, the application of the driving pulse to the front electrode of the ferroelectric sample causes surface plasma formation. An accelerating voltage application to anode leads to the acceleration of plasma electrons only when they appear in the vicinity of the output cathode grid. Since the observed current density of the electron beam is lower than that predicted by the space-charge law, the authors conclude that electrons are emitted from the plasma boundary behind the output cathode grid. It was also assumed that the plasma acquires a positive potential (the number of extracted electrons exceeds the number of ions emitted toward the front electrode and secondary electrons from the sample). Simultaneously with the surface plasma formation, production of neutrals also occurs. Based on the velocity of the neutrals, the thickness of the neutral layer should be about 1–2 mm at the time of the appearance of the HF modulation. At this time an increase in the light intensity was observed from a region about 2 mm thick near the front electrode. This increase in the light intensity can be explained by additional plasma formation. Approximately at the same instant of additional plasma formation, the potential of the front electrode changes its polarity from negative to positive. This means that at least part of the electrons emitted from the front electrode are captured inside the potential well, which has been formed by the positively charged plasma. In some sense, the formation of this plasma may play the role of a closing switch. If the duration of this perturbation is less than the time of the electromagnetic (e/m) wave propagation along the input cable, one can consider a wave process. The process of e/m wave oscillation in the cable can cause a periodical increase of electron emission from the cathode box, i.e., modulation of the electron beam amplitude. It is known that inside an asymmetric potential well, nonrelativistic electron oscillations and bunching can occur.[202] This oscillating bunch of electron space charge may have a positive feedback from the wave process if synchronism with the wave oscillations along the cable is maintained. This positive feedback is provided by a continuous extraction of electrons from the plasma boundary in the vicinity of the output cathode grid. In addition, due to the acceleration of the electron bunches, a HF current appears in the cathode holder. The appearance of this current should maintain the process of the e/m wave oscillation in the input cable; i.e., it represents the positive feedback.

3. Demonstration of microwave generation by a ferroelectric-cathode tube

The demonstration was implemented by the research group of Jerby (Drori *et al.*[19]) at Tel-Aviv University (Israel). A ferroelectric cathode was employed in a cyclotron-resonance maser (CRM). The CRM oscillator device was operated at ~7 GHz, near the cutoff frequency of a hollow cylindrical cavity. The cathode was made of a PLZT 12/65/35 ceramic with a high-dielectric constant ($\varepsilon_r \sim 4000$). Electrons were extracted from the plasma excited on the cathode surface by ~1 kV short rise-time pulses. The use of ferroelectric cathodes may advance microwave tube technology for various applications.

In general, the cathode is a key component in microwave tubes, cyclotron-resonance masers (CRMs), and free electron lasers. The features of the cathode and its sensitivity to operating conditions are crucial for the performance of the device. Ferroelectric cathodes present some attractive features in this regard. They can operate in poor vacuum conditions, at room temperature, and at low voltages. Ferroelectric cathodes do not need heating and preactivation and they are easy to fabricate and handle as compared to thermionic or field-emission cathodes.

In ferroelectric cathodes, electrons are emitted from a surface flashover plasma caused by an electric-field stress of the order of tens of kV/cm applied to the ceramic on a nanosecond time scale. This electric-field level is lower than needed for field-emission cathodes and is comparable to that of carbon-fiber cathodes.[204] Current densities up to 100 A/cm^2 have been produced by ferroelectric cathodes. Ferroelectric cathodes were proposed as electron-beam sources for free-electron em-wave generators.[9,127] In the present oscillator experiment, a ferroelectric cathode was employed in a cyclotron resonance maser (CRM) scheme. This device, operating in a gyrotron mode,[205] near cutoff, tolerates the electron energy spread and is characterized by its high gain.

Ferroelectric cathodes can be used in low repetition-rate or single-shot compact CRMs. They can be easily fabricated in various shapes for producing specified cross-sectional profiles of the electron beams, including large two-dimensional

electron-beam arrays for multibeam devices proposed recently.[206]

CONCLUSIONS

In this review we have described the main experimental and theoretical results on electron emission from ferroelectric materials published during the last 25 years by various research groups all over the world. We derived two different types of the observed electron emission, demonstrating many orders of magnitude difference in electron currents from the same ferroelectric materials. We believe that the review allows one to better understand the origin of both effects. A proper understanding is also a key problem in the development of a new generation of diverse devices based on the phenomena.

The first type of ferroelectric emission is an electron emission provoked by pyroelectric, piezoelectric effects, or spontaneous polarization inversion. In these cases, variation of temperature (pyroelectric effect), application of mechanical stress (piezoelectric effect), or spontaneous polarization inversion (polarization switching) causes a deviation of spontaneous polarization from its equilibrium state and generation of uncompensated electrostatic charges and fields on a ferroelectric polar surface. This type of electron emission is observed in the ferroelectric phase only. The emerging electron emission occurs from a negatively charged ferroelectric surface uncoated by any electrode. This electron emission provides a screening electron current into the vacuum similar to a conventional conductive current of pyroelectric, piezoelectric, or polarization inversion origin occurring via uniformly deposited electrodes. This electron emission current appears as a result of tunneling emission, and it does not exceed 10^{-7} A/cm^2. It demonstrates a pronounced size effect that makes it highly problematic that electron emission can be generated from ferroelectric thin films. The studies undertaken by use of the electron visualization technique allowed visualization of both static domain configurations and their dynamic behavior. We think that the ferroelectric origin of weak electron emission is commonly accepted.

Strong electron emission is quite different. The current density exceeds the weak emission by 9–12 orders of magnitude. We firmly believe that another physical mechanism is responsible for high density emission currents reaching 100 A/cm^2. Thorough analysis of numerous published data resulted in the recognition of the following basic features of strong emission.

(1) Strong emission is induced by quite a different experimental setup than for weak emission. The excitation of this emission occurs by using a patterned electrode deposited on a ferroelectric surface. As a result, the ferroelectric surface is divided into two zones: the first coated by an electrode (strips or grid) and the second uncoated the electrode electron emitting zone. A trigger voltage (high pulsed voltage stress is normally used) gives rise to two components of the field: normal and tangential. The normal component may lead to diverse field-induced effects: reversing the spontaneous polarization direction (for samples related to the ferroelectric phase), field-enforced phase transitions (for samples related to the antiferroelectric or the relaxor phase), and conventional electrical polarization of the dielectric (for samples related to the paraelectric phase or any other phase). However, calculations of field distribution showed that the normal component induces the field-enforced effects under the patterned electrode and near the electrode edges due to fringing fields. The tangential component of the applied field exists on the uncoated emitting zone of the surface and it may cause a surface flashover by avalanching emitting electrons along the surface.

(2) Ferroelectric materials used for strong electron emission generation are related to different phase states namely: ferroelectric, antiferroelectric, relaxor, and paraelectric. Analysis of published data showed that high current density emission is induced by applying trigger voltage pulses of any polarity. Regardless of the phase state and the mode of excitation, the measured emission current densities demonstrated nearly equal values. This allowed one to propose a plasma as the source of electrons for strong emission. Plasma formation has been proved experimentally by measurements of plasma density and electron temperature, by temporally and spatially resolved observations of ion emission, by fast framing photos, and by measurements of the energy spectra of emitted electrons and parameters of an electron diode with a ferroelectric cathode. Plasma formation can explain the above-mentioned difference in electron currents between the weak and strong electron emission.

(3) Two different modes of the surface flashover plasma generation followed by strong electron emission were observed. The first mode of plasma ignition occurs by weak electron emission induced by polarization inversion, or by a field-enforced phase transition near the edges of the patterned electrode due to the normal component of the applied field. These processes lead to the appearance of a noncompensated surface charge of ferroelectric origin with corresponding strong normal and tangential electric field components. The normal component of the electric field is responsible for weak electron field emission, followed by a surface electron avalanche due to the tangential component of the electric field. This mode of plasma excitation induced by field-enforced effects occurs only in specific phase states (ferroelectric, antiferroelectric, or relaxor) and upon a definite direction of the applied field (a bipolar triggering field for polarization inversion in the ferroelectric phase, or a monopolar field for ceramic compositions related to the antiferroelectric or relaxor states). It is very important to emphasize that the delay time of plasma generation followed by strong emission depends on the velocity of the forward growth of the ferroelectric domains inside the ferroelectric sample bulk or phase switching time (antiferroelectric, relaxor phase-ferroelectric phase). This velocity cannot exceed the velocity of sound in the material. This characteristic time for a ceramic sample 1 mm thick is in a microsecond time scale. The threshold trigger field (normal component) in this case is the coercive field needed for polarization inversion in the ferroelectric material used, or the field causing the phase transition from the antiferroelectric (relaxor) phase to the ferroelectric state possessing macroscopic polarization. It has been shown that it may be very low (e.g., for ferroelectric

TGS crystals it is about 1 kV/cm) and may be initiated even by a sinusoidal voltage, demonstrating that any rise time of the trigger voltage pulse is suitable in this mode.

The second type of surface flashover is ignited by field electron emission at triple junctions (points). However, in this case, an appearance of surface charges, which is responsible for the strong electric field followed by field electron emission at triple junctions, is caused by the conventional electric polarization in the dielectric material. This type of surface flashover has been well known for about 30 years, and it was used for so-called metal–dielectric cathodes. The plasma is initiated by a high voltage trigger pulse of any polarity applied to ferroelectrics in any phase state, as well as to linear dielectrics. The field causing field electron emission at triple junctions is enhanced by a factor equal to the dielectric permittivity of the material, which is especially high for ferroelectric ceramics. Thorough measurements showed that the plasma formation starts within the first few nanoseconds after the application of the trigger voltage pulse. So far, the delay time of strong electron emission ignited in this mode is much shorter than that in the mode where the plasma is initiated by any field-enforced phase transition or polarization inversion. Studies of both modes of flashover for the ferroelectric ceramic PLZT 7/65/35 showed that the threshold triggering voltage for initiating surface plasma by the field emission at triple junctions is three times higher than that for plasma ignited by polarization inversion. The rise time of the applied trigger voltage should be as short as possible.

Various ferroelectric electron emission devices based on both weak and strong emission have been proposed. Ferroelectric electron emissive flat panel displays, x-ray, neutron, and thermal imaging devices have been developed. Strongly emitting ferroelectric cathodes can be used for microwave radiation generation, gas spark switches, etc. Undertaken studies showed that strong plasma-assisted ferroelectric cathodes are greatly damaged by surface flashover. Poor reproducibility and a relatively short lifetime (about 10^6-10^7 shots) limit the cathodes' application, especially if they are to be operated at a high repetition rate.

It should be noted that there is no unanimous opinion about the strong electron emission effect. Due to a lack of detailed knowledge, the relation between true (weak electron emission) and plasma-assisted emission is not accepted by all research groups. One must perform temporally and spatially resolved measurements of the surface electric field in order to distinguish between these two modes of electron emission. This problem is especially important because ''true'' ferroelectric electron emission allows one to develop electron emission devices operating in a nondamaging mode. However, it should be additionally proved that ''true'' electron emission can provide the same high current densities as strong electron emission. As to the application of ferroelectric plasma-assisted strong cathodes, the main problem is the development of cathodes with a narrow energy spectrum, as well as high uniformity and reproducibility of the emitted electron current.

ACKNOWLEDGMENT

This work was supported by Ministry of Science of Israel.

[1] B. Rosenblum, P. Braunlich, and J. P. Carrico, Appl. Phys. Lett. **25**, 17 (1974).
[2] G. Rosenman and V. Pechorskii, J. Exp. Theor. Phys. **6**, 661 (1980).
[3] G. Rosenman, V. Okhapkin, Yu. Chepelev, and V. Shur, J. Exp. Theor. Phys. **39**, 477 (1984).
[4] P. Braunlich, B. Rosenblum, J. P. Carrico, L. Himmel, and P. K. Rol, Appl. Phys. Lett. **22**, 61 (1973).
[5] G. Rosenman, D. Shur, and A. Skliar, J. Appl. Phys. **79**, 7401 (1996).
[6] H. Gundel, H. Riege, J. Handerek, and K. Zioutas, CERN/PS/88-66(AR).
[7] H. Gundel, H. Riege, E. Wilson, J. Handerek, and K. Zioutas, Bull. Am. Phys. Soc. **34**, 193 (1989).
[8] H. Gundel, H. Riege, J. Handerek, and K. Zioutas, Appl. Phys. Lett. **54**, 2071 (1989).
[9] J. D. Ivers, L. Schächter, J. A. Nation, G. S. Kerslick, and R. Advani, J. Appl. Phys. **73**, 2667 (1993).
[10] B. Jiang, G. Kirkman, and N. Reinhardt, Appl. Phys. Lett. **66**, 1196 (1995).
[11] S. E. Sampayan, G. J. Caporaso, C. L. Holmes, E. J. Lauer, D. Prosnitz, D. O. Trimble, and G. A. Westenskow, Nucl. Instrum. Methods Phys. Res. A **340**, 90 (1994).
[12] T. C. Cavazos, W. L. Wilbanks, C. B. Fleddermann, and D. A. Shiffler, Appl. Phys. Lett. **65**, 2612 (1994).
[13] D. Averty, S. F. Liateni, and R. Le Bihan, Ferroelectrics **173**, 171 (1995).
[14] M. Okuyama, J. Asano, and Y. Hamakawa, Jpn. J. Appl. Phys., Part 1 **33**, 5506 (1994).
[15] Sh. Airapetov, I. I. Ivanchik, A. N. Lebedev, I. V. Levshin, and N. A. Tikhomirova, Sov. Phys. Dokl. **35**, 267 (1990).
[16] D. Shur, G. Rosenman, Ya. Krasik, and V. D. Kugel, J. Appl. Phys. **79**, 3669 (1996).
[17] M. Miyake, S. Ibuka, K. Yasuoka, and S. Ishii, Jpn. J. Appl. Phys., Part 1 **36**, 6004 (1997).
[18] H. Riege, I. Boscolo, J. Handerek, and U. Herleb, J. Appl. Phys. **84**, 1602 (1998).
[19] R. Drori, M. Einat, D. Shur, E. Jerby, G. Rosenman, R. Advani, R. J. Temkin, and C. Pralong, Appl. Phys. Lett. **74**, 335 (1999).
[20] J. D. Ivers, J. Nation, P. Wang, C. Golkowski, and D. Flechter, The 26th IEEE International Conference On Plasma Science, Monterey, CA, June, 1999 (unpublished).
[21] Ya. E. Krasik, A. Dunaevsky, and J. Felsteiner, Appl. Phys. Lett. **73**, 453 (1998).
[22] V. M. Fridkin, *Photoferroelectrics* (Springer, Berlin, 1979).
[23] I. Ivanchik, Sov. Phys. Solid State **12**, 586 (1970).
[24] G. M. Guro, I. I. Ivanchik, and N. F. Kontoniuk, Sov. Phys. JETF Lett. **5**, 9 (1967).
[25] G. M. Guro, I. I. Ivanchik, and N. F. Kontoniuk, Sov. Phys. Solid State **10**, 135 (1968).
[26] R. LeBihan and J. L. Chartier, Ferroelectrics **13**, 475 (1976).
[27] R. LeBihan and B. Abboud, Ferroelectrics **92**, 375 (1989).
[28] E. I. Boikova and G. Rosenman, Sov. Phys. Solid State **20**, 1976 (1978).
[29] G. Rosenman, Ju. Ja. Tomashpolski, E. I. Boikova, and M. A. Sevostianov, Ferroelectrics **31**, 139 (1981).
[30] G. Rosenman, E. I. Boikova, and Yu. L. Chepelev, Phys. Status Solidi A **69**, K173 (1982).
[31] A. Akhaian, A. N. Brozdnichenko, and E. V. Bursian, Sov. Phys. Solid State **20**, 912 (1978).
[32] A. Akhaian and A. N. Brozdnichenko, Sov. Phys. Solid State **25**, 1990 (1983).
[33] L. M. Beliaev and G. G. Bendrikova, Phys. Solid State **6**, 506 (1964).
[34] V. S. Kortov and R. I. Minz, Sov. Phys. Solid State **9**, 1436 (1967).
[35] G. Rosenman and E. Boikova, Phys. Status Solidi A **58**, 379 (1980).
[36] S. Rez, G. Rosenman, Yu. L. Chepelev, N. B. Angert, and A. A. Zhaskov, Sov. Tech. Phys. Lett. **5**, 568 (1979).
[37] G. Rosenman, I. S. Rez, Yu. L. Chepelev, N. B. Angert, and A. A. Zhaskov, Sov. Phys. Solid State **22**, 2032 (1980).
[38] G. Rosenman, Yu. Chepelev, and E. Boikova, Phys. Status Solidi A **117**, 259 (1990).
[39] U. Brunsmann, M. Euler, W. Kriegseis, and A. Scharmann, Phys. Status Solidi A **7**, K91 (1971).
[40] U. Brunsmann, A. Scharmann, and U. Weissler, Proceedings of the Fifth

International Symposium On EEE and Dosimetry, Zvikov, 1976 (unpublished), p. 283.
[41] B. Sujak, W. Syslo, K. Lada, and B. Jasik, Proceedings of the Sixth International Symposium On EEE and Application, Rostock, 1979 (unpublished).
[42] G. Rosenman, Yu. Chepelev, N. D. Gavrilova, V. K. Novik, and B. A. Chainov, Izv. Vuzov, Fizika (in Russian) **4**, 114 (1984).
[43] G. Rosenman, Ferroelectrics **135**, 469 (1992).
[44] G. Rosenman, E. Boikova, M. Sevostyanov, Yu. Tomaspolskii, Sov. Phys. JETF Lett. **27**, 253 (1978).
[45] G. Rosenman and E. Boikova, Sov. Phys. Solid State **22**, 121 (1980).
[46] G. Rosenman and E. Boikova, Sov. Phys. Solid State **20**, 1444 (1978).
[47] Yu. Tomashpolkii, E. Boikova, and G. Rosenman, Sov. Phys. Solid State **20**, 2019 (1978).
[48] G. Rosenman, Yu. Tomashpolskii, and E. Boikova, Ferroelectrics **3–4**, 139 (1981).
[49] B. Sujak and W. Syslo, Ferroelectrics **22**, 711 (1978).
[50] M. Kostsov, A. S. Sidorkin, V. S. Zaltzberg, and S. P. Gribkov, Sov. Phys. Solid State **24**, 1952 (1982).
[51] S. Sidorkin, A. M. Kostsov, and V. S. Zaltzberg, Sov. Phys. Solid State **27**, 1320 (1985).
[52] S. Sidorkin and A. M. Kostsov, Sov. Phys. Solid State **33**, 1383 (1991).
[53] K. Biedrzycki, Phys. Status Solidi A **93**, 503 (1986).
[54] K. Biedrzycki and B. Kosturek, Phys. Status Solidi A **100**, 327 (1987).
[55] K. Biedrzycki and R. Poprawski, Solid State Commun. **73**, 455 (1990).
[56] G. Rosenman, I. S. Rez, Yu. Chepelev, E. A. Sorokina, and E. I. Boikova, Sov. Phys. Solid State **22**, 2047 (1980).
[57] G. Rosenman, M. Tsedrik, I. Rez, S. Vasilevsky, and Yu. Chepelev, Ferroelectrics **110**, 113 (1990).
[58] D. Shur and G. Rosenman, J. Appl. Phys. **80**, 3445 (1996).
[59] A. Krumins, T. Shiosaki, and S. Koizumi, Jpn. J. Appl. Phys., Part 1 **33**, 4940 (1994).
[60] G. Rosenman, O. Malyshkina, and Yu. Chepelev, Ferroelectr. Lett. Sect. **10**, 141 (1989).
[61] V. D. Kugel, G. Rosenman, and D. Shur, J. Phys. D **28**, 2360 (1995).
[62] G. Rosenman and V. Pechorskii, Sov. Phys. Solid State **23**, 2162 (1981).
[63] G. Rosenman, O. V. Malyshkina, and Yu. L. Chepelev, Ferroelectrics **110**, 99 (1990).
[64] W. J. Merz, Phys. Rev. **95**, 690 (1954).
[65] R. Miller and A. Savage, J. Appl. Phys. **31**, 662 (1960).
[66] N. A. Tikhomirova, A. I. Baranov, A. V. Ginsberg, V. G. Monya, E. V. Chenskii, and L. A. Shuvalov, Sov. Phys. JETF Lett. **38**, 365 (1983).
[67] G. Rosenman, V. Letuchev, Yu. Chepelev, and V. Shur, Appl. Phys. Lett. **56**, 689 (1990).
[68] K. Biedrzycki and R. Le Bihan, Ferroelectrics **126**, 263 (1992).
[69] G. Rosenman and V. D. Kugel, Solid State Commun. **87**, 951 (1993).
[70] K. Biedrzycki and R. Le Bihan, Ferroelectrics **126**, 253 (1992).
[71] B. Suyak and K. Biedrzycki, Jpn. J. Appl. Phys., Suppl. **24**, 81 (1985).
[72] G. Rosenman and I. Rez, J. Appl. Phys. **73**, 1904 (1993).
[73] G. Rosenman, Ferroelectrics **133**, 235 (1992).
[74] J. Asano, T. Imai, M. Okuyama, and Y. Hamakawa, Jpn. J. Appl. Phys., Part 1 **31**, 3098 (1992).
[75] O. Auciello, M. A. Ray, D. Palmer, J. Duarte, G. E. McGurie, and D. Temple, Appl. Phys. Lett. **66**, 2183 (1995).
[76] E. Sviridov, R. Le Bihan, S. F. Liateni, and A. Desecures, Appl. Phys. Lett. **73**, 3953 (1998).
[77] G. Rosenman, V. Pechorskii, Y. Chepelev, E. Boikova, and L. Isakova, Phys. Status Solidi B **120**, 1904 (1983).
[78] G. Rosenman, Ferroelectrics **126**, 305 (1992).
[79] G. Rosenman, Ferroelectrics **118**, 451 (1991).
[80] V. D. Kugel and G. Rosenman, Appl. Phys. Lett. **68**, 2813 (1996).
[81] H. Gundel, J. Handerek, and H. Riege, J. Appl. Phys. **69**, 975 (1991).
[82] D. Shur, G. Rosenman, and Ya. Krasik, Appl. Phys. Lett. **70**, 574 (1997).
[83] D. Shur and G. Rosenman, J. Phys. D **32**, L29 (1999).
[84] G. Rosenman, D. Shur, Kh. Garb, R. Cohen, and Ya. Krasik, J. Appl. Phys. **82**, 772 (1997).
[85] W. Zhang and W. Huebner, J. Appl. Phys. **83**, 6034 (1998).
[86] N. J. Shannon, P. W. Smith, P. J. Dobson, and M. J. Shaw, Appl. Phys. Lett. **70**, 1625 (1997).
[87] Ya. E. Krasik, A. Dunaevsky, and J. Felsteiner, J. Appl. Phys. **85**, 7946 (1999).
[88] A. Dunaevsky, Ya. E. Krasik, J. Felsteiner, and S. Dorfman, J. Appl. Phys. **85**, 8464 (1999).
[89] I. Boscolo, A. Scurati, and M. Stellato, J. Appl. Phys. **85**, 8337 (1999).
[90] G. Benedek, I. Boscolo, J. Handerek, and H. Riege, J. Appl. Phys. **81**, 1396 (1997).
[91] D. Shur, G. Rosenman, Ya. Krasik, and R. Advani, J. Phys. D **31**, 1375 (1998).
[92] G. Pleyber, K. Biedrzycki, and R. Le Bihan, Ferroelectrics **141**, 125 (1993).
[93] H. Gundel, H. Riege, E. J. N. Wilson, J. Handerek, and K. Zioutas, Ferroelectrics **100**, 1 (1989).
[94] H. Gundel, J. Handerek, H. Riege, and E. J. N. Wilson, Ferroelectrics **110**, 183 (1990).
[95] D. Flechtner, C. Golkowski, J. D. Ivers, G. S. Kerslick, J. A. Nation, and L. Schachter, J. Appl. Phys. **83**, 955 (1998).
[96] G. Benedek, I. Boscolo, A. Moscatelli, A. Scurati, and J. Handerek, J. Appl. Phys. **83**, 2766 (1998).
[97] A. Dunaevsky, Ya. E. Krasik, J. Felsteiner, and S. Dorfman, J. Appl. Phys. **85**, 8474 (1999).
[98] G. H. Haertling and C. E. Land, J. Am. Ceram. Soc. **54**, 1 (1971).
[99] G. H. Haertling, Ferroelectrics **75**, 25 (1987).
[100] W. C. Stewart and L. S. Cosentino, Ferroelectrics **1**, 149 (1970).
[101] H. Gundel, H. Riege, E. J. N. Wilson, J. Handerek, and K. Zioutas, Nucl. Instrum. Methods Phys. Res. A **280**, 1 (1989).
[102] E. Fatuzzo and W. J. Merz, *Ferroelectricity* (North-Holland, Amsterdam, 1967).
[103] F. Jona and G. Shirane, *Ferroelectric Crystals* (Pergamon, Oxford, 1962).
[104] E. Land and P. D. Thacher, Proc. IEEE **57**, 5 (1969).
[105] G. H. Haertling and C. E. Land, Am. Ceram. Soc. Bull. **49**, 564 (1970).
[106] T. Cutchen, Ferroelectrics **27**, 173 (1980).
[107] K. Uchino, *Piezoelectric Actuators and Ultrasonic Motors* (Kluwer Academic, MA, 1996).
[108] J. C. Burfoot and G. W. Taylor, *Polar Dielectrics and Their Applications* (University of California Press, Berkeley, 1979).
[109] R. Landauer, J. Appl. Phys. **28**, 227 (1957).
[110] J. F. Scott, Ferroelectr. Rev. **1**, 1 (1998).
[111] J. Zelenka, *Piezoelectric Resonators and their Applications* (Elsevier, Amsterdam, 1986).
[112] R. C. Miller and A. Savage, Phys. Rev. **112**, 755 (1958).
[113] R. C. Miller and A. Savage, J. Appl. Phys. **31**, 662 (1960).
[114] V. D. Kugel, G. Rosenman, and D. Shur, J. Appl. Phys. **78**, 1165 (1995).
[115] P. Wurfel, I. P. Batra, and J. T. Yacobs, Phys. Rev. Lett. **30**, 1218 (1973).
[116] P. Wurfel and I. P. Batra, Phys. Rev. B **8**, 5126 (1973).
[117] L. Dontsova, N. Tikhomirova, and L. Shuvalov, Ferroelectrics **97**, 87 (1989).
[118] G. Rosenman and V. D. Kugel, Ferroelectrics **157**, 105 (1994).
[119] L. E. Cross, Ferroelectrics **151**, 305 (1994).
[120] C. E. Land, Ferroelectrics **7**, 45 (1974).
[121] G. H. Haerling and C. B. McCambell, Proc. IEEE, April, 450 (1972).
[122] W. Y. Pan, C. Q. Dam, Q. M. Zhang, and L. E. Cross, J. Appl. Phys. **66**, 6014 (1989).
[123] S-E. Park, M.-J. Pan, K. Markowsky, S. Yoshikawa, and E. Cross, J. Appl. Phys. **82**, 1798 (1997).
[124] B. Pokharel and D. Pandey, J. Appl. Phys. **86**, 3327 (1999).
[125] K. Uchino and S. Nomura, Ferroelectrics **50**, 191 (1983).
[126] F. Furuta, K. Y. Oh, and K. Uchino, Sens. Mater. **3**, 205 (1992).
[127] H. Riege, Nucl. Instrum. Methods Phys. Res. A **340**, 80 (1994).
[128] H. Gundel, in *Science and Technology of Electroceramic Thin Films*, edited by O. Auciello and R. Waser (Kluwer, Dordrecht, 1995).
[129] I. G. Austin and N. F. Mott, Adv. Phys. **18**, 41 (1969).
[130] B. Faust, H. Muller, and O. F. Schirmer, Ferroelectrics **153**, 297 (1994).
[131] V. Bune and V. A. Pashkov, Sov. Phys. Solid State **28**, 1701 (1986).
[132] L. Schachter, J. D. Ivers, J. A. Nation, and G. S. Kerslick, J. Appl. Phys. **73**, 8097 (1993).
[133] R. Advani, J. P. Hogge, K. Kreischer, W. Mulligan, R. Temkin, G. Kirkman, B. Jiang, and N. Reinhardt, IEEE Trans. Plasma Sci. **26**, 1347 (1998).
[134] D. Shur, Ph.D. thesis, Tel-Aviv University, 1999.
[135] I. I. Ivanchik, Ferroelectrics **111**, 147 (1990).
[136] J. T. Wang, W. Dawson, M. Chinkhota, and T. P. Chen, Nucl. Instrum. Methods Phys. Res. A **387**, 315 (1997).
[137] K. Geissler, H. Gundel, H. Riege, and J. Handerek, Appl. Phys. Lett. **56**, 895 (1990).
[138] K. Geissler, A. Meineke, H. Riege, J. Handerek, H. Granzer, and D. Suchland, Phys. Lett. A **166**, 84 (1992).

[139] K. Geissler, J. Handerek, A. Meineke, H. Riege, and K. Schmidt, Phys. Lett. A **176**, 387 (1993).
[140] K. Geissler, A. Meineke, H. Riege, and J. Handerek, Nucl. Instrum. Methods Phys. Res. A **340**, 96 (1994).
[141] K. Geissler, A. Meineke, H. Riege, S. de Silvestri, M. Nisoli, O. Svelto, I. Boscolo, and J. Handerek, Nucl. Instrum. Methods Phys. Res. A **372**, 567 (1996).
[142] H. Gundel, H. Henke, A. Meineke, H. Riege, K. Schmidt, and J. Handerek, Nucl. Instrum. Methods Phys. Res. A **340**, 102 (1994).
[143] G. Benedek and I. Boscolo, Appl. Phys. Lett. **72**, 522 (1998).
[144] W. Zhang, W. Huebner, S. E. Sampayan, and M. L. Krogh, J. Appl. Phys. **85**, 8497 (1999).
[145] S. Dorfman, A. Dunaevsky, J. Felsteiner, and Ya. E. Krasik, J. Appl. Phys. **85**, 8495 (1999).
[146] J. Kofoid, AIEE Trans. **6**, 991 (1960); **6**, 999 (1960).
[147] S. P. Bugaev and G. A. Mesyats, Sov. Phys. Dokl. **16**, 41 (1971).
[148] S. P. Bugaev, A. M. Iskol'dskii, and G. A. Mesyats, Sov. Phys. Tech. Phys. **12**, 1358 (1968).
[149] S. P. Bugaev and G. A. Mesyats, Sov. Phys. Tech. Phys. **12**, 1363 (1968).
[150] S. P. Bugaev, A. S. El'chaninov, F. Ya. Zagulov, B. M. Koval'chuk, and G. A. Mesyats, Instrum. Exp. Tech. **6**, 1557 (1970).
[151] S. P. Bugaev, V. V. Kremnev, Yu. I. Terent'ev, V. G. Shpak, and Ya. Ya. Yurike, Sov. Phys. Tech. Phys. **16**, 1547 (1972).
[152] V. P. Puchkarev and G. A. Mesyats, J. Appl. Phys. **78**, 5633 (1995).
[153] L. Schachter, Appl. Phys. Lett. **72**, 421 (1998).
[154] G. A. Mesyats, Tech. Phys. Lett. **20**, 8 (1994).
[155] H. C. Miller, IEEE Trans. Electr. Insul. **24**, 765 (1989).
[156] H. C. Miller, in *High Voltage Vacuum Insulation*, edited by R. Latham (Academic, London, 1995).
[157] C. LeGressus, Ph. Maire, and J. P. Duraud, IEEE Trans. Electr. Insul. **24**, 969 (1989).
[158] C. LeGressus, F. Valin, M. Henriot, M. Gautier, J. P. Duraud, T. S. Sudarshan, R. G. Bommakanti, and G. Blaise, J. Appl. Phys. **69**, 6325 (1991).
[159] G. Blaise, IEEE Trans. Electr. Insul. **28**, 437 (1993).
[160] S. P. Bugaev and G. A. Mesyats, Sov. Phys. Dokl. **16**, 41 (1971).
[161] R. A. Anderson and J. P. Brainard, J. Appl. Phys. **51**, 1414 (1980).
[162] A. S. Pillai and R. Hackam, J. Appl. Phys. **53**, 2983 (1982).
[163] A. A. Avdienko and M. D. Malev, Vacuum **27**, 643 (1977).
[164] A. A. Avdienko and M. D. Malev, Sov. Phys. Tech. Phys. **24**, 581 (1979).
[165] R. G. Bommakanti and T. S. Sudarshan, J. Appl. Phys. **66**, 2091 (1989).
[166] Ya. E. Krasik, A. Dunaevsky, J. Felsteiner, and A. Krokhmal, Bulletin of the 41st Annual Meeting of the DPP, APS, Seattle, Washington, November, 1999 (unpublished), p. 164.
[167] J. D. Swift and M. J. R. Schwar, *Electrical Probes for Plasma Diagnostics* (Iliffe, London, 1970).
[168] M. A. Heald and C. B. Wharton, *Plasma Diagnostics with Microwaves* (Wiley, New York, 1965).
[169] M. E. Lines and A. M. Glass, *Principles and Applications of Ferroelectrics and Related Materials* (Claredon, Oxford, 1977).
[170] S. P. Bugaev and G. A. Mesyats, Sov. Phys. Tech. Phys. **12**, 1363 (1968).
[171] S. P. Bugaev, V. V. Kremnev, Yu. I. Terent'ev, V. G. Shpak, and Ya. Ya. Yurike, Sov. Phys. Tech. Phys. **16**, 1547 (1972).
[172] J. P. Brainard and D. Jensen, J. Appl. Phys. **45**, 3260 (1974).
[173] V. D. Kugel, G. Rosenman, and D. Shur, J. Appl. Phys. **78**, 1165 (1995).
[174] T. Suzuki, Jpn. J. Appl. Phys. **13**, 1541 (1974).
[175] G. Rosenman and V. D. Kugel, Ferroelectrics **157**, 105 (1994).
[176] J. C. Burfoot and G. W. Taylor, *Polar Dielectrics and Their Applications* (University of California Press, Berkeley, CA, 1979).
[177] R. Le Bihan, S. F. Liateni, and D. Averty, Supplement a la Revue ''Le Vide science, technique et applications'' Mars 1995, Vol. 275.
[178] H. W. Gundel, Ferroelectrics **184**, 89 (1996).
[179] S. Sampayan, G. J. Caporoso, W. J. Orvis, and T. F. Wieskamp, UCRL-JC-120507, Preprint, Lawrence Livermore National Laboratory, 1995, submitted to J. Vac. Sci. Technol. (submitted).
[180] N. Nakatani, Jpn. J. Appl. Phys., Part 1 **25**, 27 (1986).
[181] A. Chynoweth, Phys. Rev. **113**, 159 (1959).
[182] G. Rosenman and V. D. Kugel, Solid State Commun. **87**, 951 (1993).
[183] G. Rosenman, Ferroelectrics **133**, 235 (1992).
[184] J. A. Nation, L. Schachter, F. M. Mako, L. K. Len, W. Peter, C. M. Tang, and T. Srinivasan-Rao, Proc. IEEE **87**, 865–889 (1999).
[185] L. Reimer, *Scanning Electron Microscopy* (Springer, Berlin, 1985).
[186] L. Reimer, *Image Formation in Low-Voltage Scanning Electron Microscopy* (SPIE, Bellingham, 1993).
[187] R. J. Temkin and R. Advani (private communication).
[188] L. H. Leonard, in *Introduction to Electron Beam Technology*, edited by R. Bakish (Wiley, New York, 1962).
[189] A. Hershcovitch, Appl. Phys. Lett. **68**, 464 (1996).
[190] A. Dunavsky, Ya. E. Krasik, J. Felsteiner, and A. Krokhmal, J. Appl. Phys. **87**, 3270 (2000).
[191] J. Ivers, D. Flechter, C. Golkowski, G. Liu, J. Nation, and L. Schachter, IEEE Trans. Plasma Sci. **27**, 707 (1999).
[192] M. Thumm, Appl. Surf. Sci. **111**, 106 (1997).
[193] R. Drori, D. Shur, E. Jerby, G. Rosenman, R. Advani, and R. Temkin, Digest of the 22nd International Conference on Infrared and Millimeter Waves, Wintergreen, VA, July 1997 (unpublished).
[194] E. W. Gray, J. Appl. Phys. **58**, 132 (1985).
[195] A. Dunaevsky, Ya. E. Krasik, and J. Felsteiner, Proceedings of the 12th Pulsed Power Conference, Monterey, 1999 (unpublished), pp. 408–411.
[196] American Piezo Ceramics, Data sheet, P.O. Box-180, Mackeyville, PA 17750.
[197] P. A. Redhead, J. P. Hobson, and E. V. Kornelsen, *The Physical Basis of Ultrahigh Vacuum* (Chapman and Hall, London, 1968), Chap. 2.
[198] J. F. O'Hanlon, *A User's Guide to Vacuum Technology* (Wiley, New York, 1989).
[199] L. Reimer, *Scanning Electron Microscopy* (Springer, Berlin, 1985).
[200] L. Reimer, *Image Formation in Low-Voltage Scanning Electron Microscopy* (SPIE, Bellingham, 1993).
[201] K. Bergmann, R. Lebert, J. Kiefer, and W. Neff, Appl. Phys. Lett. **71**, 1936 (1997).
[202] V. L. Granatstein and I. Alexeff, *High-power Microwave Sources* (Artech House, Boston, 1987).
[203] A. Dunaevsky, Ya. E. Krasik, J. Felsteiner, and A. Rosenberg, J. Appl. Phys. **86**, 4107 (1999).
[204] A. Shahadi, E. Jerby, Li Lei, and R. Drori, Nucl. Instrum. Methods Phys. Res. A **375**, 140 (1996).
[205] V. A. Flyagin, A. V. Gaponov, M. I. Petelin, and V. K. Yulpatov, *MTT* **31**, 514 (1995).
[206] E. Jerby, M. Korol, Li Lei, V. Dikhtiar, R. Milo, and I. Mastovsky, IR and MM Waves Conference Digest, VA, 1997 (unpublished), p. 65; and references therein; see also M. Korol and E. Jerby, Phys. Rev. E **55**, 5934 (1997).